AQUEOUS ALTERATION IN THE TARDA METEORITE: ISOTOPIC AND GEOCHEMICAL ANALYSES OF SECONDARY MINERALS

Bennett J.K. Wilson

A DISSERTATION SUBMITTED TO THE FACULTY OF GRADUATE STUDIES IN PARTIAL FULFILLMENT OF THE REQUIREMENTS FOR THE DEGREE OF DOCTOR OF PHILOSOPHY

GRADUATE PROGRAM IN EARTH AND SPACE SCIENCE
YORK UNIVERSITY
TORONTO, ONTARIO

August 2025

Abstract

Water appeared on some carbonaceous asteroids within the first few million years of Solar System history and modified the other accreted components in a process known as aqueous alteration. Recovered meteorites from such bodies, termed carbonaceous chondrites, are composed of diverse assemblages of secondary minerals and organic compounds that differ depending on the fluid environment the meteorite experienced. Since carbonaceous asteroids likely seeded the early planets with prebiotic organic matter, understanding the conditions that governed aqueous alteration is critical for evaluating their role in the origin of life.

This dissertation investigates the aqueous alteration history of Tarda, a new and unusual C2-ungrouped carbonaceous chondrite that fell in Morocco in 2020. The secondary mineralogy of Tarda implies exposure to significant aqueous alteration, and their investigation enables the fluid environment of Tarda to be constrained. The goal of this dissertation is to constrain the temperature, timing, evolution, and chemistry of the fluid responsible for altering the Tarda meteorite. Chapter 1 first establishes a novel, non-polar sample preparation procedure capable of polishing Tarda and other clay-rich samples for sensitive microanalytical techniques. Hexane, toluene, and mineral oil were identified as effective polishing liquids for such samples, which prevent clay minerals from swelling. Chapter 2 uses this polished surface and employs in situ secondary ion mass spectrometry (SIMS) on dolomite and magnetite to analyze oxygen, carbon, and manganese-chromium isotopes to constrain the timing, temperature, and evolution. Here, dolomite and magnetite were found to have precipitated approximately ~4.563 billion years ago at ~90˚C, from a relatively evolved fluid after significant water-rock interaction. Chapter 3 employs transmission electron microscopy (TEM), energy-dispersive spectroscopy (EDS), and atom probe tomography (APT) to investigate the nanoscale chemistry of magnetite framboids in Tarda. These

analyses reveal discrete boundary enrichments in elements such as Ti, Si, Na, Mg, Ca, and Mn, capturing a chemical record of the altering fluid from which the framboids precipitated. The observed element distributions and inferred surface charge conditions constrain the fluid to alkaline pH (>5.4) and support a chemically diverse, cation-rich environment. Together, these chapters present a multi-technique, multi-scale investigation into the aqueous alteration history of Tarda. Beyond providing new insights into Tarda itself, this work contributes to broader efforts to reconstruct parent body fluid histories and evaluate the potential for carbonaceous asteroids to host environments favorable to prebiotic organic synthesis.

Acknowledgements

First, I would like to thank my supervisor, Dr. Mike Daly, who has continually supported the projects contained in this dissertation. Mike gave me significant autonomy over my research for the past four years, enabling me to combine my interests with scientific merit. He balanced this with the guidance necessary to keep me on track, and I have continued to love what I study. Thank you.

Next, I would like to thank Dr. Kim Tait, who provided guidance and support for this PhD. She connected me with this PhD opportunity, provided the Tarda meteorite for this PhD, and provided extensive resources from the Royal Ontario Museum. Thank you.

Thank you to my committee members, Dr. Isaac Smith and Dr. Jim Whiteway for reviewing this dissertation and your guidance over the lifetime of this PhD.

A special thank you goes to Dr. Kazuhide Nagashima at the University of Hawai'i, Mānoa, whom I briefly visited for O, C, and Mn-Cr isotope collection. During this visit and all our subsequent online meetings, his kindness, expertise, and patience has been invaluable to me. Through him, I improved as a scientist, and better learned what kind of scientist I would like to be. Thank you for everything.

Another special thank you goes to Dr. Thomas Barrett at the University of Manchester, who often made himself available with little to no notice for support, advice, and discussions. Thank you for your time, kindness, and expertise.

I would also like to thank everyone else who played a role in the completion of my PhD. This includes Brian Langelier for supporting this thesis with TEM and APT; Dr. Gabriel Arcuri, for discussions and APT operation; Dr. Travis Casagrande, for discussions and FIB operation; Dr. Carmen Andrei for discussions and TEM operation; Dr. Elena Dobrică, for discussions and FIB

operation; Dr. Yanan Liu for SEM operation, Salvatore Boccia for SEM operation, Dr. Ross Findlay for reviewing, and; Veronica Di Cecco for help in the laboratory and reviewing. It was a pleasure to work with you all, and your collective expertise is unparalleled.

Additionally, I would like to thank my family, lab group, and friends for the support, numerous discussions, and shared experiences over the years. A particular emphasis goes to my friends Noah Stanton, Reilly Sawyers, and Adam Urquhart, who always kept me looking forward to things outside of this PhD.

Lastly, I would like to thank my partner, Paula Voorheis, who tried her best to keep me sane. A PhD is, at times, all consuming. She was always a reminder that the rest of life is more important.

Table of Contents

List of Tables

List of Figures

Preface

Chapter 1 is based on the following journal paper:

Wilson, B. J. K., et al. (2024). A Sample Preparation Guide for Clay-Rich Carbonaceous Chondrites. *Meteoritics and Planetary Science*, *59*(3), 560–567.

Chapter 2 is based on the following work submitted to Geochimica et Cosmochimica Acta for peer review:

Wilson, B. J. K., et al. (2024). Aqueous Alteration in the C2-ung Tarda Meteorite: In Situ Isotopic Evidence from Dolomite and Magnetite. In peer review to Geochimica et Cosmochimica Acta.

CHAPTER 1. Introduction

Some carbonaceous asteroids accreted with significant amounts of water ice (e.g. Brearley, 2006; Lee et al., 2025; Suttle et al., 2021). Heating from the decay of short-lived radiogenic isotopes subsequently released liquid water within these bodies, creating one of the earliest aqueous environments in the solar system (Brearley, 2006; Cohen & Coker, 2000; Grimm & Mcsween, 1989; Lee et al., 2025). This water then reacted with the asteroid's original components, producing a suite of new minerals and organic compounds that vary based on the starting composition and the specific conditions of the aqueous environment (Brearley, 2006; Glavin et al., 2018; Krot et al., 2013; Lee et al., 2025; Pizzarello & Shock, 2010). This process, known as aqueous alteration, played a critical role in shaping the final mineralogical and organic inventory of these asteroids prior to their potential delivery to the forming planets (Kimura et al., 2013; Pizzarello, 2006). With an improved understanding of the conditions accompanying aqueous alteration, such as the timing, temperature, chemistry, and evolution, a better understanding of products capable of contributing to the origin of life can be achieved.

Meteorites from carbonaceous asteroids, known as carbonaceous chondrites, preserve records of aqueous alteration through their secondary minerals and organic components. This dissertation focuses on Tarda, a C2-ungrouped (C2-ung) meteorite that fell in Morocco in August 2020 (Gattacceca et al., 2021). Tarda contains primary olivine chondrules and chondrule fragments, embedded within a secondary mineral assemblage produced by aqueous alteration (Bates et al., 2024; Marrocchi et al., 2021; Schrader et al., 2024). This includes a matrix dominated by smectite and serpentine, along with dolomite, magnetite, and Fe-sulfides (Bates et al., 2024; Marrocchi et al., 2021). The combination of Tarda's aqueously altered mineralogy and its ungrouped

classification presents a unique opportunity to study aqueous alteration processes in a primitive asteroid that is both petrologically distinct and relatively understudied compared to most other aqueously altered meteorites.

This dissertation was designed to approach Tarda's aqueous alteration history from multiple scales and perspectives, each chapter targeting a different but complementary aspect of the problem. Since no water remains in the Tarda meteorite, studies were performed on dolomite and magnetite, which precipitate from the altering fluid and record its characteristics (e.g. Dobrică et al., 2019; Jilly-Rehak et al., 2017; Kimura et al., 2013; Lee et al., 2014; McCain et al., 2023; White et al., 2020)

The first chapter focuses on sample preparation challenges unique to Tarda. Its unusually high abundance of swelling clays (a symptom of aqueous alteration) required the development of a non-polar, clay-sensitive polishing method. Without addressing this issue, many planned analyses (e.g., electron microprobe, SIMS, TEM) would have been compromised, since they require an extremely flat surface to operate (Gauvin & Lifshin, 2000; Höschen et al., 2015; Kita et al., 2009; Ronnhult et al., 1987; Salajková et al., 2021). This chapter establishes a necessary foundation for producing high-quality analytical surfaces from Tarda and other clay-rich, polar-sensitive samples.

Using the polished surface produced from chapter one, the second chapter uses secondary ion mass spectrometry to conduct in situ oxygen, carbon, and Mn-Cr isotopic analyses of dolomite and magnetite. Here, constraints are placed on the temperature, timing, and evolution of the altering fluid on the Tarda parent body from which dolomite and magnetite were precipitating.

The third chapter uses novel sample preparation procedures to investigate nanoscale chemical compositions of magnetite framboids in Tarda. Framboidal magnetite likely contains nanoscale chemical remnants of the fluid from which they precipitated, segregated within grain boundaries

(Kimura et al., 2013; White et al., 2020). Transmission Electron Microscopy and Atom Probe Tomography was used to range this chemistry, providing direct evidence of fluid chemistry. The potential influence of fluid chemistry on organic synthesis within the parent body was then examined.

Collectively, these chapters provide a multi-scale and multi-technique coordinated investigation into the aqueous history of Tarda. Beyond characterizing Tarda, this approach helps bridge the gap between the mineralogical, chemical, and isotopic records of aqueous processing on carbonaceous asteroids as a whole. While the fluid conditions constrained here suggest environments that could have been conducive to organic synthesis, the alteration heterogeneity observed in comparable meteorites like Tagish Lake highlight the complexity that governs these aqueous systems. These findings provide constraints for future laboratory experiments and highlight the need for coordinated analyses that pair mineral-fluid chemistry with organic distributions at small spatial scales.

1.1 References

Bates, H. C., Aspin, R., Fu, C. Y., Harrison, C. S., Feaver, E., Branagan-Harris, E., King, A. J., Bryson, J. F. J., Sridhar, S., & Nichols, C. I. O. 2024. Extent of alteration, paleomagnetic history, and infrared spectral properties of the Tarda ungrouped carbonaceous chondrite. *Meteoritics and Planetary Science*. https://doi.org/10.1111/maps.14224

Brearley, A. J. 2006. The Action of Water. *Meteorites and the Early Solar System II*, 587–624.

Cohen, B. A., & Coker, R. F. 2000. Modeling of Liquid Water on CM Meteorite Parent Bodies and Implications for Amino Acid Racemization. *Icarus*, *145*(2), 369–381. https://doi.org/10.1006/icar.1999.6329

Dobrică, E., Ogliore, R. C., Engrand, C., Nagashima, K., & Brearley, A. J. 2019. Mineralogy and oxygen isotope systematics of magnetite grains and a magnetite-dolomite assemblage in hydrated fine-grained Antarctic micrometeorites. *Meteoritics and Planetary Science*, *54*(9), 1973–1989. https://doi.org/10.1111/maps.13366

Gattacceca, J., McCubbin, F. M., Grossman, J., Bouvier, A., Bullock, E., Chennaoui Aoudjehane, H., Debaille, V., D'Orazio, M., Komatsu, M., Miao, B., & Schrader, D. L. 2021. The Meteoritical Bulletin, No. 109. *Meteoritics and Planetary Science*, *56*(8), 1626–1630. https://doi.org/10.1111/maps.13714

Gauvin, R., & Lifshin, E. 2000. Simulation of X-Ray Emission from Rough Surfaces. *Mikrochim. Acta*, *132*, 201–204.

Glavin, D. P., Alexander, D., Aponte, J. C., Dworkin, J. P., Elsila, J. E., & Yabuta, H. 2018. The Origin and Evolution of Organic Matter in Carbonaceous Chondrites and Links to Their Parent Bodies. In *Primitive Meteorites and Asteroids: Physical, Chemical, and Spectroscopic Observations Paving the Way to Exploration* (pp. 205–271).

Grimm, R. E., & Mcsween, H. Y. 1989. Water and the thermal evolution of carbonaceous chondrite parent bodies. *Icarus*, *82*(2), 244–280. https://doi.org/10.1016/0019-1035(89)90038-9

Höschen, C., Höschen, T., Mueller, C. W., Lugmeier, J., Elgeti, S., Rennert, T., & Kögel-Knabner, I. 2015. Novel Sample Preparation Technique to Improve Spectromicroscopic Analyses of Micrometer-Sized Particles. *Environmental Science and Technology*, *49*(16), 9874–9880. https://doi.org/10.1021/acs.est.5b01636

Jilly-Rehak, C., Christine E., Huss, G. R., & Nagashima, K. 2017. 53Mn–53Cr radiometric dating of secondary carbonates in CR chondrites: Timescales for parent body aqueous alteration. *Geochimica et Cosmochimica Acta*, *201*, 224–244. https://doi.org/10.1016/j.gca.2016.08.033

Kimura, Y., Sato, T., Nakamura, N., Nozawa, J., Nakamura, T., Tsukamoto, K., & Yamamoto, K. 2013. Vortex Magnetic Structure in Framboidal Magnetite Reveals Existence of Water Droplets in an Ancient Asteroid. *Nature Communications*, *4*, 1–8. https://doi.org/10.1038/ncomms3649

Kita, N. T., Ushikubo, T., Fu, B., & Valley, J. W. 2009. High precision SIMS oxygen isotope analysis and the effect of sample topography. *Chemical Geology*, *264*(1–4), 43–57. https://doi.org/10.1016/j.chemgeo.2009.02.012

Krot, A. N., Keil, K., Scott, E. R. D., Goodrich, C. A., & Weisberg, M. K. 2013. Classification of Meteorites and Their Genetic Relationships. In *Treatise on Geochemistry: Second Edition* (2nd ed., Vol. 1). https://doi.org/10.1016/B978-0-08-095975-7.00102-9

Lee, M. R., Alexander, C. M. O'D., Bischoff, A., Brearley, A. J., Fujiya, W., Le, C., Ashley, G., Dobric, E., Kooten, E. Van, Krot, A. N., Leitner, J., Marrocchi, Y., Remusat, L., Telus, M.,

Tsuchiyama, A., & Vacher, L. G. 2025. Low-Temperature Aqueous Alteration of Chondrites. *Space Science Reviews*, *221*(11). https://doi.org/10.1007/s11214-024-01132-8

Lee, M. R., Lindgren, P., & Sofe, M. R. 2014. Aragonite, breunnerite, calcite and dolomite in the CM carbonaceous chondrites: High fidelity recorders of progressive parent body aqueous alteration. *Geochimica et Cosmochimica Acta*, *144*, 126–156. https://doi.org/10.1016/j.gca.2014.08.019

Marrocchi, Y., Avice, G., & Barrat, J.-A. 2021. The Tarda Meteorite: A Window into the Formation of D-type Asteroids. *The Astrophysical Journal Letters*, *913*(1), 1–8. https://doi.org/10.3847/2041-8213/abfaa3

McCain, K. A., Matsuda, N., Liu, M. C., McKeegan, K. D., Yamaguchi, A., Kimura, M., … Tsuda, Y. 2023. Early fluid activity on Ryugu inferred by isotopic analyses of carbonates and magnetite. *Nature Astronomy*, *7*(3), 309–317. https://doi.org/10.1038/s41550-022-01863-0

Pizzarello, S. 2006. The chemistry of life's origin: A carbonaceous meteorite perspective. *Accounts of Chemical Research*, *39*(4), 231–237. https://doi.org/10.1021/ar050049f

Pizzarello, S., & Shock, E. 2010. The organic composition of carbonaceous meteorites: the evolutionary story ahead of biochemistry. *Cold Spring Harbor Perspectives in Biology*, *2*(3), 1–20. https://doi.org/10.1101/cshperspect.a002105

Ronnhult, T., Brox, B., & Fritze, G. 1987. The Influence of Surface Topography on the X-ray Intensity in Electron Microprobe Analysis (EDSNDS). In *SCANNING* (Vol. 9).

Salajková, Z., Holá, M., Prochazka, D., Ondráček, J., Pavliňák, D., Čelko, L., Gregar, F., Šperka, P., Pořízka, P., Kanický, V., De Giacomo, A., & Kaiser, J. 2021. Influence of sample surface topography on laser ablation process. *Talanta*, *222*. https://doi.org/10.1016/j.talanta.2020.121512

Schrader, D. L., Cloutis, E. A., Applin, D. M., Davidson, J., Torrano, Z. A., Foustoukos, D., Alexander, C. M. O. D., Domanik, K. J., Matsuoka, M., Nakamura, T., Zega, T. J., Brennecka, G. A., & Render, J. 2024. Tarda and Tagish Lake: Samples from the same outer Solar System asteroid and implications for D- and P-type asteroids. *Geochimica et Cosmochimica Acta*, *380*(September 2023), 48–70. https://doi.org/10.1016/j.gca.2024.07.007

Suttle, M. D., King, A. J., Schofield, P. F., Bates, H., & Russell, S. S. 2021. The aqueous alteration of CM chondrites, a review. *Geochimica et Cosmochimica Acta*, Vol. 299, pp. 219–256. https://doi.org/10.1016/j.gca.2021.01.014

White, L. F., Tait, K. T., Langelier, B., Lymer, E. A., Černok, A., Kizovski, T. V., Ma, C., Tschauner, O., & Nicklin, R. I. 2020. Evidence for sodium-rich alkaline water in the Tagish Lake parent body and implications for amino acid synthesis and racemization. *Proceedings of the National Academy of Sciences of the United States of America*, *117*(21), 11217–11219. https://doi.org/10.1073/pnas.2003276117

CHAPTER 2. A Sample Preparation Guide for Clay-Rich Carbonaceous Chondrites

Abstract

The matrix of the C2-ungrouped Tarda meteorite contains abundant smectite minerals that swell and crumble when exposed to polar liquids, causing the sample to rapidly slake. This phenomenon presents a serious challenge when polishing the meteorite, as common polishing liquids used on carbonaceous chondrites, such as water, ethanol, ethylene glycol, and isopropyl alcohol, are polar and will cause the sample to swell, making it unsuitable for some analyses. Hexane and mineral oil are nonpolar liquids that were found to not induce swelling on highly expansive montmorillonite-clay analog material and were effectively integrated into a polishing procedure for Tarda. Here, we detail a procedure for mounting, cutting, and polishing the Tarda meteorite to prepare a surface that is suitable for a variety of sensitive techniques, such as electron microprobe analysis. This work offers a practical methodology for the preparation of other clay-rich samples, which may include the recently returned Ryugu and Bennu materials.

2.1. Introduction

Carbonaceous chondrites (CCs) are primitive meteorites that may contain significantly higher abundances of organic material and clay content than other chondritic meteorites (e.g., Glavin et al., 2018; Krot et al., 2013; Pizzarello, 2006; Pizzarello & Shock, 2010, 2017; Schmitt-Kopplin et al., 2010; Weisberg et al., 2006). These organic- and clay-rich CCs represent material that was available to the young and forming Earth before life emerged, and their investigation may yield insights into the origin of life on Earth. It is, therefore, unsurprising that CCs remain a consistent focus in chondritic literature and two recent missions have collected pristine and contextualized samples from the carbonaceous asteroids 101955 Bennu and 162173 Ryugu (Lauretta et al., 2022; Lauretta et al., 2017; Morota et al., 2020; Nakamura et al., 2022; Watanabe et al., 2017; Yokoyama et al., 2022). However, with only 52 observed falls, pristine CCs available for study are incredibly limited and great care must be applied to optimize CC material during study (Meteoritical Bulletin Database, 2023).

To analyze CCs, various surface-sensitive analytical techniques are often used, such as the Electron Microprobe, Energy Dispersive Spectroscopy, Secondary-Ion Mass Spectrometry, and Electron Back Scatter Diffraction. These techniques require a flat and polished sample surface since uneven surfaces can alter secondary counts that vary with the angle of the sample topography (Gauvin & Lifshin, 2000; Höschen et al., 2015; Kita et al., 2009; Ronnhult et al., 1987; Salajková et al., 2021). Samples for surface-sensitive analyses are commonly prepared by mounting the sample in some sort of epoxy medium, grinding the surface flat, and polishing. Clay-rich CC samples, however, can contain smectite group swelling clays, which have unique properties that present challenges during sample preparation (Garvie & Trif, 2021; Rubin & Ma, 2017; Suttle et al., 2021; Tomeoka & Buseck, 1988; Zolensky et al., 2002). Smectite minerals, such as saponite,

are comprised of repeating 2:1 layers consisting of an octahedral sheet sandwiched between two tetrahedral sheets (Barton & Karathanasis, 2002; Hensen & Smit, 2002; Kumari & Mohan, 2021). Consecutive sheets are weakly bound to one another, allowing variable space between each layer (Kumari and Mohan, 2021; Barton and Karathanasis, 2002). The tetrahedral and octahedral sheets exhibit a net anionic charge due to the pervasive and inequivalent substitutions of framework cations (Chakrabarty et al., 2006; Komadel et al., 2005). Charge-compensating cations and polar molecules such as water, can occupy the interlayer space causing each layer to expand from 9.6 Å up to ~20 Å, significantly increasing the mineral volume (Chakrabarty et al., 2006; Hensen & Smit, 2002; Katti et al., 2018; Komadel et al., 2005; Kumari & Mohan, 2021).

While many geological sample preparation methods incorporate water into their polishing procedure, clay-rich CCs require less polar options. Using a polarity scale ranging from the least polar solvent Tetramethylsilane (0) to water (1), solvents used in the polishing procedure for CCs commonly include ethanol (0.654), ethylene glycol (0.790), or isopropyl alcohol (0.546) (Aoudjehane Chennaoui et al., 2021; Gucsik et al., 2016; Harrington & Righter, 2017; Izawa et al., 2010; Nakashima et al., 2023; Reichardt, 1994; Zolensky et al., 2002). However, the 2020 fall named Tarda (C2-ung) posed significant sample preparation issues as the meteorite rapidly crumbled in the presence of polar liquids, including alcohols (Aoudjehane Chennaoui et al., 2021; Garvie & Trif, 2021). This phenomenon has not been previously documented in the chondritic literature. Tarda presented a new challenge for polishing procedures and the method used to produce a surface suitable for a variety of sensitive analyses is explained here in detail using materials accessible by most analytical laboratories. This has significant applications to the preparation of other polar-sensitive and delicate samples. This may include the recently returned

Ryugu samples that presented similar polishing difficulties, as well as samples returned from Bennu and future polar-sensitive meteorites (Lauretta et al., 2022; Nakashima et al., 2023).

2.2. Materials and Methods

This study uses a 2.1 g Tarda meteorite sample (catalog number ROMESM60117) and five similarly sized montmorillonite chips (ROMESM28500) from the Royal Ontario Museum (ROM) in Toronto, Canada. An Olympus BX53M microscope with Olympus Stream Motion 2.2 software was used to image the epoxy mounts at the ROM. A JEOL JXA8230 electron probe microanalyzer (EPMA) was used to produce a composite topographical map using secondary electron (SE) imaging to assess the sample topography of the Tarda meteorite. The map was collected using an accelerated voltage of 15 kV with a beam current of ~100 nA and 11 mm working distance. Processing and collecting was done with Oxford INCA software.

A Hitatchi SU3500 Scanning Electron Microscope (SEM) was used to acquire high resolution backscatter electron (BSE) topographical images to further assess sample topography. The images were acquired with an accelerating voltage of 20 kV with a beam current of ~0.7 nA and a working distance of 10 mm.

2.3. Preparation

A Kimwipe™ with Buehler Releasing Agent™ was applied to the interior of a one-inch diameter closed-end cylindrical reusable rubber epoxy mold. The Tarda sample was placed into the mold and a Struers EpoFix™ epoxy mixture consisting of a bisphenol-A based resin, and an amine-based hardener was poured into the mold completely submerging the Tarda sample. If required, a stir stick was used to adjust the position of the Tarda sample to ensure it cured in the center of the epoxy mold, which is essential for certain analyses such as SIMS (Kita et al., 2009). If large bubbles were entrained within the epoxy mixture immediately after pouring, a stir stick

was used to gently bring the bubbles to the surface. The mold was set to cure in a fume hood under a low vacuum to further remove bubbles. Once cured, the sample was removed by inverting the reusable rubber mold and will be referred to as a cured potted butt.

To minimize mass loss, a Wells 6234 wire saw equipped with a 0.42 mm diamond-impregnated wire was used to cut the sample dry. The potted butt containing Tarda was cut in half parallel to the epoxy surface with a cutting speed of 0.7 meters per second, producing two halves each with an exposed surface. A local exhaust ventilation system was used to remove airborne particles during the cutting process. After cutting, ejected dust that settled on a clean removable surface beneath the saw was recovered.

The cut surface requires a meticulous polishing procedure to achieve a flat and smooth surface suitable for a variety of surface-sensitive analyses. This is commonly produced through an iterative process and consists of multiple steps of lapping, polishing, and rinsing, where each lapping and polishing phase uses finer particles than the previous phase until the desired polish level is achieved. In between each lapping/polishing phase, polishing debris is removed by rinsing the sample with a polishing liquid to prevent scratching in future steps. Since CCs are sensitive to water, rapidly evaporating alcohols such as ethanol, ethylene-glycol, and isopropyl alcohol are often employed (Gucsik et al., 2016; Harrington & Righter, 2017; Izawa et al., 2010; Kimura et al., 2013; King et al., 2020; Nakashima et al., 2023; Zolensky et al., 2002).

2.4. Polishing Challenges Associated with Tarda

Producing a flat surface on the Tarda meteorite is challenging. This reflects predominantly two physical characteristics:

i) Significant hardness variability: Approximately 80 vol.% of the Tarda meteorite is composed of a fine-grained phyllosilicate matrix containing abundant smectite and

serpentine (Garvie & Trif, 2021; King et al., 2021). These clays have a hardness of ~1-3 on the Mohs scale. In contrast, embedded minerals within this soft matrix include chondrules and chondrule fragments, magnetite, dolomite, olivine, and Fe-sulfides which exhibit considerably higher Mohs hardness values up to 7 (Marrocchi et al., 2021; Yesiltas et al., 2022).

ii) Sensitivity to polar liquids: The phyllosilicates in Tarda expand when exposed to common polar polishing liquids (Garvie and Trif, 2021; Aoudjehane Chennaoui et al., 2021).

Polishing soft and hard minerals to a uniform flatness is challenging and harder minerals may be plucked from the matrix which may scratch the soft phyllosilicates and ruin the polish (Camuti & Mcguire, 1999; Harrington & Righter, 2017; Nakashima et al., 2023). Additionally, polar liquids should be avoided with meteorites composed of swelling clays.

We initially attempted to polish the Tarda meteorite using isopropyl alcohol. Upon inspection of the first lapping and rinsing iteration, the smectite minerals had swelled and subsequently dried, crumbling and creating several deep cavities (Figure 2.1). Original textures were severely disrupted in the sample.

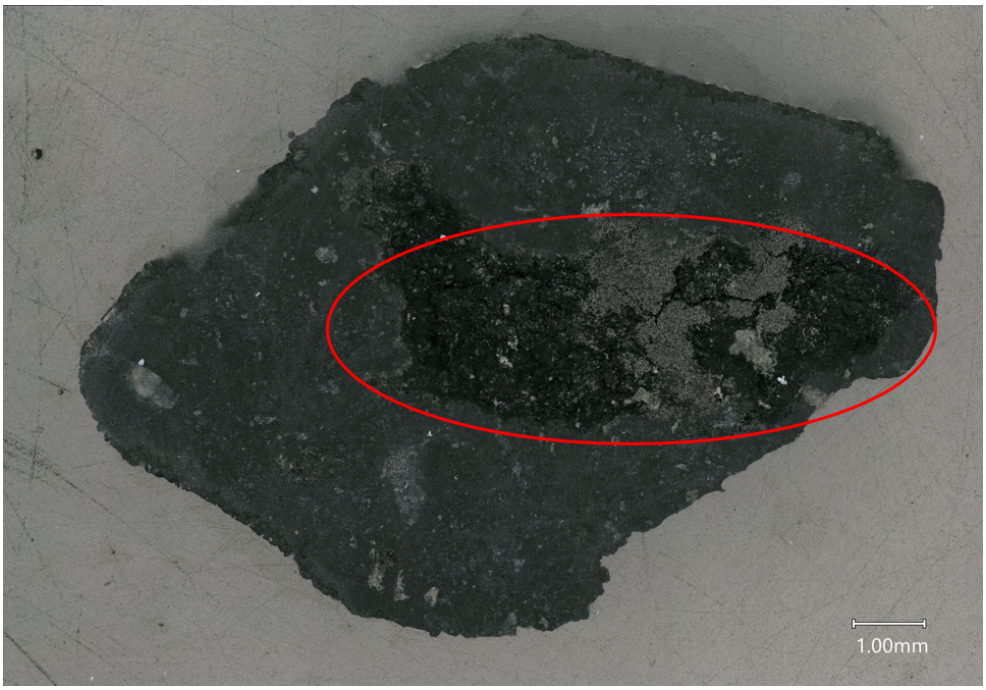

Figure 2.1: Reflected-light photograph for one of the two Tarda sample halves. Red oval highlights an ~4-mm-long cavity with interior features resembling desiccation cracks and was the most significant zone of alteration.

2.5. Testing Polishing Liquids

A polishing liquid compatible with swelling smectite minerals is required to polish clay-rich samples such as Tarda. To avoid further surficial damage to the Tarda meteorite, the most expansive smectite mineral named montmorillonite was used as an analogue material. Five small montmorillonite chips from Otay, California were provided by the ROM to test reactivity with six liquids. Ranging from 0 to 1, each liquid had a different polarity (P) as identified by Reichardt (1994). The liquids were:

i) Three polar solvents: >99% ethylene glycol (P = 0.790), >99% ethanol (P = 0.654), and >99% isopropyl alcohol (P = 0.546) (Reichardt, 1994).

ii) Two non-polar solvents: >98.5% n-hexane (hereafter hexane; P = 0.009) and >99.8% toluene (P = 0 .099).

iii) One non-polar polishing oil: Johnson and Johnson scented baby mineral oil.

Each montmorillonite chip was embedded in epoxy replicating the embedding procedure used for Tarda and 120 grit sandpaper was used to sand each epoxy surface down until montmorillonite became exposed at the surface.

The first three mounted montmorillonite chips were placed in a fume hood, and each had 0.5 ml of one of the three polar solvents poured on its surface. Each solvent was allowed to rest on the sample until it evaporated, replicating the polishing procedure. After approximately five minutes, each montmorillonite chip exposed to isopropyl alcohol, ethylene glycol, or ethanol significantly swelled, ranging from 40 to 90 mm (Figure 2.2).

The fourth montmorillonite chip was exposed to the mineral oil. The mineral oil did not interact with the montmorillonite and was wiped off after 10 minutes.

The fifth montmorillonite chip was placed in a fume hood and exposed to a series of three liquids to control for swelling variations across montmorillonite chips. It was first exposed to 0.5 ml of hexane (non-polar), which quickly evaporated with no reaction with the montmorillonite (Figure 2.3H1, H2). Next, the montmorillonite was subjected to 0.5 mL of toluene (non-polar), which also evaporated with no reaction from the montmorillonite (Figure 2.3T1, T2). Lastly, 0.5 ml of isopropyl alcohol (polar) was exposed to the montmorillonite surface and was found to swell, severely disrupting the original texture (Figure 2.3I1, I2).

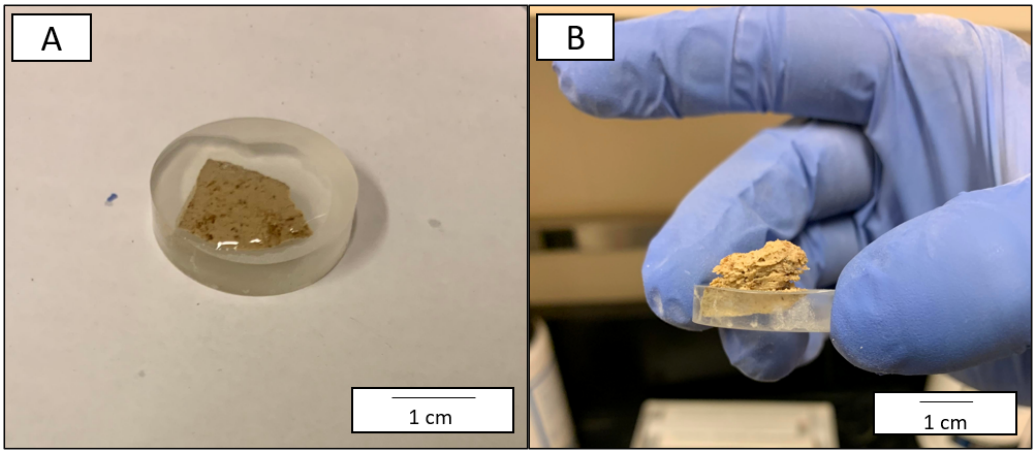

Figure 2.2: Mounted montmorillonite chip before (A) and after (B) being exposed to 0.5 mL of ethylene-glycol.

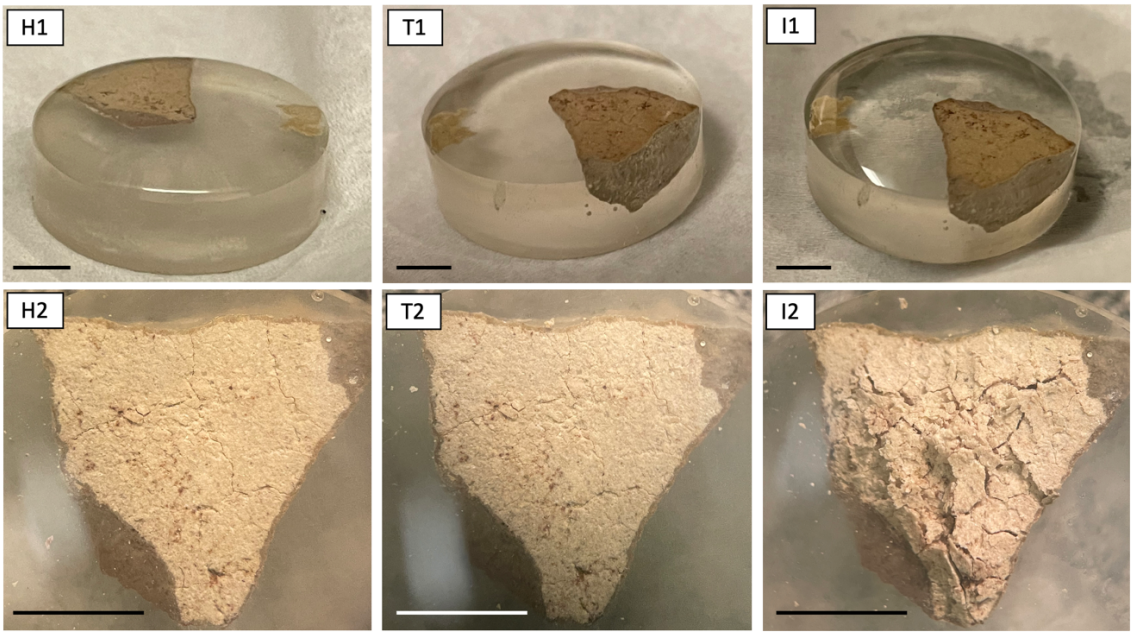

Figure 2.3: Before and after photos of montmorillonite being exposed to hexane (H1, H2), toluene (T1, T2) and isopropyl alcohol (I1, I2). Only isopropyl alcohol caused montmorillonite to swell. Scale bars are 0.5 cm.

Hexane, toluene, and mineral oil did not cause montmorillonite to swell, and each was successfully used to hand, or machine polish the Tarda meteorite, explained in the following section. In the successful preparation method used to polish the Tarda sample, the scented baby mineral oil was used as a non-toxic polishing lubricant to suspend the diamond powder during the final polish. Toluene and hexane can be interchanged during the polishing process and were used

as solvents capable of safely removing polishing debris from the sample surface and dissolving the baby mineral oil after the polish has been achieved. While hexane evaporates more quickly than toluene (within tens of seconds), it is a less toxic solvent and was implemented in the polishing procedure for the Tarda meteorite (Bates et al., 2016; Filley et al., 2004).

2.6. Polishing Recipe

Incorporating mineral oil and hexane, we give a detailed description of each step used to polish the Tarda meteorite, listed below:

i) Dry polish sample to 1200 grit: Using a series of silicon-carbide and corundum sandpaper sheets, Tarda was polished dry from 220 to 1200 grit over the course of six steps (220, 400, 600, 800, 1000, 1200 grit). During the polishing phase, the Tarda sample was polished in small (~10 cm diameter) circles using only hand pressure for 3-5 minutes for each iteration. In between each polish, hexane was used to rinse the sample surface to clear polishing debris away in preparation for the next iteration. If debris remained, a Kimwipe™ soaked in hexane was used to gently wipe the surface. At 1200 grit (15 micrometer), the cleaned surface was shiny and flat but scratches were still visible. Of note, while we employed a dry polish during this step, a wet polish could be achieved if desired by charging the sandpaper sheets with mineral oil.

ii) Improve cohesion (optional): At 1200 grit, the surface of Tarda was reimpregnated with Struers EpoFix™ epoxy to fill pore space and exposed cavities. Tarda was placed back into the 1-inch epoxy mold, face up. The mixture was poured over its surface and was set to cure in a fume hood under vacuum for 24 hours, to allow bubbles to escape from pore space. Afterwards, the surface was re-exposed by coarsely polishing down the

epoxy surface until dust began to appear. Step 1 was then repeated to achieve a polish to 1200 grit.

iii) Final polish: This step may be completed by hand or by machine polish.

a. Hand-polish: A Struers 300 mm diameter DP-Floc polishing pad was charged with mineral oil and 0.5-micrometer diamond powder to get a slurry consistency. It was then hand-polished in (~10 cm diameter) circles using hand pressure for 8-10 minutes.

b. Machine-polish: A Struers 300 mm diameter DP-Floc polishing pad was attached to a Buehler Metasev™ 250 automatic polisher and charged with mineral oil and 0.5-micrometer diamond powder to get a slurry consistency. The Tarda sample was loaded into the automatic polisher with a pin load of approximately one pound of pressure. The pad was then spun at 200 rpm for one minute

iv) Sample cleaning: After the final polish was completed, the sample was rinsed with hexane and subsequently placed face-up in a prepared clean glass container filled with hexane to dissolve the mineral oil. The container was periodically agitated by hand to gently mobilize the hexane. After approximately one minute, the sample was removed and the hexane within the container was dumped and replenished with new hexane. This was repeated several times to ensure the mineral oil was continually diluted and dissolved from the sample. Complete dissolution was assumed once the baby mineral oil scent disappeared from the sample. Once removed and dry, if polishing residue remained on the surface, a Kimwipe™ soaked in hexane was used to gently wipe the surface clean. The epoxy surrounding the sample should now have a mirror finish, which indicates an excellent polish on the sample. The sample is polished for a variety of sensitive techniques such as electron microprobe analysis (Figure 2.4).

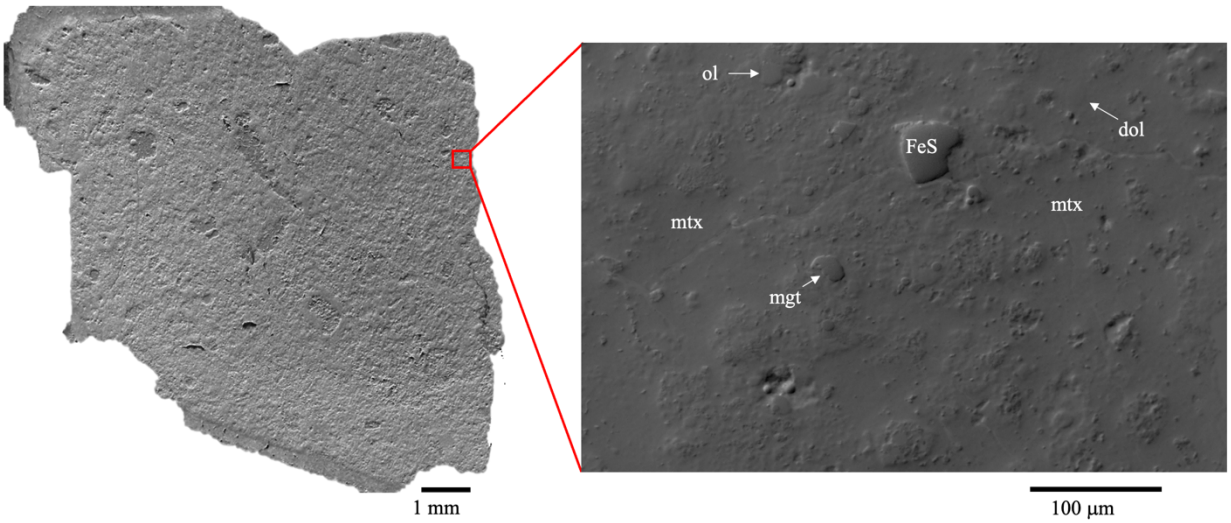

Figure 2.4: SEM secondary electron image of Tarda (left) and backscattered electron topography (BSE-TOPO) image (right) showing sample topography that remains after polishing. Olivine (ol), iron sulphides (FeS), and magnetite (mgt) are more resistant to polishing compared to the softer dolomite (dol) and phyllosilicate matrix (mtx).

2.7. Discussion

The polishing procedure outlined here uses equipment and chemicals available to most well-equipped geological laboratories. This recipe enables an inexpensive manual or machine polish on polar-sensitive CC samples that is appropriate for a suite of analyses that require a highly polished surface. This procedure is adaptable at many steps and may easily serve as a guide to complement existing laboratory workflows. For example, a variety of polishing pads and particles may be substituted (e.g., Buehler, 2022), non-polar lubricants can be used during the lapping process, and other non-polar lubricants such as kerosene have been used to polish phyllosilicate-rich soil samples, which may serve to replace mineral oil (Camuti & Mcguire, 1999).

While suitable for a variety of equipment, the final surface has produced a mirror epoxy finish, but with minor sample topography. This is largely unavoidable when polishing CCs due to the hardness difference between sample clasts and matrix, however, minor changes in the physical polishing procedures may further improve sample flatness.

To our knowledge, Tarda is the first carbonaceous material reported to display such high sensitivity to polar polishing liquids. This phenomenon, however, may have been unknowingly encountered in at least two previous studies since similar polishing difficulties were reported in Tagish Lake samples which were polished using isopropyl alcohol, and in the recently returned Ryugu samples which were polished using ethanol (Nakashima et al., 2023; Zolensky et al., 2002). To combat the crumbling associated with the ethanol-based polish in the clay-rich Ryugu samples, Nakashima et al, (2023) employed a dry polishing technique. While this technique prevents swelling in the sample clays, they report undesirable fracturing of anhydrous minerals associated with dry polishing, lowering the quality of mineral grains available for further study. Since the recipe detailed here uses a wet and non-polar polish, both fracturing and crumbling can be avoided, offering a distinct advantage over other methods.

It is currently unclear whether rapid slaking in the presence of polar liquids occur in only a few clay-rich CCs governed by atypical compositions or abundances of matrix smectite, or whether such polishing difficulties often go unreported. To explore this, future work employing transmission electron microscopy (TEM) will serve to identify the nature and species of the smectite minerals within the matrix of Tarda to investigate physical properties that may contribute to significant swelling.

2.8. Conclusion

CCs are primitive organic and water-bearing remnants of the early solar system that may represent material delivered to the early Earth. As such, CCs receive significant attention in literature, and carbon-rich asteroids have been the target for Hayabusa2 and OSIRIS-REx return sample missions. The C2-ungrouped Tarda meteorite fell to Earth and was recovered in Morocco in 2020 and is the first reported CC that has an adverse reaction with polar liquids, possibly due to

an unusual phyllosilicate-rich matrix or a reporting bias. Here, we provide a polar-sensitive polishing procedure capable of hand- and machine-polishing the Tarda meteorite. Surfaces produced with this polishing method are suitable for a variety of surface-sensitive equipment, such as electron microprobe analyses, and can be applied to future polar-sensitive carbonaceous material.

2.9. References

Aoudjehane Chennaoui, H., Agee, C.B., Ziegler, K., Garvie, L.A.J., Irving, A., Sheikh, D., Carpenter, P.K., et al. 2021. Tarda (C2-Ung): A New and Unusual Carbonaceous Chondrite Meteorite Fall from Morocco. *52nd Lunar and Planetary Science Conference*.

Barton, C.D., and Karathanasis, A.D. 2002. CLAY MINERALS. In *Encyclopedia of Soil Science*, edited by R. Lal, 187–92. New York, USA: Marcel Dekker, Inc.

Bates, M.N., Reed, B.R., Liu, S., Eisen, E.A., and Hammond, S.K. 2016. Solvent Exposure and Cognitive Function in Automotive Technicians. *NeuroToxicology* 57 (December): 22–30.

Buehler. 2022. Grinding and Polishing Guide. https://www.buehler.com/blog/grinding-and-polishing-guide/. 2022.

Camuti, K.S., and Mcguire, P.T. 1999. Preparation of Polished Thin Sections from Poorly Consolidated Regolith and Sediment Materials. *Sedimentary Geology*. Vol. 128.

Chakrabarty, D., Gautam, S., Mitra, S., Gil, A., Vicente, M.A., and Mukhopadhyay, R. 2006. Dynamics of Absorbed Water in Saponite Clay: Neutron Scattering Study. *Chemical Physics Letters* 426 (4–6): 296–300.

Filley, C.M., Halliday, W., and Kleinschmidt-Demasters, B.K. 2004. The Effects of Toluene on the Central Nervous System. *Journal of Neuropathology and Experimental Neurology* 63 (1): 1–12.

Garvie, L.A.J., and Trif, L. 2021. Bulk Mineralogy of the Tarda (C2-Ung) 2020 Fall: Results from Powder XRD and Thermal (TG-DSC-MSEGA) Analysis. *52nd Lunar and Planetary Science Conference*.

Gauvin, R., and Lifshin, E. 2000. Simulation of X-Ray Emission from Rough Surfaces. *Mikrochim. Acta* 132: 201–4.

Glavin, D.P., Conel, C.M.O'D., Aponte, J.C., Dworkin, J.P., Elsila, J.E., and Yabuta, H. 2018. *The Origin and Evolution of Organic Matter in Carbonaceous Chondrites and Links to Their Parent Bodies*. *Primitive Meteorites and Asteroids: Physical, Chemical, and Spectroscopic Observations Paving the Way to Exploration*. Elsevier Inc.

Gucsik, A., Gyollai, I., Nishido, H., Ninagawa, K., Izawa, M.M.R., Jäger, C., Ott, U., et al. 2016. Cathodoluminescence and Raman Spectromicroscopy of Forsterite in Tagish Lake Meteorite: Implications for Astromineralogy. *International Journal of Spectroscopy* 2016 (February): 1–8.

Harrington, R., and Righter, K. 2017. Carbonaceous Chondrite Thin Section Preparation. In *80th Annual Meeting of the Meteoritical Society*.

Hensen, E.J.M., and Smit, B. 2002. Why Clays Swell. *Journal of Physical Chemistry B* 106 (49): 12664–67.

Höschen, C., Höschen, T., Mueller, C.W., Lugmeier, J., Elgeti, S., Rennert, T., and Kögel-Knabner, I. 2015. Novel Sample Preparation Technique to Improve Spectromicroscopic Analyses of Micrometer-Sized Particles. *Environmental Science and Technology* 49 (16): 9874–80.

Izawa, M.R.M., Flemming, R.L., McCausland, P.J.A., Southam, G., Moser, D.E., and Barker, I.R. 2010. Multi-Technique Investigation Reveals New Mineral, Chemical, and Textural Heterogeneity in the Tagish Lake C2 Chondrite. *Planetary and Space Science* 58 (10): 1347–64.

Katti, D.R., Thapa, K.B., and Katti, K.S. 2018. The Role of Fluid Polarity in the Swelling of Sodium-Montmorillonite Clay: A Molecular Dynamics and Fourier Transform Infrared Spectroscopy Study. *Journal of Rock Mechanics and Geotechnical Engineering* 10 (6): 1133–44.

Kimura, Y., Sato, T., Nakamura, N., Nozawa, J., Nakamura, T., Tsukamoto, K., and Yamamoto, K. 2013. Vortex Magnetic Structure in Framboidal Magnetite Reveals Existence of Water Droplets in an Ancient Asteroid. *Nature Communications* 4 (October): 1–8.

King, A.J., Bates, H.C., Schofield, P.F., and Russell, S.S. 2021. The Bulk Mineralogy and Water Contents of the Carbonaceous Chondrite Falls Kolang and Tarda. *52nd Lunar and Planetary Science Conference*.

King, A.J., Phillips, K.J.H., Strekopytov, S., Vita-Finzi, C., and Russell, S.S. 2020. Terrestrial Modification of the Ivuna Meteorite and a Reassessment of the Chemical Composition of the CI Type Specimen. *Geochimica et Cosmochimica Acta* 268: 73–89.

Kita, N.T., Ushikubo, T., Fu, B., and Valley, J.W. 2009. High Precision SIMS Oxygen Isotope Analysis and the Effect of Sample Topography. *Chemical Geology* 264 (1–4): 43–57.

Komadel, P., Madejova, J., and Bujdak, J. 2005. Preparation and Properties of Reduced-Charge Smectites – a Review. *Clays and Clay Minerals* 53 (4): 313–34.

Krot, A.N., Keil, K., Scott, E.R.D., Goodrich, C.A., and Weisberg, M.K. 2013. *Classification of Meteorites and Their Genetic Relationships*. *Treatise on Geochemistry: Second Edition*. 2nd ed. Vol. 1. Elsevier Ltd.

Kumari, N., and Mohan, C. 2021. Basics of Clay Minerals and Their Characteristic Properties. In *Clay and Clay Minerals*, edited by Gustavo Morari Do Nascimento, 1–29. IntechOpen.

Lauretta, D.S., Adam, C.D., Allen, A.J., Ballouz, R., Barnouin, O.S., Becker, K.J., Becker, T., et al. 2022. Spacecraft Sample Collection and Subsurface Excavation of Asteroid (101955) Bennu. *Science* 377: 1–7.

Lauretta, D.S., Balram-Knutson, S.S., Beshore, E., Boynton, W. V., Drouet d'Aubigny, C., DellaGiustina, D.N., Enos, H.L., et al. 2017. OSIRIS-REx: Sample Return from Asteroid (101955) Bennu. *Space Science Reviews* 212 (1–2): 925–84.

Marrocchi, Y., Avice, G., and Barrat, J.-A. 2021. The Tarda Meteorite: A Window into the Formation of D-Type Asteroids. *The Astrophysical Journal Letters* 913 (1): 1–8.

Meteoritical Bulletin Database. Accessed September 20, 2023. https://www.lpi.usra.edu/meteor/metbull.php

Morota, T., Sugita, S., Cho, Y., Kanamaru, M., Tatsumi, E., Sakatani, N., Honda, R., et al. 2020. Sample Collection from Asteroid (162173) Ryugu by Hayabusa2: Implications for Surface Evolution. *Asteroids* 368: 654–59.

Nakamura, T., Matsumoto, M., Amano, K., Enokido, Y., Zolensky, M.E., Mikouchi, T., Genda, H., et al. 2022. Formation and Evolution of Carbonaceous Asteroid Ryugu: Direct Evidence from Returned Samples. *Science*, 1–9.

Nakashima, D., Fujioka, Y., Katayama, K., Morita, T., Kikuiri, M., Amano, K., Kagawa, E., et al. 2023. Development of Preparation Methods of Polished Sections of Returned Samples from Asteroid Ryugu by the Hayabusa2 Spacecraft. *Meteoritics and Planetary Science*, 1–16.

Pizzarello, S. 2006. The Chemistry of Life's Origin: A Carbonaceous Meteorite Perspective. *Accounts of Chemical Research* 39 (4): 231–37.

Pizzarello, S., and Shock, E. 2010. The Organic Composition of Carbonaceous Meteorites: The Evolutionary Story Ahead of Biochemistry. *Cold Spring Harbor Perspectives in Biology* 2 (3): 1–20.

Pizzarello, S., and Shock, E. 2017. Carbonaceous Chondrite Meteorites: The Chronicle of a Potential Evolutionary Path between Stars and Life. *Origins of Life and Evolution of Biospheres* 47 (3): 249–60.

Reichardt, C. 1994. Solvatochromic Dyes as Solvent Polarity Indicators. *Chemical Reviews* 94: 2319–58.

Ronnhult, T., Brox, B., and Fritze, G. 1987. The Influence of Surface Topography on the X-Ray Intensity in Electron Microprobe Analysis (EDSNDS). *SCANNING* 9: 81–87.

Rubin, A.E., and Ma, C. 2017. Meteoritic Minerals and Their Origins. *Chemie Der Erde*. Elsevier GmbH.

Salajková, Z., Holá, M., Prochazka, D., Ondráček, J., Pavliňák, D., Čelko, L., Gregar, F., et al. 2021. Influence of Sample Surface Topography on Laser Ablation Process. *Talanta* 222 (January).

Schmitt-Kopplin, P., Gabelica, Z., Gougeon, R.D., Fekete, A., Kanawati, B., Harir, M., Gebefuegi, I., et al. 2010. High Molecular Diversity of Extraterrestrial Organic Matter in Murchison Meteorite Revealed 40 Years after Its Fall. *Proceedings of the National Academy of Sciences of the United States of America* 107 (7): 2763–68.

Suttle, M.D., King, A.J., Schofield, P.F., Bates, H., and Russell, S.S. 2021. The Aqueous Alteration of CM Chondrites, a Review. *Geochimica et Cosmochimica Acta*. Elsevier Ltd.

Tomeoka, K., and Buseck, P.R. 1988. Matrix Mineralogy of the Orgueil CI Carbonaceous Chondrite. *Geochimica et Cosmochimica Acta* 52: 1627–40.

Watanabe, S. ichiro, Tsuda, Y., Yoshikawa, M., Tanaka, S., Saiki, T., and Nakazawa, S. 2017. Hayabusa2 Mission Overview. *Space Science Reviews* 208 (1–4): 3–16.

Weisberg, M.K., McCoy, T.J., and Krot, A.N. 2006. Systematics and Evaluation of Meteorite Classification. *Meteorites and the Early Solar System II*, 19–52.

Yesiltas, M., Kebukawa, Y., Glotch, T.D., Zolensky, M., Fries, M., Aysal, N., and Tukel, F.S. 2022. Compositional and Spectroscopic Investigation of Three Ungrouped Carbonaceous Chondrites. *Meteoritics and Planetary Science* 1687 (9): 1665–87.

Yokoyama, T., Nagashima, K., Nakai, I., Young, E.D., Abe, Y., Aléon, J., Alexander, C.M.O., et al. 2022. Samples Returned from the Asteroid Ryugu Are Similar to Ivuna-Type Carbonaceous Meteorites. *Science*, 1–7.

Zolensky, M.E., Nakamura, K., Gounelle, M., Mikouchi, T., Kasama, T., Tachikawa, O., and Tonui, E. 2002. Mineralogy of Tagish Lake: An Ungrouped Type 2 Carbonaceous Chondrite. *Meteoritics and Planetary Science* 37 (5): 737–61.

CHAPTER 3. Aqueous Alteration in the C2-ung Tarda Meteorite: In Situ Isotopic Evidence from Dolomite and Magnetite

Abstract

The Tarda meteorite is a recently recovered C2-ungrouped carbonaceous chondrite that preserves evidence of early Solar System aqueous alteration. Tarda was found to share reflectance spectra with P-type asteroids, possibly enabling these elusive asteroids to be studied in the laboratory for the first time. Furthermore, Tarda has been shown to share many petrological and isotopic affinities with Tagish Lake – a pristine C2-ungrouped chondrite that is widely considered to source a D-type asteroid. Thus Tarda, Tagish Lake, and their respective spectral classes are probably genetically related, and potentially source a shared parent body. Despite their similarities, however, Tagish Lake hosts different lithologies and carbonate species than Tarda, suggesting distinct aqueous alteration histories between the two meteorites. Here, we present in-situ oxygen, carbon, and ^{53}Mn–^{53}Cr isotopic analyses of dolomite and magnetite in Tarda using Secondary Ion Mass Spectrometry to (i) investigate the conditions associated with aqueous alteration on the early Tarda parent body, and to (ii) compare our findings with Tagish Lake to assess heterogeneous aqueous alteration of their unique and likely shared parent body. For dolomite, we found that δ^{13}C ranged from 56.6‰ to 72.3‰, while δ^{18}O ranged from 22.5‰ to 27.8‰ with an average Δ^{17}O of 0.2 ± 1.6. Dolomite additionally contained widespread ^{53}Cr excesses that, if interpreted to have chronological significance, corresponds to a live [(^{53}Mn/^{55}Mn)$_0$] value of $(3.08 \pm 0.52) \times 10^{-6}$. For magnetite, the δ^{18}O values ranged from -5.5‰ to 5.8‰ with an average Δ^{17}O of 2.4‰ ± 1.7. Oxygen isotope thermometry of a co-precipitating dolomite–magnetite pair indicates alteration temperatures of ~90°C. Compared to Tagish Lake, we find that dolomite in Tarda contains systematically lower O-isotope signatures than carbonates in Tagish Lake, with variations in δ^{13}C

that are generally similar but possibly show a weak positive correlation. Temporally, the carbonates in both meteorites have identical ages within uncertainty. We conclude that Tarda has experienced greater aqueous alteration than Tagish Lake, likely due to increased water-rock interaction and/or higher temperatures.

3.1 Introduction

Some primitive planetesimals accreted with water-rich ices which subsequently melted, presumably due to short-lived radiogenic heating (e.g. Brearley, 2006; Grimm & Mcsween, 1989; Lee et al., 2025). The resultant fluid then interacted with each affected planetesimal in a process known as aqueous alteration, causing pervasive modification of the accreted minerals and organics (e.g. Glavin et al., 2018; Krot et al., 2013; Pizzarello, 2006; Pizzarello & Shock, 2010, 2017; Remusat, 2014; Suttle et al., 2021). The conditions that accompany aqueous alteration, however, are highly variable and can be recorded by the diversity and abundance of secondary minerals and organic compounds that formed under distinct alteration conditions within and between each early asteroid (Brearley, 2006; Glavin et al., 2018; Lee et al., 2025). Using fragments of such bodies that fell to the Earth as meteorites, their aqueous alteration histories can be investigated using secondary minerals such as magnetite and various carbonate species, since they are common products of aqueous alteration which can record the isotopic signature of the fluid (e.g. Brearley, 2006; Dobrică et al., 2019; Fujiya et al., 2020, 2019, 2013, 2012; Jilly-Rehak et al., 2017a, 2017b, 2014; Kimura et al., 2013; Lee et al., 2025, 2014; Lindgren et al., 2017; McCain et al., 2023). The oxygen and/or carbon isotopic signatures of dolomite and magnetite can constrain the evolution of the fluid from which they precipitated, while formation temperatures of secondary minerals can be constrained from the oxygen isotopes from a co-precipitating dolomite and magnetite pair (e.g. Jilly-Rehak et al., 2017a; Rowe et al., 1994; Telus et al., 2019; Yokoyama et al., 2023).

Additionally, when the carbonates contain high Mn and low Cr, the ^{53}Mn-^{53}Cr isotope systematics using the short-lived radionuclide ^{53}Mn that decays to ^{53}Cr with its half-life of ~3.7 Myr can be used to date the timing of carbonate precipitation, offering insights into the duration and timing of aqueous activity (e.g. Birck & Allègre, 1985; 1988). Together, these isotope systems provide a robust geochemical framework for interpreting the environment from which the meteorite formed.

In this study, we use Secondary Ion Mass Spectrometry (SIMS) to apply these tools to the Tarda meteorite, an aqueously altered petrologic type-2 (C2) ungrouped carbonaceous chondrite that fell to Morocco in 2020 and was recovered the following day (Gattacceca et al., 2021). Tarda is the first meteorite that exhibits reflectance spectra most consistent with P-type asteroids, potentially enabling this spectral class to be studied in the laboratory for the first time (Schrader et al., 2024). Petrologically, Tarda is dominated by a serpentine- and smectite-rich matrix (~72 vol%) that contains olivine chondrules and chondrule fragments (~10 vol%), magnetite (~8 vol%), Fe-sulfides (~8 vol%), and carbonates (~2 vol%) (Bates et al., 2024; Marrocchi et al., 2021; Yesiltas et al., 2022). Dolomite and magnetite are both common products of aqueous alteration in the Tarda meteorite, enabling the aqueous alteration history of the meteorite to be studied.

Previous studies on the Tarda meteorite have found that bulk $\delta^{18}O$ oxygen isotope values for Tarda ($\delta^{18}O$ = 15.943, 16.434, 17.034, 17.924, 20.607, 20.842, 21.971) plot between CI (Ivuna-type) and CY (Yamato-type) chondrites, and bulk $\Delta^{17}O$ values ($\Delta^{17}O = -0.135 \pm 0.303$) plot beneath both CI, and CY chondrites and the terrestrial fractionation line (TFL), distinct from all other grouped carbonaceous chondrites (Gattacceca et al., 2021). While Tarda is ungrouped, several studies have, however, identified widespread petrological and geochemical similarities between Tarda and Tagish Lake, which is a C2-ungrouped chondrite generally considered to source a D-type asteroid (Hiroi et al., 2001; Schrader et al., 2024). Examples of these similarities

include bulk C/H wt%, bulk $\Delta^{17}O$, thermogravitational analyses, infrared reflectance spectra, and paleomagnetic properties, ultimately suggesting a genetic relationship between the two meteorites and their spectral reflectance types (Bates et al., 2024; Marrocchi et al., 2021; Schrader et al., 2024). Tarda and Tagish Lake, however, have notable differences that likely reflect heterogeneous parent body alteration. For instance, Tagish Lake has multiple observed lithologies (such as carbonate-poor and carbonate-rich) and contains various carbonates such as calcite, dolomite, and siderite, while we have only observed one lithology in Tarda, with dolomite as the sole observed carbonate (Bates et al., 2024; Blinova et al., 2014; Brown et al., 2000; Izawa et al., 2010a; Schrader et al., 2024; Zolensky et al., 2002). These may contribute to their differing spectral reflectance types (e.g. Gilmour et al., 2019). In this study, we present in-situ oxygen, carbon, and ^{53}Mn-^{53}Cr isotope measurements of dolomite and magnetite in Tarda to constrain the evolution, temperature, and timing of aqueous alteration. We compare the results with carbonates in Tagish Lake to explore the heterogeneity of aqueous alteration within their likely shared parent body. Since Tarda and Tagish Lake have rare spectral links to P- and D-type asteroids respectively, this work may have significant applications to prepare for the Lucy mission, set to extensively survey spectral D-, P-, and C-type Trojan asteroids (e.g. Levison et al., 2021; Olkin et al., 2021), and JAXA's Martian Moon eXploration (MMX) mission to explore Phobos and Deimos which have D-type spectral signatures (e.g. Kuramoto et al., 2022; Nakamura et al., 2021).

3.2 Analytical Methods

This study uses a 2.1-g Tarda meteorite specimen loaned from the Royal Ontario Museum (catalog number: ROMESM60117). Using the sample preparation method detailed in Wilson et al. (2024), the specimen was mounted in Struers EpoFix epoxy and cut in half to form two flat sample surfaces. Both cut surfaces were polished using mineral oil and hexane since they are non-

polar liquids which prevent the clay-rich sample surface from slaking. Two highly polished 1-inch-diameter potted butts were produced with thicknesses beneath 5 mm to minimize epoxy degassing during SIMS analysis. A ~30 nm gold coat was applied to the sample surface to minimize charging.

Large (>10 μm) and crack-free dolomite and magnetite crystals were targeted and imaged with the Hitatchi 3500SU Shottky Scanning Electron Microscope (SEM) at the Open Centre for the Characterization of Advanced Materials (OCCAM) in Toronto, Canada. Images were collected using a 20 kV accelerating voltage and a 0.7 nA beam current. Elemental compositions of the carbonates were determined using semi-quantitative Energy Dispersive X-ray Spectroscopy (EDX) over 100 seconds.

To collect secondary and backscattered electron images, a FEI Helios 660 dual-beam focused ion beam SEM (FIB-SEM) instrument was used at the Advanced Electron Microscopy Center (AEMC) at the University of Hawai‘i at Mānoa. To easily identify each region of interest for the SIMS measurements, we marked each grain using a gallium ion beam. The regions were imaged using the ion beam at 30 kV accelerating voltage and a low current of 7.7 pA to pinpoint the areas of interest. Once the grains were located, they were sputtered for approximately 30 seconds using a higher ion beam current of 0.23 nA and a 3×3 μm² raster to remove the gold coating and any surface contamination. The working distance for this microscope is 4 mm, and the stage was tilted at 52° to have the ion beam perpendicular to the sample surface.

3.2.1. Secondary Ion Mass Spectrometry

Large dolomite and magnetite grains were targeted for in-situ oxygen, carbon, and ^{53}Mn-^{53}Cr isotopic analyses with the CAMECA ims-1280 ion microprobe at the University of Hawai’i at Mānoa. Prior to SIMS analysis, both Tarda samples spent ~24 hours in a vacuum oven set to 50˚C

to degas. The oxygen isotope system was analyzed prior to ^{53}Mn-^{53}Cr to ensure any contamination resulting from the ^{16}O- ion beam was not recorded. All reported isotope ratios were calculated by first summing the ion intensities and then taking the ratio, instead of averaging the ratio for each cycle in the measurements to minimize the additive positive bias (Ogliore et al., 2011).

3.2.2. Oxygen

Oxygen isotopes were measured in magnetite and dolomite, each requiring one analytical session. All oxygen isotopes were collected using a $^{133}Cs^+$ ion source with an accelerating voltage of 10 kV and a primary beam current of ~30 pA focused to a diameter of ~1 μm. Each target location was presputtered for 45 seconds in a 2 x 2 μm raster to remove the gold coat and then measured for 20 cycles. Using a Faraday cup for $^{16}O^-$ measurements and electron multipliers for $^{17,18}O^-$ measurements, each cycle measured all oxygen isotopes simultaneously (6 s), followed by a measurement of $^{16}OH^-$ for interference monitoring (0.8 s). The mass resolving power (MRP) for $^{16}O^-$ and $^{18}O^-$ was ~2100, while the MRP for $^{17}O^-$ was ~5350 to resolve the interference from $^{16}OH^-$ on $^{17}O^-$. For both the dolomite and magnetite oxygen analysis, the $^{16}OH^-$ tail contributed ~30 ppm of $^{16}OH^-$ counts to the raw $^{17}O^-$ counts and was subtracted based on the measured $^{16}OH^-$ of each measurement. The $^{16}OH^-$ contribution is typically ~1.6‰ and 0.03‰ in dolomite and magnetite (up to 2.7‰ and 0.03‰), respectively.

Since instrumental isotope fractionation of oxygen from dolomite changes as a function of Fe content, multiple dolomite standards with varying Fe content were used to build a correction curve to correct for this bias (Figure A1; Śliwiński et al., 2016a). The dolomite standards used in this study were UW6250, dol1001, dol1026, and dol1055, with Fe# = (Fe/(Mg+Fe) ranging from 0.00 to 0.34 (Śliwiński et al., 2016a, Xu et al., 2022). The data are fitted with a Hill function proposed by Śliwiński et al. (2016a). The instrumental mass fractionation on magnetite measurements is

corrected using a polycrystalline magnetite standard from Chile (Nagashima et al., 2020). To account for possible crystallographic orientation effects (Huberty et al., 2010), we measured ~21 points from different and randomly oriented crystals of the magnetite standard to determine the mean value and uncertainty; 2-standard deviation (2SD) among the measurements was 2.1‰ in $\delta^{18}O$.

We report oxygen isotope compositions as per mil deviations from the standard mean ocean water (SMOW), using the formula:

$$\delta^{17,18}O = \left[\frac{(^{17,18}O/^{16}O)_{sample}}{(^{17,18}O/^{16}O)_{SMOW}} - 1\right] \times 1000 \qquad (3.1)$$

where $^{18}O/^{16}O_{SMOW}$ = 0.0020052 and $^{17}O/^{16}O_{SMOW}$ = 0.00038. Reported deviations from the terrestrial fractionation line is calculated as $\Delta^{17}O_{sample} = \delta^{17}O_{sample} - \delta^{18}O_{sample} \times 0.52$. The reported uncertainty considers both the standard error of the cycles in each measurement and the standard deviation of the standard measurements.

3.2.3. Carbon

Carbon isotopes were measured in dolomite, requiring two analytical sessions. The data from each session were processed separately. Both carbon isotopes were measured using a $^{133}Cs^{+}$ source with an accelerating voltage of 10 kV and a primary beam current of ~450 pA focused to a diameter of ~3 μm. Each target location was presputtered for 30 seconds in a 2x2 μm raster to remove the gold coat and then measured for 10 cycles. Using a Faraday cup for $^{12}C^{-}$ counts and an electron multiplier for $^{13}C^{-}$ counts, each cycle measured both carbon isotopes simultaneously (12 s), followed by a measurement of $^{12}CH^{-}$ for interference monitoring (1 s). The MRP during the collection of $^{13}C^{-}$ was ~3300 to resolve the interference from $^{12}CH^{-}$ on $^{13}C^{-}$. The contribution of $^{12}CH^{-}$ on $^{13}C^{-}$ was negligible.

Carbon isotope fractionation from dolomite changes as a function of Fe content (Śliwiński et al., 2016b). Multiple in-house dolomite standards with Fe# ranging from 0.00 to ~0.66 were used to build a correction curve using the Hill function to correct for this bias (Figure A2; Figure A3).

We report carbon isotope compositions as per mil deviations from the Pee Dee Belemnite (PDB) using the formula:

$$\delta^{13}C = \left[\frac{(^{13}C/^{12}C)_{sample}}{(^{13}C/^{12}C)_{PDB}} - 1\right] \times 1000 \qquad (3.2)$$

where $(^{13}C/^{12}C)_{PBD} = 0.0112372$. The reported uncertainty considers both the standard error of the cycles in each measurement and the standard deviation of the standard measurements.

3.2.4. Mn-Cr

^{53}Mn-^{53}Cr measurements were measured in dolomite over one analytical session. They were collected with a Hyperion $^{16}O^-$ source with an accelerating voltage of -13 kV and a primary beam current of ~500 pA focused to a diameter of ~5 μm. Each location was presputtered for 300 seconds with a 5x5 μm raster to remove the gold coat and surface contamination, then was measured with 3x3 raster for 50 cycles. Each cycle measured $^{52}Cr^+$ and $^{53}Cr^+$ simultaneously (45 s), followed by a peak jump to $^{55}Mn^+$ (2 s), all of which were measured on EM detectors. The MRP for the collection of $^{53}Cr^+$ was ~6500 to resolve the interference of $^{52}CrH^+$ on $^{53}Cr^+$. Additionally, the EM background noise was measured at the end of the session for ~7 hours, resulting in a noise contribution of ~0.01-0.03 count/s which was subtracted.

Measured $^{55}Mn/^{53}Cr$ ratios were corrected using a relative sensitivity factor (RSF), determined from a synthetic calcite standard, MACS-3NP (Jochum et al., 2019). The RSF is defined here as

$$RSF = \left[\frac{(^{55}Mn^+/^{52}Cr^+)_{SIMS}}{(^{55}Mn^+/^{52}Cr^+)_{TRUE}}\right] \qquad (3.3)$$

and was calculated for this measurement as 0.64±0.05 (2SD). Reference values for the true $^{55}Mn/^{52}Cr$ ratio were used from Jochum et al. (2019), and $^{53}Cr/^{52}Cr$ reference values were used from Papanastassiou (1986).

3.3 Results

3.3.1. Characterization of Dolomite and Magnetite

Dolomite is the only carbonate observed in the Tarda meteorite, predominantly occurring as irregularly shaped grains with embayed margins entrained within the Tarda matrix (Figure 3.1A,B). The dolomite grains are typically less than 20 μm in diameter, however, some large dolomite grains (~50+ μm) are present. Most dolomite grains look similar; however, some dolomite grains contain fewer mineral inclusions (such as magnetite) than others. No obvious zoning was observed from backscatter electron images. Most dolomite crystals are associated with magnetite, either entrained within the dolomite grain (Figure 3.1A), or nearby (Figure 3.1B). Compositionally, the dolomite crystals in Tarda are very similar to the values reported from Tarda and Tagish Lake by Schrader et al. (2024), varying predominantly in Mn+Fe content (Figure 3.2).

Magnetite generally exists as four morphologies in the Tarda meteorite: (1) magnetite plaquettes (Figure 3.1A); (2) magnetite framboids (Figure 3.1A,B); (3) equant/irregular magnetite (Figure 3.1C), and; (4) magnetite spherules (Figure 3.1D). Of these morphologies, magnetite most commonly occurs as framboids, typically as small (<10μm) clusters of sub-micron sized magnetite crystals that vary in crystal definition and packing proximity. The other magnetite morphologies (equant, plaquettes, and spherules), however, typically exist as larger crystals but rarely exceed 10 μm in diameter.

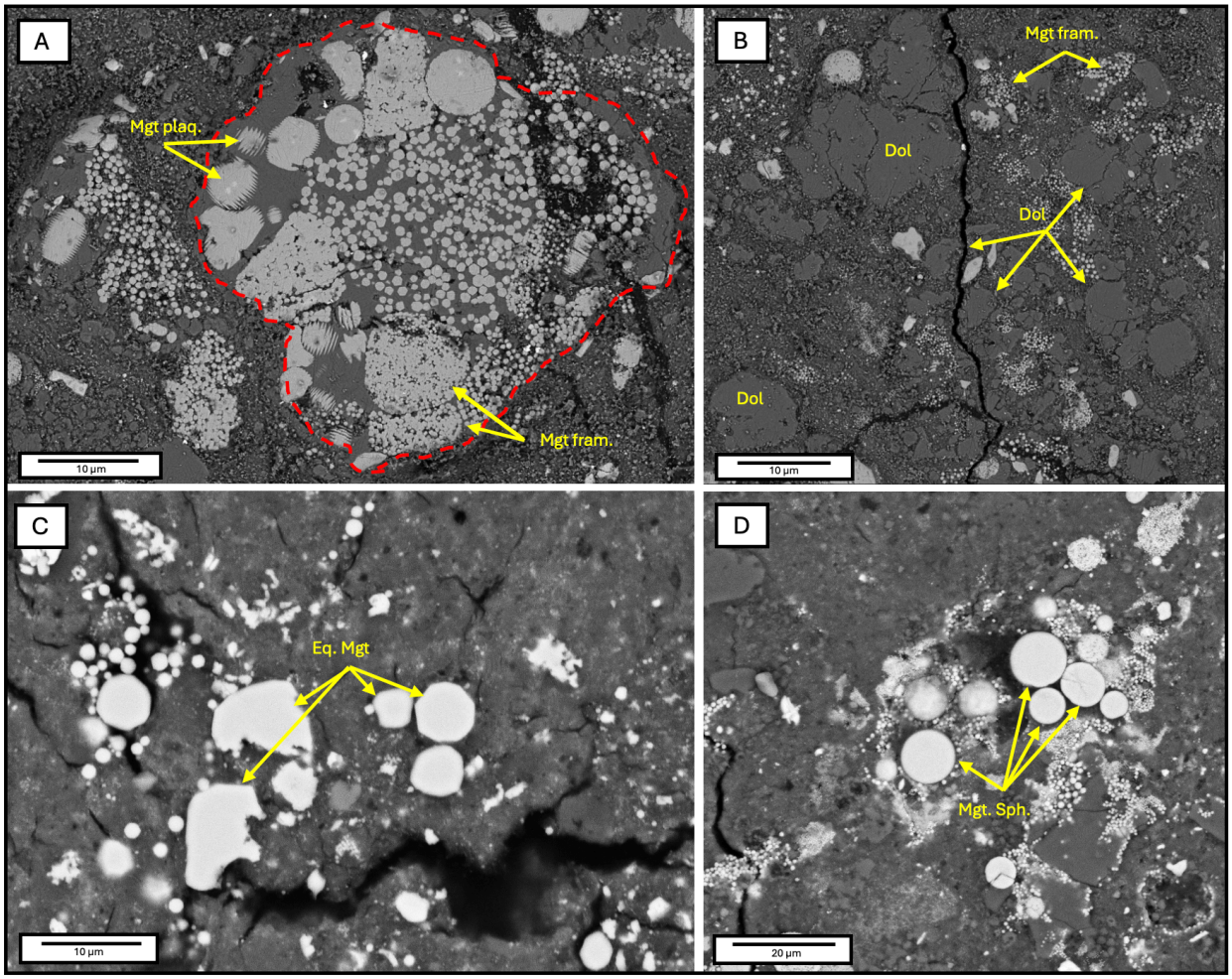

Figure 3.1: Backscatter electron images identifying different occurrences of dolomite and magnetite in the Tarda meteorite. Panel A shows examples of framboidal magnetite (Mgt fram.) and magnetite plaquettes (Mgt plaq.) within a dolomite grain (outlined in red). Panel B shows dolomite grains (Dol), some of which are associated with minor framboidal magnetite. Examples of Equant magnetite (Eq. Mgt) and magnetite spherules (Mgt. Sph.) are shown in Panels C and D respectively.

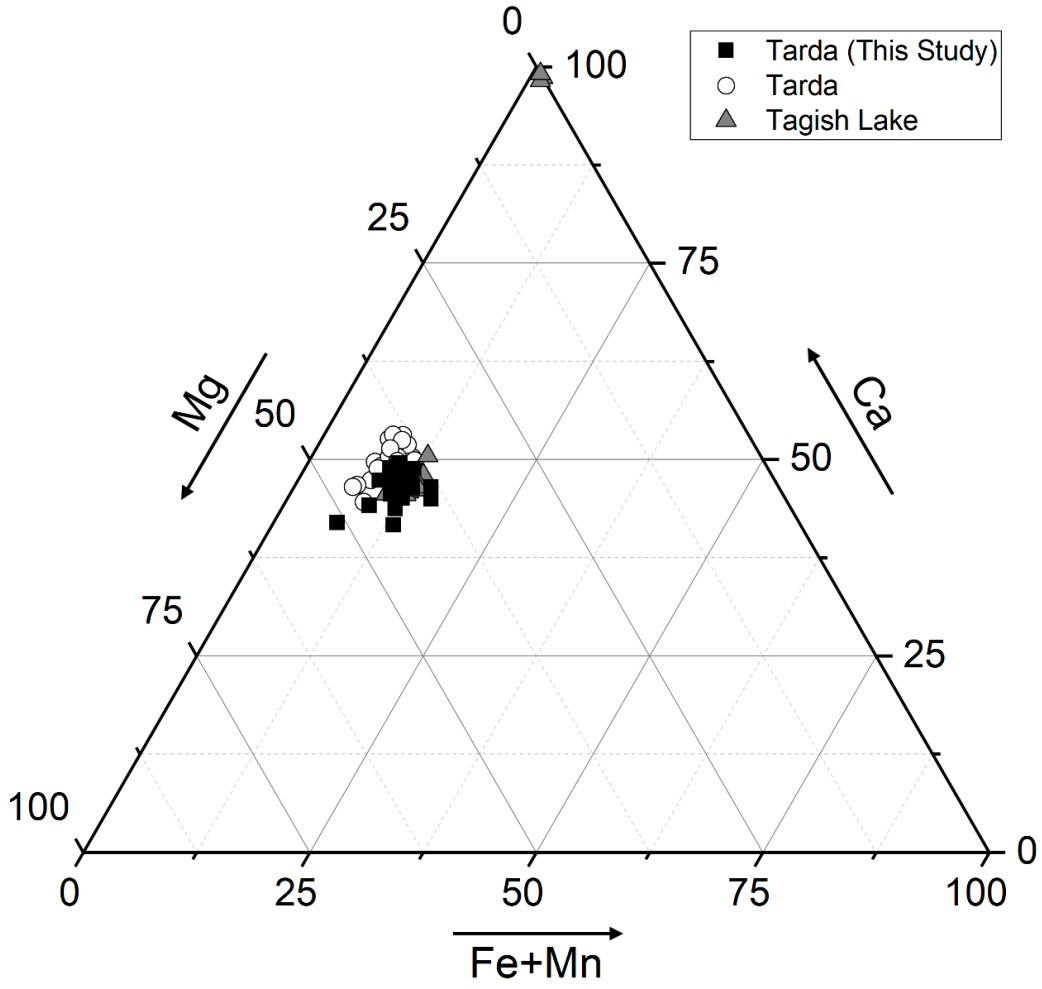

Figure 3.2: Fe+Mn, Mg, and Ca ternary plot of carbonates in Tarda and Tagish Lake. Literature values are from Schrader et al. (2024).

3.3.2. Oxygen Isotopic Composition of Dolomite and Magnetite

Oxygen isotope analyses were conducted on 21 distinct dolomite crystals and 29 distinct magnetite crystals (Table 3.1 and Table 3.2). Dolomite was found to plot close to the terrestrial fractionation line (TFL) with an average $\Delta^{17}O$ (‰) value of 0.15 ± 1.6 (2SD) and records some variation in $\delta^{18}O$ and $\delta^{17}O$ values, ranging from 22.5‰ to 27.8‰ and from 11.5‰ to 15.1‰, respectively (Figure 3.3). These values plot closest to dolomites from CI chondrites and Ryugu but are distinctly lower than them.

Magnetite $\delta^{18}O$ and $\delta^{17}O$ values range from -5.5‰ to 5.8‰ and -0.1‰ to 5.3‰ respectively, plotting consistently above the TFL with an average $\Delta^{17}O$ of 2.4‰ ± 1.7 (2SD), with the highest $\Delta^{17}O$ (‰) value plotting at 4.0 ± 1.5‰ (2σ) well resolved from 0‰ (Figure 3.3).

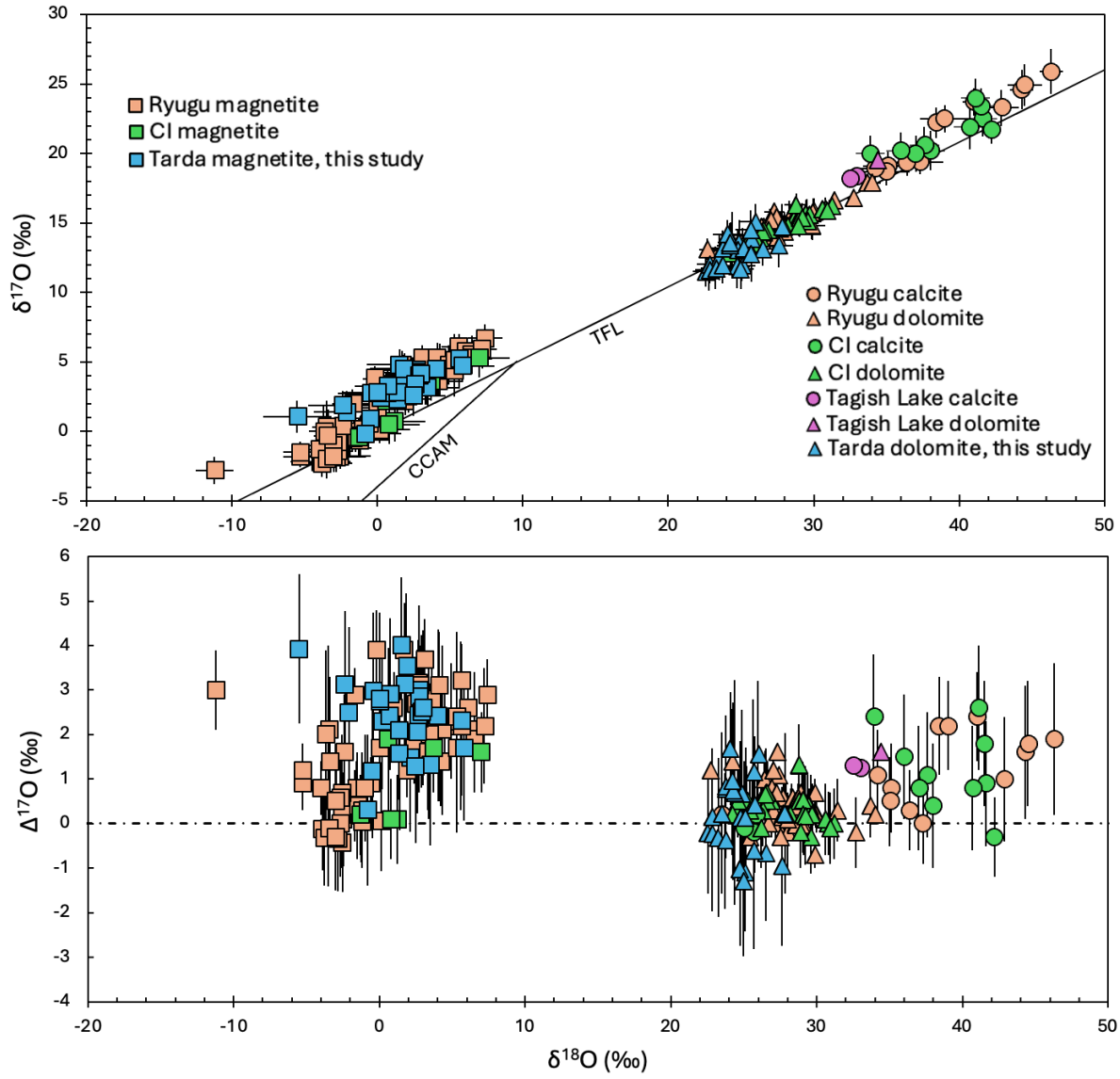

Figure 3.3: Triple-O isotope measurements for magnetite and dolomite in Tarda, compared to magnetite and/or carbonates in Ryugu, CI's, and Tagish Lake from literature (Fujiya et al., 2023; Kita et al., 2024; Leshin et al., 2001; McCain et al., 2023; Nakamura et al., 2022; Piralla et al., 2020; Yokoyama et al., 2023).

3.3.3. Carbon Isotopic Composition of Dolomite

We report carbon isotopes for 15 dolomite crystals (Table 3.1). The majority of the $\delta^{13}C$ analyses plot between 65.2‰ and 72.3‰, however, two points plot distinctly lower at 56.6 ± 4.8‰ and 57.8 ± 3.9‰ (2SD; Figure 3.4). This is generally consistent with carbonates in CI's and Tagish Lake and Ryugu dolomite (Alexander et al., 2015; Fujiya et al., 2019; Grady et al., 2002,1998; McCain et al., 2023).

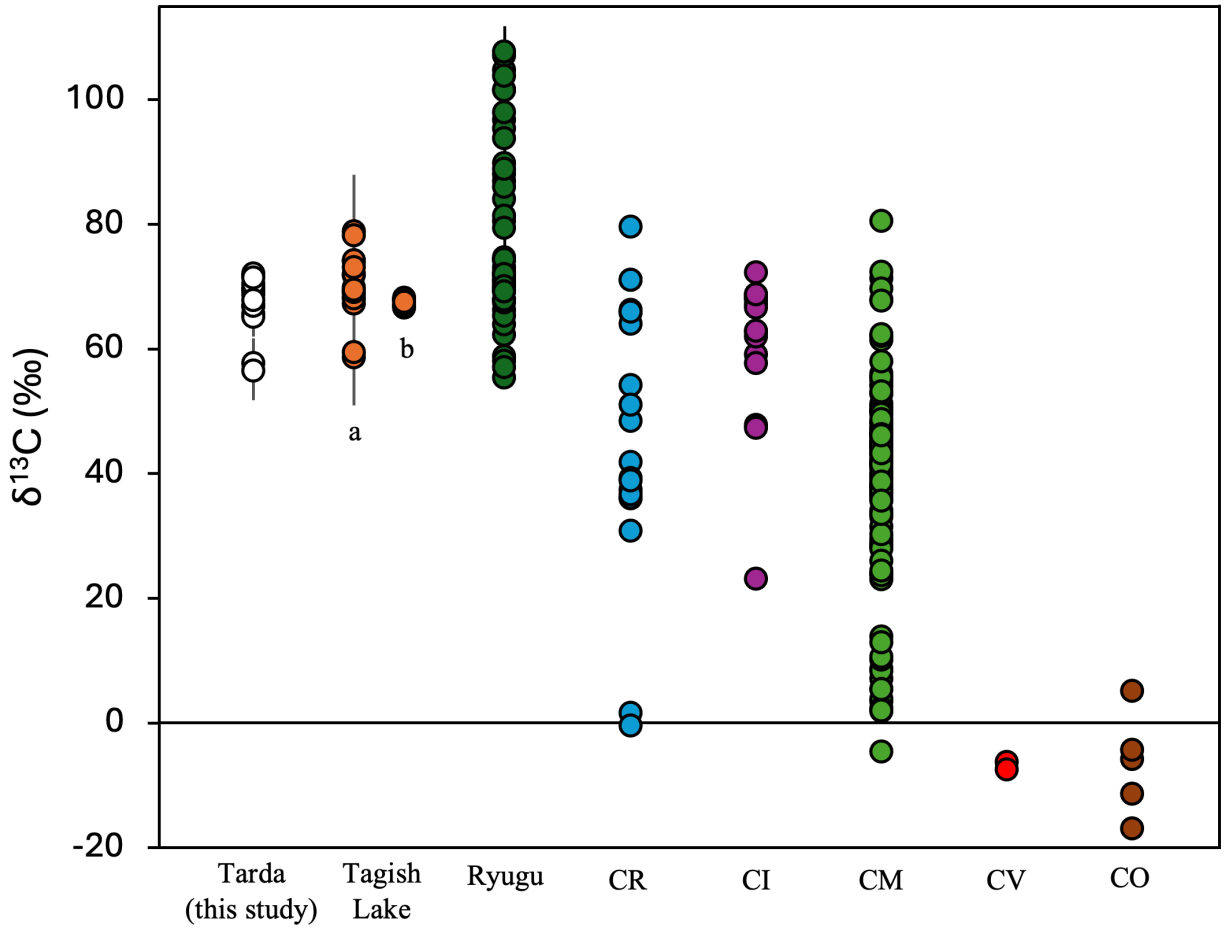

Figure 3.4: $\delta^{13}C$ analyses for 15 dolomite grains from the Tarda meteorite (white circles) compared to published $\delta^{13}C$ carbonate values (Alexander et al., 2015; Fujiya et al., 2019, 2023; Grady et al., 2002, 1988; McCain et al., 2023). Error bars are presented as 2σ, many of which are smaller than the symbols. The "a" and "b" corresponds to Tagish Lake $\delta^{13}C$ carbonate analyses from Fujiya et al. (2019) and Grady et al. (2002) respectively.

3.3.4. Mn-Cr Carbonate Dating

The Mn-Cr isotope system was measured for six dolomite grains in the Tarda meteorite. Each analyzed dolomite contained well resolved ^{53}Cr excesses, with $\delta^{53}Cr$ ranging from 453‰ to ~5900‰. With the exception of one dolomite grain (ID# D6, Table 3.1), the ^{53}Cr excesses correlate linearly with $^{55}Mn/^{52}Cr$ measurements indicating in-situ decay of ^{53}Mn (Figure 3.5). If this linear trend is interpreted as an isochron, the abundance of live ^{53}Mn relative to stable ^{55}Mn [initial ($^{53}Mn/^{55}Mn$) ratio, $(^{53}Mn/^{55}Mn)_0$] at the time when the dolomites formed can be calculated from the isochron slope and corresponds to $(3.08 \pm 0.52) \times 10^{-6}$, with uncertainty expressed as 2σ.

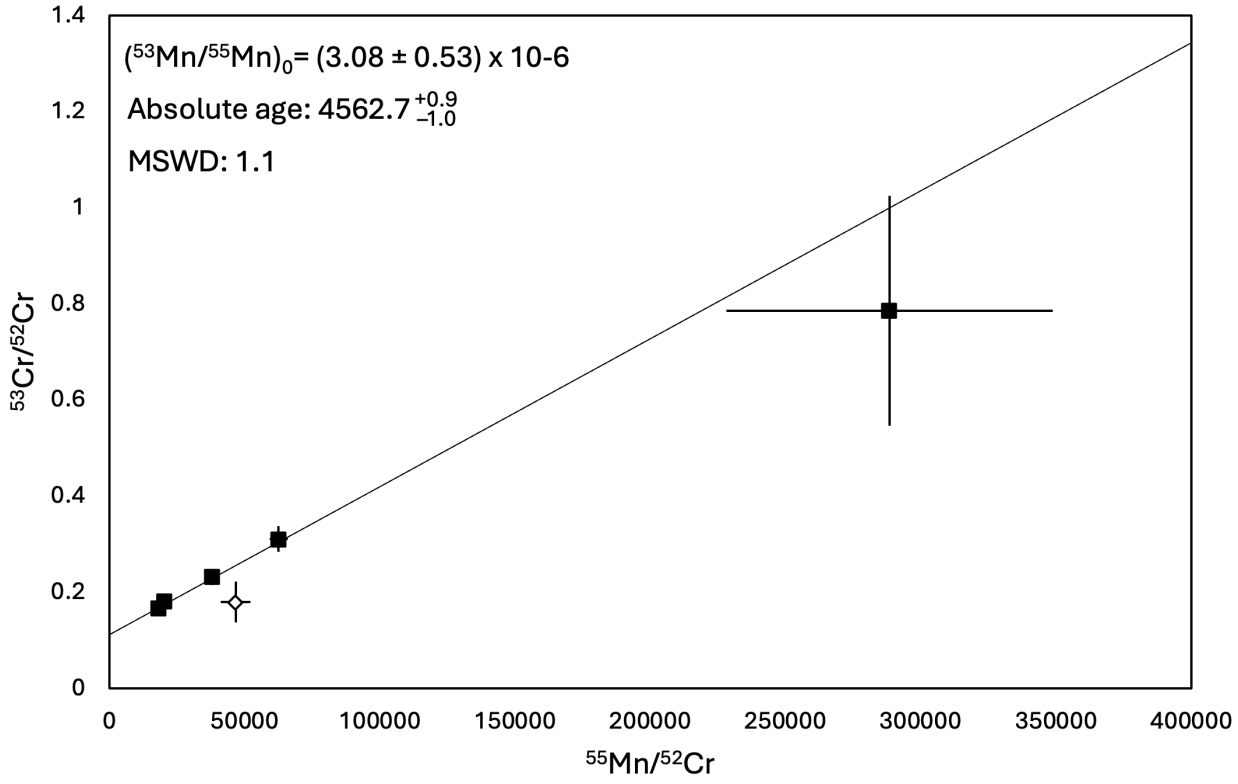

Figure 3.5: Plot of $^{53}Cr/^{52}Cr$ vs $^{55}Mn/^{52}Cr$ for a six dolomite grains in the Tarda meteorite. The data was fitted using model 1 from isoplotR, shown as a solid black line (Vermeesch, 2018). The white diamond marker identifies an outlier (analysis ID D6), which was not used in the trendline/isochron calculation

Table 3.1: Oxygen, carbon, and manganese-chromium isotopic compositions of dolomite crystals in the Tarda meteorite.

Analysis ID	$\delta^{18}O$ (‰)	2σ	$\delta^{17}O$ (‰)	2σ	$\Delta^{17}O$ (‰)	2σ	$\delta^{13}C$ (‰)	2σ	$^{53}Cr/^{52}Cr$	2σ	$\delta^{53}Cr$ (‰)	2σ	$^{55}Mn/^{52}Cr$	2σ
D2	-	-	-	-	-	-	70.0	2.1	0.17996	0.01607	586.2	141.4	20575.7	1154.5
D3	27.8	1.1	14.7	1.7	0.2	1.8	69.6	1.5	0.16489	0.00900	453.3	78.9	18446.5	415.5
D4	24.9	0.9	13.6	1.6	0.7	1.9	69.5	1.3	0.31026	0.02694	1734.6	237.3	62563.2	3361.9
D5	22.5	0.8	11.5	1.1	-0.2	1.4	57.8	3.9	0.78478	0.23907	5916.8	2107.1	288444.8	60250.3
D6	25.1	0.9	11.9	1.1	-1.1	1.3	68.9	1.3	0.17908	0.04238	578.3	373.5	46662.3	5500.0
D7b	22.8	0.9	12.0	1.4	0.1	1.6	71.8	1.4	-	-	-	-	-	-
D10	27.6	1.0	13.4	1.6	-1.0	1.8	67.0	1.7	-	-	-	-	-	-
D11	24.4	1.1	13.4	2.4	0.7	2.5	56.6	4.8	-	-	-	-	-	-
D12	-	-	-	-	-	-	-	-	0.23117	0.01621	1037.5	142.6	38161.5	1165.7
D13	26.0	1.1	15.1	1.3	1.6	1.6	70.5	1.3	-	-	-	-	-	-
D14	26.5	0.8	13.1	1.2	-0.7	1.5	65.7	1.8	-	-	-	-	-	-
D15	23.5	1.0	12.5	1.4	0.2	1.8	-	-	-	-	-	-	-	-
D16	22.8	1.0	11.6	1.5	-0.2	1.7	72.3	1.4	-	-	-	-	-	-
D18	23.8	0.9	13.1	1.2	0.8	1.6	-	-	-	-	-	-	-	-
D19	23.7	0.9	13.2	1.2	0.8	1.6	-	-	-	-	-	-	-	-
D20	24.7	0.9	11.8	1.5	-1.0	1.7	71.5	1.4	-	-	-	-	-	-
D21	25.0	0.9	11.7	1.5	-1.3	1.7	65.2	3.2	-	-	-	-	-	-
D23	23.3	1.0	11.8	1.5	-0.3	1.8	67.1	2.5	-	-	-	-	-	-
D24	25.8	1.0	13.8	1.3	0.4	1.5	67.9	1.6	-	-	-	-	-	-
D25	23.7	0.8	11.9	1.3	-0.4	1.5	-	-	-	-	-	-	-	-
DM1D1	24.8	1.0	13.0	1.6	0.1	1.7	-	-	-	-	-	-	-	-
DM1D2	25.7	1.0	14.5	1.4	1.2	1.6	-	-	-	-	-	-	-	-
DM1D3	25.1	1.0	13.2	1.4	0.1	1.6	-	-	-	-	-	-	-	-
DM1D4	25.2	0.8	13.9	1.7	0.7	2.0	-	-	-	-	-	-	-	-
DM2D1	24.1	1.0	14.2	1.0	1.7	1.3	-	-	-	-	-	-	-	-
DM3D1	25.7	0.9	12.7	2.0	-0.6	2.2	-	-	-	-	-	-	-	-
DM3D2	24.2	0.8	13.6	1.4	1.0	1.6	-	-	-	-	-	-	-	-

Table 3.2: Oxygen isotopes compositions for 29 distinct magnetite crystals in the Tarda meteorite.

Analysis ID	$\delta^{18}O$ (‰)	2σ	$\delta^{17}O$ (‰)	2σ	$\Delta^{17}O$ (‰)	2σ
M1	2.7	2.6	4.4	1.4	3.0	1.9
M8	2.1	2.3	2.6	1.2	1.5	1.7
M10	1.4	2.4	2.3	1.5	1.6	1.7
M11	-2.1	2.3	1.4	1.5	2.5	1.9
M13A	5.6	2.2	5.3	1.2	2.3	1.7
M16	-0.5	2.4	0.9	0.9	1.2	1.5
M17A	2.7	2.3	4.2	1.4	2.8	1.7
M18	1.7	2.2	4.0	1.5	3.1	1.8
M19M1	4.0	2.3	4.5	1.3	2.4	1.9
M20	0.2	2.2	2.4	1.0	2.3	1.5
M21	2.7	2.2	3.8	1.2	2.4	1.7
M22	2.7	2.4	3.8	1.2	2.4	1.6
M24	0.6	2.3	2.7	0.9	2.4	1.5
M25	-5.5	2.3	1.1	1.2	3.9	1.7
M27	-0.4	2.3	2.8	1.1	3.0	1.8
M28	1.4	2.3	2.8	0.9	2.1	1.5
M28M2	1.5	2.3	4.8	1.1	4.0	1.5
M31	3.5	2.2	3.1	1.4	1.3	1.8
M32	0.0	2.3	2.8	0.9	2.7	1.6
M33	1.9	2.3	4.5	1.1	3.5	1.6
M34A	2.9	2.2	4.0	1.3	2.5	1.7
DM1M1	0.7	2.3	3.3	1.3	2.9	1.7
DM1M2	-0.8	2.5	-0.1	1.1	0.3	1.7
DM2M1	3.0	2.3	4.2	1.2	2.6	1.7
DM2M2	0.0	2.4	2.8	1.3	2.8	1.9
DM2M3	-2.4	2.4	1.9	1.0	3.1	1.7
DM3M1	5.8	2.2	4.7	1.2	1.7	1.6
DM3M2	2.6	2.2	3.4	1.5	2.1	1.8
DM3M3	2.5	2.2	2.6	1.4	1.3	1.7

3.4 Discussion

3.4.1. Terrestrial Weathering

The dolomite crystals analyzed in this study have O-isotopic signatures that plot close to the TFL; thus, we must ensure that the measured O-isotope signatures are extraterrestrial. It is unlikely that the dolomite analyzed in this study are terrestrial contamination products for several reasons: (1) The Tarda meteorite was recovered the day after it was seen to fall, allowing very limited time for terrestrial crystal growth or modification (Gattacceca et al., 2021); (2) dolomite is extremely difficult to produce in aqueous environments under ambient pressure and temperature (e.g. Cai et al., 2021; Land, 1998; Warren, 2000); (3) Tarda dolomite displays a systematic enrichment of $\delta^{13}C$ consistent with other meteorite groups (Figure 3.4) and; (4) the systematic excesses of ^{53}Cr within the Tarda dolomite implies the dolomite crystals are ancient, forming while the short-lived radionuclide ^{53}Mn was still alive (Figure 3.5).

3.4.2. Correlations Between Morphologies and Isotope Ratios

Carbonaceous chondrites that have undergone aqueous alteration are thought to originate from parent asteroids that formed by accreting two primary components: (1) anhydrous minerals characterized by low $^{18}O/^{16}O$ and low $\Delta^{17}O$, and; (2) water ice with high $^{18}O/^{16}O$ and high $\Delta^{17}O$ (e.g. Clayton & Mayeda, 1984; Ireland et al., 2020; Jilly-Rehak et al., 2017a; Rowe et al., 1994; Suttle et al., 2021; Yurimoto et al., 2008). These components are believed to have distinct nebular sources, distinguishable by their oxygen isotope compositions (e.g. Clayton & Mayeda, 1984). The earliest minerals to precipitate from the isotopically heavy water are expected to inherit the heaviest oxygen isotope signatures. In contrast, minerals that form later, following the mixture of the two components, should show progressively lighter and lower $\Delta^{17}O$ oxygen isotope signatures, potentially allowing the evolution of the system and the crystallization sequence to be tracked (e.g.,

Bland et al., 2009; Clayton & Mayeda, 1984; Rowe et al., 1994; Tyra et al., 2016). Here, we investigate the morphology of the analyzed dolomite and magnetite and attempt to identify any potential trends to the observed isotopic data present in Table 3.1 and Table 3.2.

As presented in section 3.3.1, nearly all instances of dolomite occur as irregular and embayed crystals. Some, however, look 'cleaner' with fewer inclusions (e.g. Figure A4C vs Figure A4D), but this appears to have no systematic influence on the resultant triple-O, C, or Mn-Cr isotope ratios.

Magnetite in Tarda, however, has numerous morphologies consisting of framboids, plaquettes, spherules, and irregular/equant grains. These morphologies have also been found in Ryugu samples, Bennu samples, Tagish Lake, hydrated fine-grained Antarctic micrometeorites, CI, CM, and CR chondrites (Chan et al., 2016; Dobrică et al., 2023, 2019; Hua & Buseck, 1998; Kita et al., 2024; Lauretta et al., 2024; McCain et al., 2023; Rubin & Ma, 2017; Zolensky et al., 2002). At least on Ryugu, each magnetite morphology is likely produced in a crystallization sequence governed by changing fluid conditions, in the order of spherulitic, plaquette/framboidal, and finally equant/elongated (Tsuchiyama et al., 2022).

Recent analyses of Ryugu samples have additionally revealed nanoscale features associated with magnetite spherulites, including radiating fibers, nanometric pores, and lattice dislocations, indicating rapid growth of this morphology under nonequilibrium aqueous conditions (Dobrică et al. 2023). SIMS studies of spherulitic and spherical magnetite in Ryugu found porous crater textures correlated with higher $\delta^{18}O$ & $\Delta^{17}O$ values (implying earlier formation) and greater abundances of Si and water, compared to the results from equant magnetite which exhibited smooth crater textures (Aléon et al., 2024; Kita et al., 2024; Yokoyama et al., 2022). These porous crater textures are attributed to heterogeneous sputtering of the magnetite crystal, caused by the

presence of silicates and water-rich amorphous nanometer-sized pores (Aléon et al., 2024; Dobrică et al., 2023; Kita et al., 2024).

In Tarda, most of our analyzed magnetite crystals were equant (n=20), with lesser plaquettes (n=7), spherules (n=1), and framboids (n=1). We did not observe any obvious radiating features or poorly defined crystal edges in the analyzed magnetite crystals using SEM, which is typically diagnostic for spherulites (Dobrică et al., 2023; Kita et al., 2024).

The average $\Delta^{17}O$ results for each magnetite morphology is unresolvable between their mutual uncertainties which makes assessing precipitation order challenging. However, there usually exists a correlation between $\delta^{18}O$ and $\Delta^{17}O$ since increased mixing between water and anhydrous rock is expected to lower both values. Despite only one measurement, the analyzed spherule contains the highest $\delta^{18}O$ suggesting it precipitated earlier than the other morphologies. This is consistent with the findings of Tsuchiyama et al. (2022) in Ryugu samples.

3.4.3. Isotope Thermometry

When precipitating from water, magnetite and dolomite each exhibit distinct oxygen isotope fractionation behaviors, both of which additionally vary as a function of temperature (e.g. Zheng, 1991, 1999, 2011). Theoretically determined fractionation factors describe these relationships, with dolomite being more sensitive to temperatures changes than magnetite (Figure 3.6; Eq. 3.4, 3.5; Zheng, 1991, 2011). For dolomite, fractionation relative to water is greatest at 0˚C, fractionating at +40‰ and decreases exponentially with increasing temperature (Figure 3.6; Eq. 3.4; Zheng, 2011). As temperatures increase for the magnetite-water system, however, $\delta^{18}O$ in magnetite fractionates from 0 to approximately -8‰ relative to water, plateauing at temperatures around ~200˚C (Figure 3.6; Eq. 3.5; Zheng, 1991). The difference between Eq. 3.4 and Eq. 3.5 produces a dolomite-magnetite fractionation curve that assumes both minerals co-precipitate from

the same aqueous fluid in equilibrium (Eq. 3.6). If so, the temperature of the system can be calculated (Jilly-Rehak et al., 2017a; Eq. 3.6).

$$\text{Dolomite} - \text{water: } 10^3 \ln a = \frac{4.06 \times 10^6}{T^2} - \frac{4.65 \times 10^3}{T} + 1.71 \qquad (3.4)$$

$$\text{Magnetite} - \text{water: } 10^3 \ln a = \frac{3.02 \times 10^6}{T^2} - \frac{12.00 \times 10^3}{T} + 3.31 \qquad (3.5)$$

$$\text{Dolomite} - \text{magnetite: } 10^3 \ln a = \frac{1.04 \times 10^6}{T^2} - \frac{7.35 \times 10^3}{T} - 1.60 \qquad (3.6)$$

Dolomite and magnetite are frequently associated in Tarda, however, it is difficult to determine whether they grew from the same fluid. Using the same scheme as Jilly-Rehak et al. (2017a), we will assume local fluid co-precipitation of dolomite and magnetite has occurred if: (1) Both secondary minerals occur in the same clast or lithology; (2) both minerals are frequently in contact with no obvious indication that one predates the other, and; (3) both minerals lie on the same oxygen 3-isotope mass-dependent fractionation line (unresolvable $\Delta^{17}O$).

One dolomite-magnetite assemblage satisfied these conditions, enabling oxygen thermometry to be calculated. Multiple analyses were collected from this assemblage; two from magnetite and four from dolomite (Figure 3.7). While all four dolomites have $\Delta^{17}O$ values within uncertainty of both magnetite in this assemblage (Table A1), if the crystallization sequence of magnetite morphologies in Tarda is indeed similar to Ryugu (section 3.4.2), then the equant magnetite (ID: DM1M2) likely formed closest to dolomite in the crystallization sequence, so was selected (Figure

3.7). The dolomite analysis (ID: DM1D2) was selected owing to its close proximity to the equant magnetite (ID: DM1M2; Figure 3.7).

Oxygen isotope thermometry from these two analyses results in a system temperature of $90.4\ ^{+29.9}_{-25.0}$ ˚C, with uncertainties (2σ) reflecting the uncertainty of the $\delta^{18}O$ values for the dolomite and magnetite used in the calculation (Figure 3.6). This temperature generally agrees with previous estimates for both Tarda and Tagish Lake. Petrographic observations by Blinova et al. (2014) and Zolensky et al. (2002) estimated peak metamorphic temperatures in Tagish Lake to be ≥150˚C and ≥300˚C respectively, although both found localized regions that likely experienced less intense alteration. Furthermore, Schrader et al. (2024) reported that sulfides equilibrated between 100-135˚C for both Tarda and Tagish Lake using pyrrhotite-pentlandite geothermometry, suggesting a minimum peak alteration temperature for both meteorites.

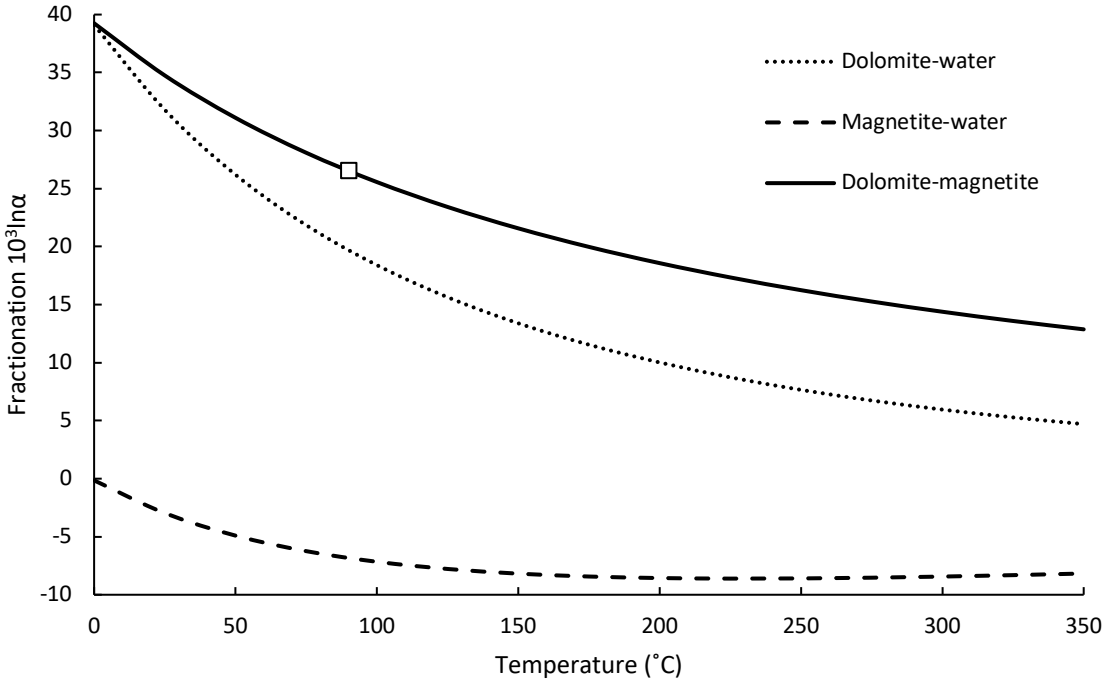

Figure 3.6: Diagram displaying fractionation curves for the dolomite-water system (dotted line) and the magnetite water system (dashed line) as a function of temperature. Fractionation is presented as $10^3 \ln\alpha$, where $\alpha = (^{18}O/^{16}O_{mineral})/(^{18}O/^{16}O_{water})$. The square marker displays the temperature of the co-precipitating pair (Figure 3.7).

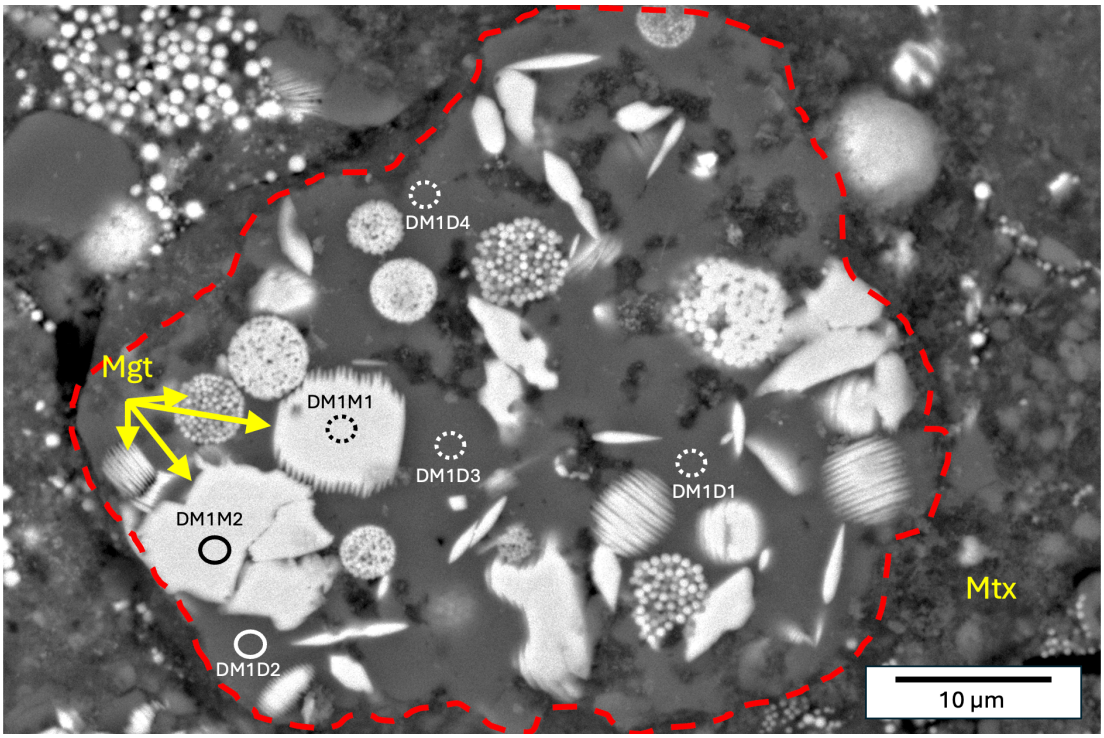

Figure 3.7: BSE SEM image of a large dolomite grain (outlined in red) with many occurrences of magnetite entrained within (examples labeled Mgt). Circles show areas where SIMS measurements were collected, each corresponding to an analysis ID (Table 3.1; Table 3.2). Solid circles show the analysis locations for SIMS measurements that were used for isotope thermometry. Surrounding matrix is labeled Mtx.

3.4.4. Mn-Cr

3.4.4.1. Isochron Chronological Significance

When discussing the age of dolomite based on ^{53}Cr excesses correlated with $^{55}Mn/^{52}Cr$, it is first important to discuss whether this correlation has chronological significance. Indeed, it is possible that a similar correlation could arise if the analyzed dolomite was contaminated with a Cr-rich fluid, in which case a linear correlation between $\delta^{53}Cr$ and $1/^{52}Cr$ (nA/cps) would also be expected. Our data shows the $\delta^{53}Cr$ and $1/^{52}Cr$ are more poorly correlated (MSWD of 3.4) than the ^{53}Cr excesses correlated with $^{55}Mn/^{52}Cr$ (MSWD of 1.1), supporting the analysis has chronological significance (Figure 3.8). Furthermore, we observe significant variation in both total ^{55}Mn contents (Figure 3.8) and Mn/Cr ratios (Figure 3.5) across the dolomite grains suggesting that they

formed in chemically distinct microenvironments which further support a chronological significance.

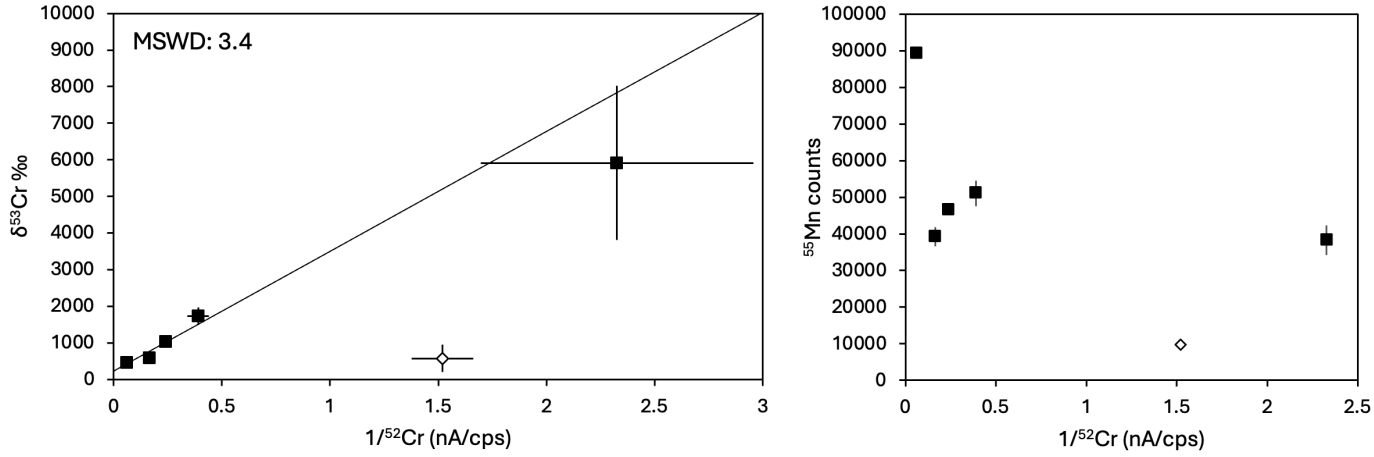

Figure 3.8: Plots of $\delta^{53}Cr$ vs $1/^{52}Cr$ and ^{55}Mn vs $1/^{52}Cr$ for each analyzed dolomite. The white diamond marker identifies the outlier (Analysis ID: D6) that was not used in the age calculation in results, nor the trendline or MSWD calculated here. The $1/^{52}Cr$ values are listed as average counts per cycle normalized to beam current, whereas the ^{55}Mn values are listed as average counts normalized to the cycles per run. The data for the left plot was fitted using model 1 from isoplotR (Vermeesch, 2018).

3.4.4.2. Mn-Cr Age Adjustment

Unlike other measured isotopic systems measured here, SIMS analysis of the Mn-Cr system requires two different elements to be sputtered from the sample and detected. This introduces a complication, since the relative ionization rate of each element sputtered from the target mineral varies depending on the elemental composition of the mineral matrix (Doyle et al., 2016; McCain et al., 2020; Sugawara et al., 2024; Sugiura et al., 2010). This is corrected for using the relative sensitivity factor (RSF; Eq. 3.3) although some studies use the inverse (e.g. McCain et al., 2020, 2023). Best practice involves calculating the RSF by matrix-matching the target mineral to an equivalent mineral standard that contains similar abundances of the isotope system of interest. A unique problem is presented for the Mn-Cr system in carbonates, however, since natural carbonates rarely contain measurable quantities of Cr, rendering natural standards unviable (Sugawara et al.,

2024). While synthetic Cr-bearing calcite standards have been manufactured and adopted for SIMS use, manufacturing Cr-bearing homogenous dolomite standards remain difficult (Jilly-Rehak et al., 2014; Land, 1998; Sugiura et al., 2010; Warren, 2000). Thus, many studies that analyze the Mn-Cr system in dolomite, including this one, have been forced to use the RSF values with a non-matrix-matched calcite standard, likely biasing the results (Bischoff et al., 2021; Fujiya et al., 2013; Jilly-Rehak et al., 2017b, 2014; Nakamura et al., 2022; Visser et al., 2020; Yokoyama et al., 2023).

Recently, however, Mn- and Cr-bearing dolomite standards have been synthesized through two methods: (1) Shallow ^{52}Cr-implantation into natural dolomite (McCain et al., 2023; Steele et al., 2017) and; (2) solid-state transformation of amorphous calcium magnesium carbonate (Sugawara et al., 2022). While both methods are improvements, the ^{52}Cr-implantation method was used to obtain their RSF using depth-profiling measurements from shallow implants, while unknown measurements were done with spot analysis that collect samples over much deeper depths. Since RSF is known to vary as a function of depth during SIMS measurements, the RSF reported by McCain et al., (2023) while investigating the Mn-Cr system of dolomite in Ryugu, reflects the shallow standard measurements used in their RSF calculation and thus are not applicable to the spot measurements used for unknowns (Sugawara et al., 2024; Sugiura et al., 2010). This issue is avoided when using the solid-state transformation method to produce a dolomite standard, however, the Cr abundance for these standards is higher than natural samples which may have a minor effect on RSF. Nonetheless, Sugawara et al., (2024) found this standard improved the RSF from ~0.7 to ~0.8-0.9. Additionally, they analyzed the $(^{53}Mn/^{55}Mn)_0$ of the same Ivuna dolomite grain that Yokoyama et al. (2022) analyzed with a calcite standard, producing matrix-matched results that were increased by 26 ± 19%. Since our measurement protocol is similar to that of Sugawara et al. (2024), we may use this conversion factor to adjust our non-

matrix-matched ($^{53}Mn/^{55}Mn)_0$ value to likely produce a more accurate age. Applying this correction to the Tarda dolomite analyzed here, the new ($^{53}Mn/^{55}Mn)_0$ value is $3.88 \pm 0.79 \times 10^{-6}$. The attached uncertainty (2σ) was calculated by propagating the uncertainty of the original ($^{53}Mn/^{55}Mn)_0$ for Tarda and the uncertainty associated with the conversion factor.

3.4.4.3. Age of Tarda Dolomite Compared to Literature Carbonates

The Mn-Cr system is a relative dating technique which records the decay time between the initial (assumed homogeneous) solar system $^{53}Mn/^{55}Mn$ ratio, and the ($^{53}Mn/^{55}Mn)_0$ of the minerals that precipitated later. In order to calculate accurate absolute ages using the Mn-Cr system, the measured ($^{53}Mn/^{55}Mn)_0$ must be anchored to another object where both the ($^{53}Mn/^{55}Mn)_0$ and absolute age are known. This is measured using Eq. 3.7:

$$\Delta T_{1-2} = \frac{1}{\lambda} ln[(^{53}Mn/^{55}Mn)_1/(^{53}Mn/^{55}Mn)_2] \qquad (3.7)$$

where λ = 3.7 Ma, $(^{53}Mn/^{55}Mn)_1$ is the measurement of the unknown, $(^{53}Mn/^{55}Mn)_2$ is the measurement for the time anchor, and ΔT_{1-2} is the relative time difference between the unknown and the time anchor. We have anchored our measurements, and all compared literature values to the extensively studied quenched angrite named D'Orbigny, where the ($^{53}Mn/^{55}Mn)_0$ was measured as $(3.47 \pm 0.12) \times 10^{-6}$ and corresponds to a Pb-Pb age of 4563.37 Ma (Brennecka & Wadhwa, 2012; McKibbin et al., 2015). A detailed discussion for why D'Orbigny was chosen can be found in Jilly-Rehak et al. (2017b).

In our results, we use a non-matrix-matched standard to report the ($^{53}Mn/^{55}Mn)_0$ of Tarda dolomite to be $(3.08 \pm 0.52) \times 10^{-6}$, corresponding to an age of $4562.7^{+0.9}_{-1.0}$ with an RSF of 0.64±0.05. However, in the previous section, the RSF adjustment from matrix-matched dolomite standards in Sugawara et al. (2024) produces an updated ($^{53}Mn/^{55}Mn)_0$ of $(3.88 \pm 0.79) \times 10^{-6}$, yielding an updated age of $4564.0^{+1.0}_{-1.2}$. While this recalculated age for the dolomites in Tarda may

indeed be closer to the true precipitation age, we note that experimental procedures and instruments used may vary significantly between previous studies, and thus, the conversion factor identified by Sugawara et al. (2024) may not be applicable as a blanket correction for all studies. Thus, it is most useful to compare the original dolomite precipitation age in Tarda with the other reported carbonate precipitation ages from literature.

The absolute age of the dolomites in the Tarda meteorite is in excellent agreement with the ages of dolomites from Tagish Lake, and CIs, and dolomites and calcites from CM and CR group chondrites, which generally fall between 4562 and 4565 Ma (approximately 2 to 5 million years after CAIs formed; Figure 3.9). This indicates that the Tarda parent body underwent aqueous alteration within the same timeframe as most other water-rich planetesimals. This synchronization was likely driven by radiogenic heating from the decay of short-lived ^{26}Al, which would have driven internal melting and liquid water availability only if these bodies accreted at similar times while sufficient ^{26}Al remained (Cohen & Coker, 2000).

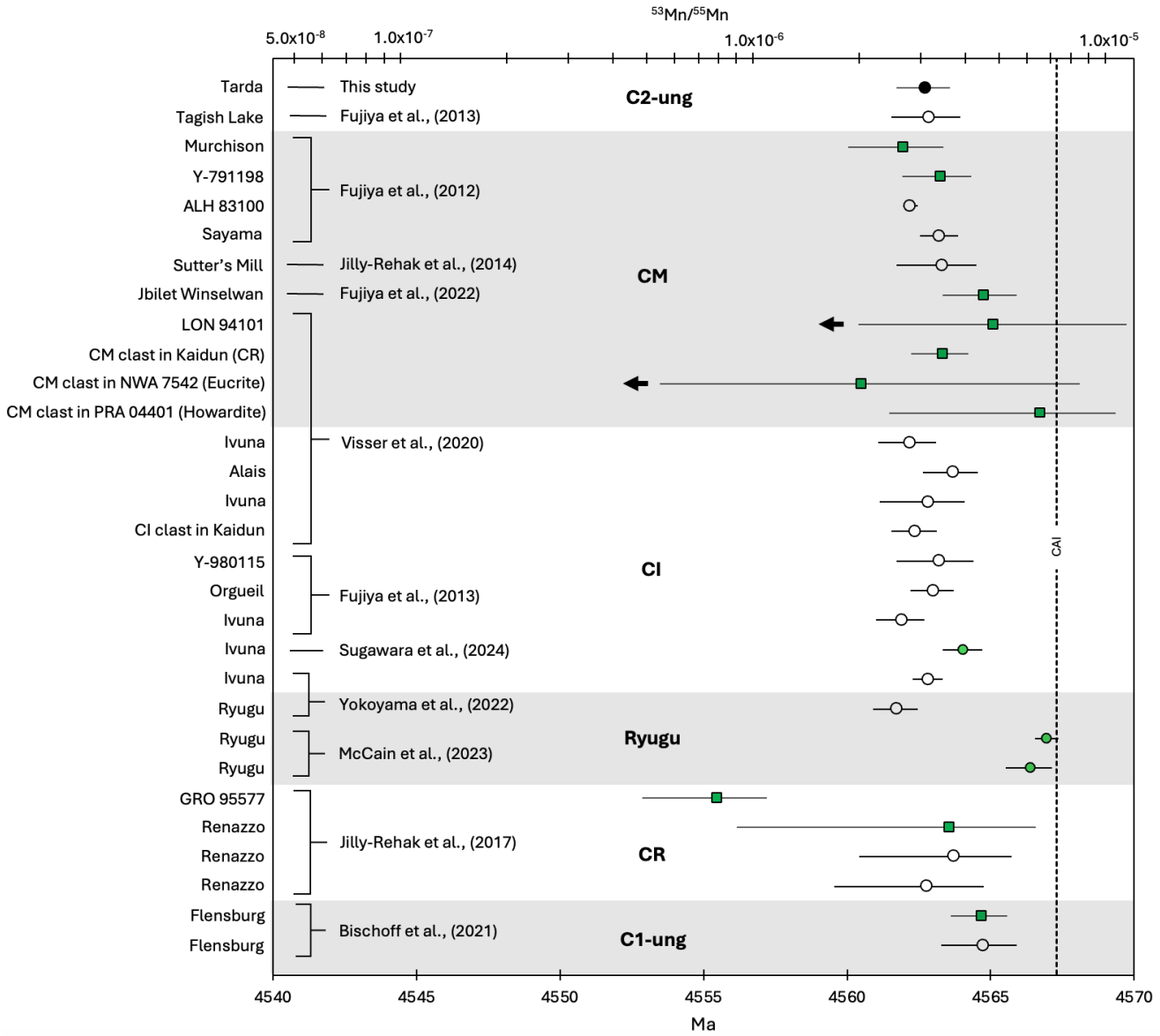

Figure 3.9: Mn-Cr ages of dolomite in Tarda (black markers) compared to literature values. All values were anchored to the D'Orbigny angrite. The CAI age at 4567.3 Ma (Connelly et al., 2012) is shown for comparison. Ages produced from dolomite grains are displayed as circular markers, while ages produced from calcite grains have square markers. Markers filled in green highlight studies that used a matrix-matched standard.

3.4.4.4. Why does analysis D6 fall of the isochron?

Of the six dolomites measured for Mn-Cr age dating, only dolomite D6 (Figure A6) deviates from the interpreted isochron in Figure 3.5 due to lower $\delta^{53}Cr$ excesses than expected for the system (Figure 3.5; Table 3.1). This dolomite, however, has some notable geochemical differences

when compared to the other dolomite crystals analyzed for Mn-Cr, which provide context for its deviation. The $\Delta^{17}O$ value for dolomite D6 was measured as –1.1 ± 1.3‰, lower than the average $\Delta^{17}O$ of 0.23‰ (n=3) for the other dolomites that were analyzed for Mn-Cr systematics (n=5). Although the values overlap within error, this difference may suggest that dolomite D6 precipitated from a more evolved and potentially later fluid. EDS analysis further reveals that dolomite D6 has a higher Mg content than all other dolomites analyzed in this study, with lower Mn, Fe, and Ca abundances. Together, these data suggests that dolomite D6 may have experienced a distinct alteration history compared to the others. We propose two scenarios to best explain this data:

1. A later aqueous alteration event occurred in which a low-$\Delta^{17}O$, Mg-rich fluid partially altered dolomite D6. If this process selectively leached Cr from the system, the ^{55}Mn-^{52}Cr ratio would have increased and shifted off the isochron.
2. Dolomite D6 formed from a later aqueous alteration event from an Mg-rich, Mn-depleted fluid, when there was less live ^{53}Mn available to decay. This would have lowered the final ^{53}Cr inventory of the crystal, deviating from the original isochron.

Due to a lack of apparent zoning and alteration textures present in dolomite D6 (Figure A6) we believe that the second scenario best explains this data.

Here we attempt to provide an age for dolomite D6. Despite only having one dolomite available to plot, if we assume the initial $^{53}Cr/^{52}Cr$ for this dolomite is consistent with the previous dolomites, we can force the trendline through the same Y intercept that was calculated in Figure 3.5. This assumption is likely somewhat incorrect as dolomite D6 would have formed later, raising the initial $^{53}Cr/^{52}Cr$ of the crystal. Thus, the calculated trendline from the Y-intercept to dolomite D6 will likely be steeper than it would be otherwise therefore producing a slightly older age. Nonetheless, if this trendline is indeed an isochron, it may well serve as an upper limit to the true age of this

dolomite. The slope of this trendline corresponds to a $(^{53}Mn/^{55}Mn)_0$ value of $1.5 \pm 1.1 \times 10^{-6}$, corresponding to an age of $4558.7^{+3.0}_{-7.6}$ Ma anchored to the D'Orbigny angrite. If this age is real, this suggests that dolomite-forming fluid conditions may have extended for several millions of years, either as a single prolonged fluid event or as several episodes, possibly resulting from impact events. Furthermore, the lack of other young dolomite grains measured suggests that the fluid from which this dolomite precipitated may have been highly localized.

3.4.5. Isotope Constraints on Fluid Conditions

Multiple previous studies have identified significant similarities between Tarda and Tagish Lake, including petrology and modal abundances, elemental and isotopic signatures (such as bulk Cr and Ti isotopes, bulk C, H, and N), reflectance spectra, and paleomagnetic remanence (etc), ultimately suggesting a genetic relationship between the two meteorites (Bates et al., 2024; Marrocchi et al., 2021; Schrader et al., 2024). Thus, it is likely that Tarda and Tagish Lake source the same parent body, or at least, formed in the same nebular neighborhood from similar initial components. Despite widespread similarities, both meteorites appear to have different aqueous alteration histories. One obvious difference is that Tagish Lake is brecciated and contains at least a carbonate-poor and carbonate-rich lithology, with multiple carbonate mineral species including calcite, dolomite, and siderite, possibly reflecting multiple records of alteration within the same sample (Blinova et al., 2014; Brown et al., 2000; Grady et al., 2002; Hildebrand et al., 2006; Izawa et al., 2010a; Nakamura et al., 2003; Schrader et al., 2024; Zolensky et al., 2002). On the other hand, we have observed only one lithology in Tarda, with dolomite as the only carbonate. The abundance of phyllosilicates is similar between the two meteorites, however, leading Schrader et al. (2024) to suggest that Tarda and Tagish Lake may have had been similarly aqueously altered but were altered under different fluid compositions (Bates et al., 2024; Schrader et al., 2024). Here,

we compare O- and C-isotope systematics between Tarda and Tagish Lake to evaluate the aqueous alteration histories of the two meteorites.

3.4.5.1. Oxygen Isotopes

As mentioned in section 3.4.2, the progressive mixing of low $^{18}O/^{16}O$ and low $\Delta^{17}O$ anhydrous rock with high $^{18}O/^{16}O$ and high $\Delta^{17}O$ water will continually modify the oxygen isotope ratio of the fluid from which the minerals will precipitate from and inherit, possible allowing the evolution of the fluid to be tracked (e.g. Rowe et al., 1994). Whether this mixing has occurred in an open system driven by kilometer scale fluid migration (Young, 2001; Young et al., 1999), a closed system involving fluid-rock interaction confined to the millimeter scale (Clayton & Mayeda, 1984), or under a system where rock and water move together on an unlithified parent body remains debated, although most evidence (in particular for the CM chondrites) appears to favour a closed system due to a general lack of observed permeability and fluid flow features in carbonaceous chondrites (Bland et al., 2009; Fujiya, 2018; Jilly-Rehak et al., 2017a). We will discuss this section assuming a closed system since no evidence of extensive permeability such as veining or extensive fracture networks were observed.

Under a two-component closed system, the oxygen isotopic composition of carbonates and magnetite in carbonaceous chondrites are influenced by:

(i) The initial O-isotope composition of the water-ice and rock.

(ii) The degree of local mixing between the water-ice and rock prior to the mineral formation, depending on temperature and the amount of water and rock in the system (W/R ratio).

(iii) O-isotope fractionation factors of the forming mineral relative to water (section 3.4.3).

Since Tarda and Tagish Lake likely source the same parent body or, at least, form from the same nebular neighborhood from similar components, we assume that the initial O-isotopic composition of the anhydrous rock and water ice (i) were identical between Tarda and Tagish Lake, although Blinova et al., (2014) suggest at least some degree of protolith heterogeneity between different chips of Tagish Lake. Nonetheless, this assumption is strengthened by similar O-isotope signatures for anhydrous minerals and bulk rock between both meteorites (Brown et al., 2000; Gattacceca et al., 2021; Hildebrand et al., 2006; Marrocchi et al., 2021; Ushikubo & Kimura, 2021; Figure 3.10). Additionally, O-isotope fractionation factors for each mineral (iii) are constant, varying only with temperature (Zheng, 2011). Thus, any differences in O-isotope signatures observed in the secondary minerals of Tarda and Tagish Lake likely primarily reflect different degrees of local aqueous alteration, corresponding to differences in temperature, W/R ratios, or degree of mixing.

Compared to the limited O-isotope composition in Tagish Lake carbonates, the average O-isotope compositions for dolomite in Tarda is lower in both $\Delta^{17}O$ (0.2 ± 1.6) and $\delta^{18}O$ (24.7 ± 2.8), with the $\Delta^{17}O$ closer to the bulk-rock values for the two meteorites (Figure 3.10). This implies that the dolomite in the Tarda meteorite precipitated from a more evolved fluid in comparison to the carbonates in Tagish Lake. Under the assumed two-component closed system model, this is unlikely to occur due to local differences in W/R between the source region of Tarda and Tagish Lake, since the bulk O-isotopes and phyllosilicate abundance is similar between the two meteorites (Bates et al., 2024; Schrader et al., 2024). Thus, the difference in O-isotope values of carbonates between Tarda and Tagish Lake appear to correspond best to the extent of mixing between the water and rock and/or temperature. If the dolomite in Tarda formed after more substantial mixing, the O-isotope signature of the dolomite would reflect greater contribution from the lighter and

more ^{16}O-rich O-isotope signature of the anhydrous rock, lowering the $\Delta^{17}O$ and $\delta^{18}O$ of the dolomite which matches observations (Figure 3.10).

Alternatively, it may be possible that the carbonates formed at similar times in both meteorites, but the dolomite in Tarda formed under warmer conditions. In this scenario, dolomite would fractionate with a lighter $\delta^{18}O$ on the same O mass-dependent fractionation line (Zheng, 2011). Isotopic exchange would also likely occur more readily between the water and the protolith material in the warmer system, lowering the final $\Delta^{17}O$ of the precipitated dolomite (Clog et al., 2024), which also matches our observations (Figure 3.10). The average $\delta^{18}O$ in Tarda dolomite is 8.6‰ lighter than the average $\delta^{18}O$ of carbonates in Tagish Lake. If the dolomites in Tarda formed under equilibrium conditions at ~90˚C (discussed in section 3.4.3) and temperature was solely responsible for decreasing the $\delta^{18}O$ by the observed ~8.6‰ for Tarda, this would require the carbonates in Tagish Lake to be formed under equilibrium conditions at ~23˚C. Temporally, Mn-Cr dating for carbonates in both Tarda and Tagish Lake show unresolvable ages, suggesting that the carbonates of Tarda and Tagish Lake formed within error of the measurement (Figure 3.9).

Lastly, the model should consider that dolomite is preferentially formed in Tarda compared to Tagish Lake. Little work has been done to constrain why dolomite may form in a particular system and its formation mechanisms remain poorly understood even in terrestrial environments (e.g. Cai et al., 2021; Land, 1998; Warren, 2000; Yang et al., 2022). The difficulty to experimentally produce dolomite is, fittingly, known as “the dolomite problem” (e.g. Cai et al., 2021; Land, 1998; Warren, 2000; Yang et al., 2022). Nonetheless, terrestrial laboratory experiments and O-isotopes in carbonaceous chondrites (particularly the CMs) generally suggest that dolomite likely forms at higher temperatures than calcite, is aided by the presence of negatively charged phyllosilicates,

and typically correlates with more extensive aqueous alteration (Brearley, 2006; Clog et al., 2024; Lee et al., 2025, 2014; Liu et al., 2019; Yang et al., 2022). Aqueous alteration models of CI-, CM-, and CV-type planetesimals are in general agreement and additionally demonstrate that dolomite likely forms after increased water-rock interaction, although many additional parameters are considered (Zolensky et al., 1989; Zolotov, 2012). Thus, we conclude that the lower $\delta^{18}O$ and $\Delta^{17}O$ values observed in Tarda dolomite most likely reflect precipitation under warmer conditions and/or after greater water-rock interaction in comparison with carbonates in Tagish Lake.

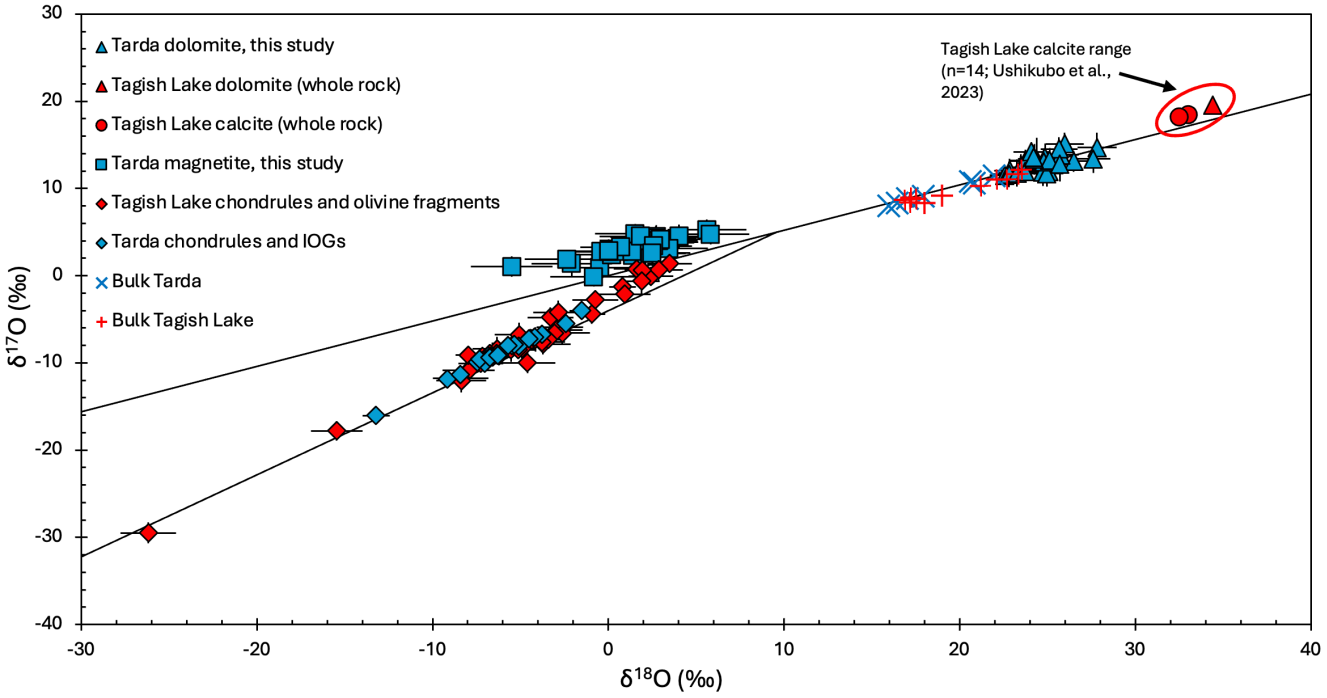

Figure 3.10: Oxygen isotope compositions for various components of Tarda and Tagish Lake. We compare secondary minerals in Tarda to bulk rock (Brown et al., 2000; Gattacceca et al., 2021; Hildebrand et al., 2006), olivine grains and chondrules (Marrocchi et al., 2021; Ushikubo & Kimura, 2021), and Tagish Lake carbonates (Leshin et al., 2001; Ushikubo et al., 2023) from literature.

3.4.5.2. Carbon Isotopes

Compared to oxygen isotopes signatures, the $\delta^{13}C$ signatures in carbonaceous chondrites have a less clear origin and generally requires more complicated interpretations (Alexander et al., 2015; Fujiya et al., 2020, 2019; Grady et al., 1988; Guo & Eiler, 2007; Vacher et al., 2018, 2017).

Carbonates in carbonaceous chondrites contain variable $\delta^{13}C$ signatures, ranging from ~-20 to +80‰, with large variations existing even in individual meteorites such as Murchison (Alexander et al., 2015; Fujiya et al., 2019, 2015; Grady et al., 1988; Telus et al., 2019; Vacher et al., 2017, 2018; Figure 3.4). Using the chemistry of comets as an analogue, the inherited $\delta^{13}C$ signature of carbonates is thought to reflect distinct contributions from ices enriched in volatile carbon species including CO, CO_2, and CH_4, as well as soluble and insoluble organic matter (Alexander et al., 2015; Fujiya et al., 2019; Hässig et al., 2017; Mumma & Charnley, 2011).

There is not yet a consensus on what is driving the large variations in $\delta^{13}C$, however, proposed models suggest this may be a result of initial $\delta^{13}C$ heterogeneity, local temperature differences (affecting the fractionation factor relative to CO-CO_2), the progressive escape of ^{13}C-depleted methane as aqueous alteration advances, and/or evolution towards lighter $\delta^{13}C$ as isotopically light C is released from organic matter (Alexander et al., 2015; Fujiya et al., 2020, 2019; Grady et al., 1988; Guo & Eiler, 2007; Vacher et al., 2017, 2018). Since most of these proposed models would predict systematic isotopic variation of both $\delta^{13}C$ and $\delta^{18}O$ in carbonates, correlations between the two are often investigated but are typically weak and complex, if present at all.

The $\delta^{13}C$ vs $\delta^{18}O$ values reported for the dolomites in Tarda (Figure 3.11) show no robust correlation, instead they are roughly clustered in both $\delta^{13}C$ vs $\delta^{18}O$, suggesting they formed from a similarly evolved fluid and similar temperature, and possibly close in time. When these are compared to those of Tagish Lake, we appear to see two different trends depending on the dataset for Tagish Lake carbonates. Using datasets from Grady et al. (2002) and Fujiya et al. (2019), the carbonate $\delta^{13}C$ values between both meteorites generally shows good agreement but the $\delta^{18}O$ values in Tarda is systemically lower (Figure 3.11). In contrast, both $\delta^{13}C$ vs $\delta^{18}O$ values from calcites in Ushikubo et al. (2023) are systematically higher than those of Tarda, forming a positive

correlation (Figure 3.11). If we take the latter data set for Tagish Lake, the systematic difference in $\delta^{13}C$ vs $\delta^{18}O$ between Tarda and Tagish Lake may be, at least in part, explained by isotope fractionation of carbon (in equilibrium with CO-CO_2 gas) and oxygen (in equilibrium with aqueous fluid) as the temperature changes (Alexander et al., 2015), with dolomite formation in Tarda being warmer consistent with the conclusion derived from O-isotope systematics (section 3.4.5.1). When we take the data from Grady et al. (2002), then Tarda and Tagish Lake carbonates experienced process(es) that changed $\delta^{18}O$ values selectively without changing $\delta^{13}C$ values, which may indicate increased water-rock interaction. Taking all the data together, we may be observing a poorly resolved and weakly positive correlation between $\delta^{18}O$ and $\delta^{13}C$ between Tarda and Tagish Lake possibly due to higher temperatures and greater mixing between low $\delta^{18}O$ (anhydrous silicates) and low $\delta^{13}C$ reservoir(s), however, more robust $\delta^{18}O$ and $\delta^{13}C$ measurements are required in carbonates, particularly for Tagish Lake.

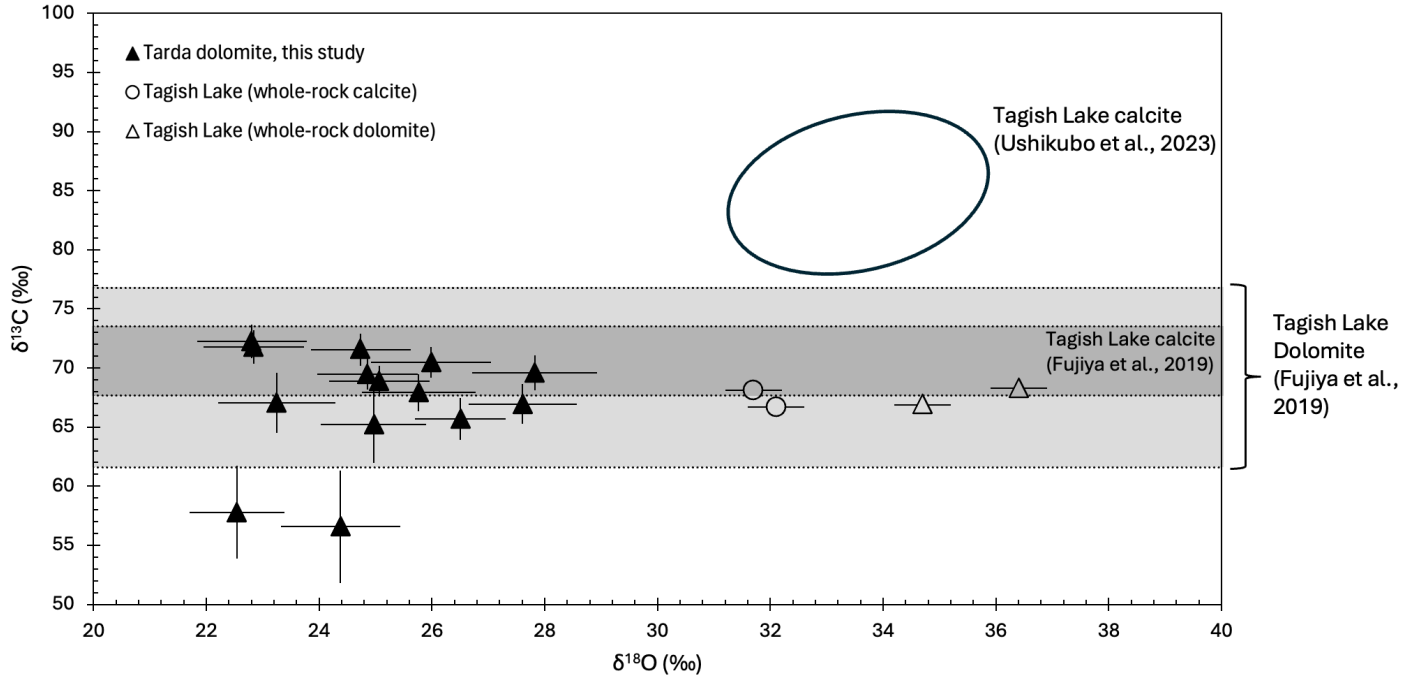

Figure 3.11: $\delta^{13}C$ vs $\delta^{18}O$ for carbonates in Tarda and Tagish Lake. Whole-rock carbonate measurements for Tagish Lake are from Grady et al., (2002). The light and dark grey banners

display $\delta^{13}C$ averages of in situ dolomite (n=4) and calcite (n=12) measurements respectively, reported by Fujiya et al. (2019). The black oval approximates the range of in situ calcite measured in Tagish Lake (n=13) analyzed by Ushikubo et al. (2023).

3.5 Conclusion

Tarda is an aqueously altered C2-ung meteorite fall with reflectance spectra most consistent with P-type asteroids. Tarda likely shares a genetic history with Tagish Lake, a C2-ung meteorite that is widely considered to source a D-type asteroid, possibly indicating a link between both reflectance types (DeMeo et al., 2015; Hiroi et al., 2001; Izawa et al., 2010b; Schrader et al., 2024). Despite their probable shared genetic history, we show that Tarda and Tagish Lake have differing oxygen isotope compositions, indicating distinct aqueous alteration histories. Tarda and Tagish Lake, thus, provide an excellent opportunity to study aqueous alteration heterogeneity on rarely recovered D- and/or P-type asteroids, and may be analogues for upcoming missions to P-, and D-, and C-type Trojan asteroids (e.g. Levison et al., 2021; Olkin et al., 2021), and to Phobos and Deimos which are spectrally similar to D-type asteroids (e.g. Kuramoto et al., 2022; Nakamura et al., 2021).

To investigate the conditions of aqueous alteration in Tarda, we performed in situ oxygen isotope analyses in magnetite, and in situ oxygen, carbon, and Mn-Cr measurements in dolomite. Our primary results include:

1. The dolomite analyzed here is chemically similar to dolomite in Tagish Lake and other fragments of Tarda.
2. Oxygen isotopes for dolomite plot along the TFL with $\delta^{18}O$ values ranging from +22.5‰ to +27.8‰, most similar to dolomite in Ryugu and CI-type meteorites.
3. $\delta^{18}O$ values of magnetite plot between -5.5‰ to +5.8‰, with $\Delta^{17}O$ values of ~2.5‰, most similar to those of Ryugu magnetite.

4. Relative to the other magnetite morphologies, spherical magnetite systematically inherited the highest $\delta^{18}O$ values.
5. Most $\delta^{13}C$ values in Tarda dolomite plot at ~70‰, comparable to dolomite and calcite in Tagish Lake, and dolomite in Ryugu and CI-type meteorites.
6. The correlation between ^{53}Cr excesses and $^{55}Mn/^{52}Cr$ forms a slope of $(3.08 \pm 0.52) \times 10^{-6}$.

From these results, the following interpretations were drawn:

1. Most magnetite precipitated before dolomite, with the spherical morphology likely precipitating first.
2. Oxygen isotope thermometry between a co-precipitating dolomite and magnetite pair suggests a system temperature of ~$90.4\ ^{+29.9}_{-25.0}$ °C.
3. Anchored to the D'Orbigny angrite, dolomite in Tarda precipitated at approximately $4562.7^{+0.9}_{-1.0}$ Ma, similar to Tagish Lake, Ryugu, and CI, CM, and CR group chondrites, suggesting the Tarda/Tagish Lake parent body accreted at similar times. A chemically distinct dolomite crystal (D6) may have precipitated later at $4558.7^{+3.0}_{-7.6}$ Ma, potentially indicating the presence of a later aqueous event.
4. While $\delta^{13}C$ isotope data is similar between Tarda and Tagish Lake, Tarda contains a lighter triple O-isotope signature indicating it experienced more significant aqueous alteration. The $\delta^{18}O$ vs $\delta^{13}C$ may show a weak positive correlation, but more analyses are required to improve the resolution. We conclude that Tarda exhibits a higher degree of aqueous alteration likely due to increased water-rock interaction and/or higher temperatures than Tagish Lake.

3.6 Supplementary Materials

Supplementary Material can be found in Appendix A and contains: (i) SIMS Bias corrections for Fe# on $\delta^{18}O$ and $\delta^{13}C$ used for dolomite measurements; (ii) contextual imaging of some representative SIMS sites; (iii) data used and considered for oxygen isotope thermometry; (iv) an image of dolomite grain D6, and; (v) a note on the availability of O and C isotope data for carbonates and magnetite in Tagish Lake.

3.7 Data availability

Data are available through Borealis Data at https://doi.org/10.5683/SP3/WDN8YA

3.8 References

Aléon, J., Mostefaoui, S., Bureau, H., Vangu, D., Khodja, H., Nagashima, K., … Yurimoto, H. 2024. Hydrogen in magnetite from asteroid Ryugu. Meteoritics and Planetary Science, 59(8), 2058–2072.

Alexander, C. M. O'D., Bowden, R., Fogel, M. L., & Howard, K. T. 2015. Carbonate abundances and isotopic compositions in chondrites. Meteoritics and Planetary Science, 50(4), 810–833.

Bates, H. C., Aspin, R., Fu, C. Y., Harrison, C. S., Feaver, E., Branagan-Harris, E., King, A. J., Bryson, J. F. J., Sridhar, S., & Nichols, C. I. O. 2024. Extent of alteration, paleomagnetic history, and infrared spectral properties of the Tarda ungrouped carbonaceous chondrite. Meteoritics and Planetary Science, 59(9), 2411–2431.

Birck, J.-L., & Allègre, C. J. 1985. Evidence for the presence of 53Mn in the early solar system. Geophysical Research Letters, 12(11), 745–748.

Birck, J.-L., & Allègre, C. J. 1988. Manganese-chromium isotope systematics and the development of the early Solar System. Nature, 331(6157), 579–584.

Bischoff, A., Alexander, C. M. O'D., Barrat, J. A., Burkhardt, C., Busemann, H., Degering, D., … Wölfer, E. 2021. The old, unique C1 chondrite Flensburg – Insight into the first processes of aqueous alteration, brecciation, and the diversity of water-bearing parent bodies and lithologies. Geochimica et Cosmochimica Acta, 293, 142–186

Bland, P. A., Jackson, M. D., Coker, R. F., Cohen, B. A., Webber, J. B. W., Lee, M. R., Duffy, C. M., Chater, R. J., Ardakani, M. G., McPhail, D. S., McComb, D. W., & Benedix, G. K. 2009. Why aqueous alteration in asteroids was isochemical: High porosity ≠ high permeability. Earth and Planetary Science Letters, 287(3–4), 559–568.

Blinova, A. I., Zega, T. J., Herd, C. D. K., & Stroud, R. M. 2014. Testing variations within the Tagish Lake meteorite-I: Mineralogy and petrology of pristine samples. Meteoritics and Planetary Science, 49(4), 473–502.

Brearley, A. J. 2006. The Action of Water. Meteorites and the Early Solar System II, 587–624.

Brennecka, G. A., & Wadhwa, M. 2012. Uranium isotope compositions of the basaltic angrite meteorites and the chronological implications for the early Solar System. Proceedings of the National Academy of Sciences of the United States of America, 109(24), 9299–9303.

Brown, P. G., Hildebrand, A. R., Zolensky, M. E., Grady, M., Clayton, R. N., Mayeda, T. K., … Mazur, T. R. 2000. The Fall, Recovery, Orbit, and Composition of the Tagish Lake Meteorite: A New Type of Carbonaceous Chondrite. Science, 790, 320–325.

Cai, W. K., Liu, J. H., Zhou, C. H., Keeling, J., & Glasmacher, U. A. 2021. Structure, genesis and resources efficiency of dolomite: New insights and remaining enigmas. Chemical Geology, Vol. 573.

Chan, Q. H. S., Zolensky, M. E., Martinez, J. E., Tsuchiyama, A., & Miyake, A. 2016. Magnetite plaquettes are naturally asymmetric materials in meteorites. American Mineralogist, 101(9), 2041–2050.

Clayton, R. N., & Mayeda, T. K. 1984. The oxygen isotope record in Murchison and other carbonaceous chondrites. In Earth and Planetary Sctence Letters (Vol. 67).

Clog, M., Lindgren, P., Modestou, S., McDonald, A., Tait, A., Donnelly, T., Mark, D., & Lee, M. 2024. Clumped isotope and Δ17O measurements of carbonates in CM carbonaceous chondrites: New insights into parent body thermal and fluid evolution. Geochimica et Cosmochimica Acta, 369, 1–16.

Cohen, B. A., & Coker, R. F. 2000. Modeling of Liquid Water on CM Meteorite Parent Bodies and Implications for Amino Acid Racemization. Icarus, 145(2), 369–381.

Connelly, J. N., Bizzarro, M., Krot, A. N., Nordlund, Å., Wielandt, D., & Ivanova, M. A. 2012. The absolute chronology and thermal processing of solids in the solar protoplanetary disk. Science, 338(6107), 651–655.

DeMeo, F. E., Alexander, C. M. O'D., Walsh, K. J., Chapman, C. R., & Binzel, R. P. 2015. The compositional structure of the asteroid belt. In Asteroids IV (pp. 13–41).

Dobrică, E., Ishii, H. A., Bradley, J. P., Ohtaki, K., Brearley, A. J., Noguchi, T., … Tsuda, Y. 2023. Nonequilibrium spherulitic magnetite in the Ryugu samples. Geochimica et Cosmochimica Acta, 346, 65–75.

Dobrică, E., Ogliore, R. C., Engrand, C., Nagashima, K., & Brearley, A. J. 2019. Mineralogy and oxygen isotope systematics of magnetite grains and a magnetite-dolomite assemblage in hydrated fine-grained Antarctic micrometeorites. Meteoritics and Planetary Science, 54(9), 1973–1989.

Doyle, P. M., Jogo, K., Nagashima, K., Huss, G. R., & Krot, A. N. 2016. Mn-Cr relative sensitivity factor in ferromagnesian olivines defined for SIMS measurements with a Cameca ims-1280 ion microprobe: Implications for dating secondary fayalite. Geochimica et Cosmochimica Acta, 174, 102–121.

Fujiya, W. 2018. Oxygen isotopic ratios of primordial water in carbonaceous chondrites. Earth and Planetary Science Letters, 481, 264–272.

Fujiya, W., Aoki, Y., Ushikubo, T., Hashizume, K., & Yamaguchi, A. 2020. Carbon isotopic evolution of aqueous fluids in CM chondrites: Clues from in-situ isotope analyses within calcite grains in Yamato-791198. Geochimica et Cosmochimica Acta, 274, 246–260.

Fujiya, W., Hoppe, P., Ushikubo, T., Fukuda, K., Lindgren, P., Lee, M. R., Koike, M., Shirai, K., & Sano, Y. 2019. Migration of D-type asteroids from the outer Solar System inferred from carbonate in meteorites. Nature Astronomy, Vol. 3, pp. 910–915.

Fujiya, W., Kawasaki, N., Nagashima, K., Sakamoto, N., Alexander, C. M. O'D, Kita, N. T., … Yurimoto, H. 2023. Carbonate record of temporal change in oxygen fugacity and gaseous species in asteroid Ryugu. Nature Geoscience, 16(8), 675–682.

Fujiya, W., Sugiura, N., Hotta, H., Ichimura, K., & Sano, Y. 2012. Evidence for the late formation of hydrous asteroids from young meteoritic carbonates. Nature Communications, 3.

Fujiya, W., Sugiura, N., Marrocchi, Y., Takahata, N., Hoppe, P., Shirai, K., Sano, Y., & Hiyagon, H. 2015. Comprehensive study of carbon and oxygen isotopic compositions, trace element abundances, and cathodoluminescence intensities of calcite in the Murchison CM chondrite. Geochimica et Cosmochimica Acta, 161, 101–117.

Fujiya, W., Sugiura, N., Sano, Y., & Hiyagon, H. 2013. Mn-Cr ages of dolomites in CI chondrites and the Tagish Lake ungrouped carbonaceous chondrite. Earth and Planetary Science Letters, 362, 130–142.

Gattacceca, J., McCubbin, F. M., Grossman, J., Bouvier, A., Bullock, E., Chennaoui Aoudjehane, H., Debaille, V., D'Orazio, M., Komatsu, M., Miao, B., & Schrader, D. L. 2021. The Meteoritical Bulletin, No. 109. Meteoritics and Planetary Science, 56(8), 1626–1630.

Gilmour, C. M., Herd, C. D. K., & Beck, P. 2019. Water abundance in the Tagish Lake meteorite from TGA and IR spectroscopy: Evaluation of aqueous alteration. Meteoritics and Planetary Science, 54(9), 1951–1972.

Glavin, D. P., Alexander, D., Aponte, J. C., Dworkin, J. P., Elsila, J. E., & Yabuta, H. 2018. The Origin and Evolution of Organic Matter in Carbonaceous Chondrites and Links to Their

Parent Bodies. In Primitive Meteorites and Asteroids: Physical, Chemical, and Spectroscopic Observations Paving the Way to Exploration (pp. 205–271).

Grady, M. M., Verchovsky, A. B., Franchi, I. A., Wright, I. P., & Pillinger, C. T. 2002. Light element geochemistry of the Tagish Lake C12 chondrite: Comparison with CI1 and CM2 meteorites. Meteoritics and Planetary Science, 37(5), 713–735.

Grady, M. M., Wright, I. P., Swart, P. K., & Pillinger, C. T. 1988. The carbon and oxygen isotopic composition of meteoritic carbonates. Geochimica et Cosmochimica Acta, 52(12), 2855–2866.

Grimm, R. E., & Mcsween, H. Y. 1989. Water and the Thermal Evolution of Carbonaceous Chondrite Parent Bodies (Vol. 82).

Guo, W., & Eiler, J. M. 2007. Temperatures of aqueous alteration and evidence for methane generation on the parent bodies of the CM chondrites. Geochimica et Cosmochimica Acta, 71(22), 5565–5575.

Hässig, M., Altwegg, K., Balsiger, H., Berthelier, J. J., Bieler, A., Calmonte, U., Dhooghe, F., Fiethe, B., Fuselier, S. A., Gasc, S., Gombosi, T. I., Le Roy, L., Luspay-Kuti, A., Mandt, K., Rubin, M., Tzou, C. Y., Wampfler, S. F., & Wurz, P. 2017. Isotopic composition of CO2 in the coma of 67P/Churyumov-Gerasimenko measured with ROSINA/DFMS. Astronomy and Astrophysics, 605.

Hildebrand, A. R., McCausland, P. J. A., Brown, P. G., Longstaffe, F. J., Russell, S. D. J., Tagliaferri, E., Wacker, J. F., & Mazur, M. J. 2006. The fall and recovery of the Tagish Lake meteorite. Meteoritics and Planetary Science, 41(3), 407–431.

Hiroi, T., Zolensky, M. E., & Pieters, C. M. 2001. The Tagish Lake meteorite: A possible sample from a D-type asteroid. Science, 293(5538), 2234–2236.

Hua, X., & Buseck, P. R. 1998. Unusual forms of magnetite in the Orgueil carbonaceous chondrite. Meteoritics and Planetary Science, 33, 215–220.

Huberty, J. M., Kita, N. T., Kozdon, R., Heck, P. R., Fournelle, J. H., Spicuzza, M. J., Xu, H., & Valley, J. W. 2010. Crystal orientation effects in δ18O for magnetite and hematite by SIMS. Chemical Geology, 276(3–4), 269–283.

Ireland, T. R., Avila, J., Greenwood, R. C., Hicks, L. J., & Bridges, J. C. 2020. Oxygen Isotopes and Sampling of the Solar System. Space Science Reviews, Vol. 216.

Izawa, M. R. M., Nesbitt, H. W., MacRae, N. D., & Hoffman, E. L. 2010a. Composition and Evolution of the Early Oceans: Evidence from the Tagish Lake Meteorite. Earth and Planetary Science Letters, 298(3–4), 443–449.

Izawa, M. R. M., Flemming, R. L., King, P. L., Peterson, R. C., & McCausland, P. J. A. 2010b. Mineralogical and spectroscopic investigation of the Tagish Lake carbonaceous chondrite by X-ray diffraction and infrared reflectance spectroscopy. Meteoritics and Planetary Science, 45(4), 675–698.

Jilly-Rehak, C. E., Huss, G. R., Nagashima, K., & Schrader, D. L. 2017a. Low-temperature aqueous alteration on the CR chondrite parent body: Implications from in situ oxygen-isotope analyses. Geochimica et Cosmochimica Acta, 222, 230–252.

Jilly-Rehak, C. E., Huss, G. R., & Nagashima, K. 2017b. 53Mn–53Cr radiometric dating of secondary carbonates in CR chondrites: Timescales for parent body aqueous alteration. Geochimica et Cosmochimica Acta, 201, 224–244.

Jilly-Rehak, C. E., Huss, G. R., Krot, A. N., Nagashima, K., Yin, Q. Z., & Sugiura, N. 2014. 53Mn-53Cr dating of aqueously formed carbonates in the CM2 lithology of the Sutter's Mill carbonaceous chondrite. Meteoritics and Planetary Science, 49(11), 2104–2117.

Jochum, K. P., Garbe-Schönberg, D., Veter, M., Stoll, B., Weis, U., Weber, M., Lugli, F., Jentzen, A., Schiebel, R., Wassenburg, J. A., Jacob, D. E., & Haug, G. H. 2019. Nano-Powdered Calcium Carbonate Reference Materials: Significant Progress for Microanalysis? Geostandards and Geoanalytical Research, 43(4), 595–609.

Kimura, Y., Sato, T., Nakamura, N., Nozawa, J., Nakamura, T., Tsukamoto, K., & Yamamoto, K. 2013. Vortex Magnetic Structure in Framboidal Magnetite Reveals Existence of Water Droplets in an Ancient Asteroid. Nature Communications, 4, 1–8.

Kita, N. T., Kitajima, K., Nagashima, K., Kawasaki, N., Sakamoto, N., Fujiya, W., … Yurimoto, H. 2024. Disequilibrium oxygen isotope distribution among aqueously altered minerals in Ryugu asteroid returned samples. Meteoritics and Planetary Science, 59(8), 2097–2116.

Krot, A. N., Keil, K., Scott, E. R. D., Goodrich, C. A., & Weisberg, M. K. 2013. Classification of Meteorites and Their Genetic Relationships. In Treatise on Geochemistry: Second Edition (2nd ed., Vol. 1).

Kuramoto, K., Kawakatsu, Y., Fujimoto, M., Araya, A., Barucci, M. A., Genda, H., … Yokota, S. 2022. Martian moons exploration MMX: sample return mission to Phobos elucidating formation processes of habitable planets. Earth, Planets and Space, Vol. 74.

Land, L. S. 1998. Failure to Precipitate Dolomite at 25˚C from Dilute Solution Despite 1000-Fold Oversaturation after 32 Years. In Aquatic Geochemistry (Vol. 4).

Lauretta, D. S., Connolly, H. C., Aebersold, J. E., Alexander, C. M. O'D., Ballouz, R. L., Barnes, J. J., … Wolner, C. W. V. 2024. Asteroid (101955) Bennu in the laboratory: Properties of the sample collected by OSIRIS-REx. Meteoritics and Planetary Science, 2486(9), 2453–2486.

Lee, M. R., Alexander, C. M. O'D., Bischoff, A., Brearley, A. J., Fujiya, W., Le, C., Ashley, G., Dobric, E., Kooten, E. Van, Krot, A. N., Leitner, J., Marrocchi, Y., Remusat, L., Telus, M.,

Tsuchiyama, A., & Vacher, L. G. 2025. Low-Temperature Aqueous Alteration of Chondrites. Space Science Reviews, 221(11).

Lee, M. R., Lindgren, P., & Sofe, M. R. 2014. Aragonite, breunnerite, calcite and dolomite in the CM carbonaceous chondrites: High fidelity recorders of progressive parent body aqueous alteration. Geochimica et Cosmochimica Acta, 144, 126–156.

Leshin, A., Farquhar, J., Guan, Y., Pizzarello, S., Jackson, T. L., & Thiemens, M. H. 2001. Oxygen Isotopic Anatomy of Tagish Lake: Relationship to Primary and Secondary Minerals in CI and CM Chondrites. 32nd Lunar and Planetary Science Conference.

Levison, H. F., Olkin, C. B., Noll, K. S., Marchi, S., Bell, J. F., Bierhaus, E., … Wong, I. 2021. Lucy mission to the Trojan asteroids: Science goals. Planetary Science Journal, Vol. 2.

Lindgren, P., Lee, M. R., Starkey, N. A., & Franchi, I. A. 2017. Fluid evolution in CM carbonaceous chondrites tracked through the oxygen isotopic compositions of carbonates. Geochimica et Cosmochimica Acta, 204, 240–251.

Liu, D., Xu, Y., Papineau, D., Yu, N., Fan, Q., Qiu, X., & Wang, H. 2019. Experimental evidence for abiotic formation of low-temperature proto-dolomite facilitated by clay minerals. Geochimica et Cosmochimica Acta, 247, 83–95.

Marrocchi, Y., Avice, G., & Barrat, J.-A. 2021. The Tarda Meteorite: A Window into the Formation of D-type Asteroids. The Astrophysical Journal Letters, 913(1), 1–8.

McCain, K. A., Liu, M.-C., & McKeegan, K. D. 2020. Calibration of matrix-dependent biases in isotope and trace element analyses of carbonate minerals. Journal of Vacuum Science & Technology B, Nanotechnology and Microelectronics: Materials, Processing, Measurement, and Phenomena, 38(4).

McCain, K. A., Matsuda, N., Liu, M. C., McKeegan, K. D., Yamaguchi, A., Kimura, M., … Tsuda, Y. 2023. Early fluid activity on Ryugu inferred by isotopic analyses of carbonates and magnetite. Nature Astronomy, 7(3), 309–317.

McKibbin, S. J., Ireland, T. R., Amelin, Y., & Holden, P. 2015. Mn-Cr dating of Fe- and Ca-rich olivine from "quenched" and "plutonic" angrite meteorites using Secondary Ion Mass Spectrometry. Geochimica et Cosmochimica Acta, 157, 13–27.

Mumma, M. J., & Charnley, S. B. 2011. The chemical composition of comets –emerging taxonomies and natal heritage. Annual Review of Astronomy and Astrophysics, 49, 471–524.

Nagashima, K., Thomen, A., Krot, A. N., Huss, G. R., Kim, N. K., & Park, C. 2020. Investigation of Instrumental Fractionation in SIMS Analyses of Magnesium, Silicon, and Oxygen Isotopes in Silicates and Oxides. 51st Lunar and Planetary Science Conference.

Nakamura, E., Kobayashi, K., Tanaka, R., Kunihiro, T., Kitagawa, H., Potiszil, C., … Tsuda, Y. 2022. On the origin and evolution of the asteroid Ryugu: A comprehensive geochemical perspective. Proceedings of the Japan Academy Series B: Physical and Biological Sciences, 98(6), 227–282.

Nakamura, T., Ikeda, H., Kouyama, T., Nakagawa, H., Kusano, H., Senshu, H., … Kawakatsu, Y. 2021. Science operation plan of Phobos and Deimos from the MMX spacecraft. Earth, Planets and Space, 73(1).

Nakamura, T., Noguchi, T., Zolensky, M. E., & Tanaka, M. 2003. Mineralogy and noble-gas signatures of the carbonate-rich lithology of the Tagish Lake carbonaceous chondrite: Evidence for an accretionary breccia. Earth and Planetary Science Letters, 207(1–4), 83–101.

Ogliore, R. C., Huss, G. R., & Nagashima, K. 2011. Ratio estimation in SIMS analysis. Nuclear Instruments and Methods in Physics Research, Section B: Beam Interactions with Materials and Atoms, 269(17), 1910–1918.

Olkin, C. B., Levison, H. F., Vincent, M., Noll, K. S., Andrews, J., Gray, S., … Caplinger, M. 2021. Lucy mission to the Trojan asteroids: Instrumentation and encounter concept of operations. Planetary Science Journal, 2(5).

Papanastassiou, D. A. 1986. Chromium Isotopic Anomalies in the Allende Meteorite. The Astrophysical Journal, 308, 27–30.

Piralla, M., Marrocchi, Y., Verdier-Paoletti, M. J., Vacher, L. G., Villeneuve, J., Piani, L., Bekaert, D. V., & Gounelle, M. 2020. Primordial water and dust of the Solar System: Insights from in situ oxygen measurements of CI chondrites. Geochimica et Cosmochimica Acta, 269, 451–464.

Pizzarello, S. 2006. The chemistry of life's origin: A carbonaceous meteorite perspective. Accounts of Chemical Research, 39(4), 231–237.

Pizzarello, S., & Shock, E. 2010. The organic composition of carbonaceous meteorites: the evolutionary story ahead of biochemistry. Cold Spring Harbor Perspectives in Biology, 2(3), 1–20.

Pizzarello, S., & Shock, E. 2017. Carbonaceous Chondrite Meteorites: The Chronicle of a Potential Evolutionary Path between Stars and Life. Origins of Life and Evolution of Biospheres, 47(3), 249–260.

Remusat, L. 2014. Organic material in meteorites and the link to the origin of life. BIO Web of Conferences, 2, 1–10.

Rowe, M. W., Clayton, Robert. N., & Toshiko, K. Mayeda. 1994. Oxygen isotopes in separated components of CI and CM meteorites. Geochimica et Cosmochimica Acta, 58(23), 5341–5347.

Rubin, A. E., & Ma, C. 2017. Meteoritic minerals and their origins. Chemie Der Erde, Vol. 77, pp. 325–385.

Schrader, D. L., Cloutis, E. A., Applin, D. M., Davidson, J., Torrano, Z. A., Foustoukos, D., Alexander, C. M. O'D., Domanik, K. J., Matsuoka, M., Nakamura, T., Zega, T. J., Brennecka, G. A., & Render, J. 2024. Tarda and Tagish Lake: Samples from the same outer Solar System asteroid and implications for D- and P-type asteroids. Geochimica et Cosmochimica Acta, 380(September 2023), 48–70.

Śliwiński, M. G., Kitajima, K., Kozdon, R., Spicuzza, M. J., Fournelle, J. H., Denny, A., & Valley, J. W. 2016a. Secondary Ion Mass Spectrometry Bias on Isotope Ratios in Dolomite–Ankerite, Part I: δ18O Matrix Effects. Geostandards and Geoanalytical Research, 40(2), 157–172.

Śliwiński, M. G., Kitajima, K., Kozdon, R., Spicuzza, M. J., Fournelle, J. H., Denny, A., & Valley, J. W. 2016b. Secondary Ion Mass Spectrometry Bias on Isotope Ratios in Dolomite–Ankerite, Part II: δ13C Matrix Effects. Geostandards and Geoanalytical Research, 40(2), 173–184.

Steele, R. C. J., Heber, V. S., & McKeegan, K. D. 2017. Matrix effects on the relative sensitivity factors for manganese and chromium during ion microprobe analysis of carbonate: Implications for early Solar System chronology. Geochimica et Cosmochimica Acta, 201, 245–259.

Sugawara, S., Fujiya, W., Kagi, H., Yamaguchi, A., & Hashizume, K. 2022. Heat-Induced Dolomitization of Amorphous Calcium Magnesium Carbonate in a CO2-Filled Closed System. ACS Omega, 7(49), 44670–44676.

Sugawara, S., Fujiya, W., Kawasaki, N., Sakamoto, N., Yamaguchi, A., & Yurimoto, H. 2024. Update on the 53Mn-53Cr ages of dolomite in the Ivuna CI chondrite and asteroid Ryugu sample. Geochimica et Cosmochimica Acta, 382, 40–50.

Sugiura, N., Ichimura, K., Fujiya, W., & Takahata, N. 2010. Mn/Cr relative sensitivity factors for synthetic calcium carbonate measured with a NanoSIMS ion microprobe. Geochemical Journal, 44, 11–16.

Suttle, M. D., King, A. J., Schofield, P. F., Bates, H., & Russell, S. S. 2021.The aqueous alteration of CM chondrites, a review. Geochimica et Cosmochimica Acta, Vol. 299, pp. 219–256.

Telus, M., Alexander, C. M. O'D., Hauri, E. H., & Wang, J. 2019. Calcite and dolomite formation in the CM parent body: Insight from in situ C and O isotope analyses. Geochimica et Cosmochimica Acta, 260, 275–291.

Tsuchiyama, A., Matsumoto, M., Matsuno, J., Nakamura, T., Noguchi, T., Yasutake, M., … Watanabe, S. 2022. 3D Morphologies of Magnetite, Sulfides, Carbonates and Phosphates in Ryugu Samples and Their Crystallization Sequence During Aqueous Alteration. 85th Annual Meeting of The Meteoritical Society 2022, 15, 7944–7951.

Tyra, M., Brearley, A., & Guan, Y. 2016. Episodic carbonate precipitation in the CM chondrite ALH 84049: An ion microprobe analysis of O and C isotopes. Geochimica et Cosmochimica Acta, 175, 195–207.

Ushikubo, T., Yamaguchi, A., Weisberg, M. K., Kimura, M., & Ebel, D. S. 2023. Evidence for High δ13C and Δ17O Fluid in Small Bodies Accreted in a Cold and Distant Region from the Sun. 54th Lunar and Planetary Science Conference.

Ushikubo, T., & Kimura, M. 2021. Oxygen-isotope systematics of chondrules and olivine fragments from Tagish Lake C2 chondrite: Implications of chondrule-forming regions in protoplanetary disk. Geochimica et Cosmochimica Acta, 293, 328–343.

Vacher, L. G., Marrocchi, Y., Villeneuve, J., Verdier-Paoletti, M. J., & Gounelle, M. 2017. Petrographic and C & O isotopic characteristics of the earliest stages of aqueous alteration of CM chondrites. Geochimica et Cosmochimica Acta, 213, 271–290.

Vacher, L. G., Marrocchi, Y., Villeneuve, J., Verdier-Paoletti, M. J., & Gounelle, M. 2018. Collisional and alteration history of the CM parent body. Geochimica et Cosmochimica Acta, 239, 213–234.

Vermeesch, P. 2018. IsoplotR: A free and open toolbox for geochronology. Geoscience Frontiers, 9(5), 1479–1493.

Visser, R., John, T., Whitehouse, M. J., Patzek, M., & Bischoff, A. 2020. A short-lived 26Al induced hydrothermal alteration event in the outer solar system: Constraints from Mn/Cr ages of carbonates. Earth and Planetary Science Letters, 547.

Warren, J. 2000. Dolomite: occurrence, evolution and economically important associations. Earth-Science Reviews, 52, 1–81.

Wilson, B. J. K., Cecco, V. E. D. I., Garvie, L. A. J., Tait, K. T., & Daly, M. G. 2024. A sample preparation guide for clay-rich carbonaceous chondrites. Meteoritics and Planetary Science, 59(3), 560–567.

Yang, L., Yu, L., Liu, K., Jia, J., Zhu, G., & Liu, Q. 2022. Coupled effects of temperature and solution compositions on metasomatic dolomitization: Significance and implication for the formation mechanism of carbonate reservoir. Journal of Hydrology, 604.

Yesiltas, M., Kebukawa, Y., Glotch, T. D., Zolensky, M., Fries, M., Aysal, N., & Tukel, F. S. 2022. Compositional and spectroscopic investigation of three ungrouped carbonaceous chondrites. Meteoritics and Planetary Science, 1687(9), 1665–1687.

Yokoyama, T., Nagashima, K., Nakai, I., Young, E. D., Abe, Y., Aléon, J., Alexander, C. M. O'D, Amari, S., Amelin, Y., & Bajo, K. 2023. Samples returned from the asteroid Ryugu are similar to Ivuna-type carbonaceous meteorites. Science, 379, eabn7850.

Young, E. D. 2001. The hydrology of carbonaceous chondrite parent bodies and the evolution of planet progenitors. Philosophical Transactions of the Royal Society of London A: Mathematical, Physical and Engineering Sciences, 2095–2110.

Young, E. D., Ash, R. D., England, P., & Rumble, D. 1999. Fluid flow in chondritic parent bodies: Deciphering the compositions of planetesimals. Science, 286(5443), 1331–1335.

Yurimoto, H., Krot, A. N., Choi, B. G., Aleon, J., Kunihiro, T., & Brearley, A. J. 2008. Oxygen isotopes of chondritic components. Reviews in Mineralogy and Geochemistry, 68, 141–186.

Zheng, Y.-F. 1991. Calculation of oxygen isotope fractionation in metal oxides. Geochimica et Cosmochimica Acta, 55(8), 2299–2307.

Zheng, Y.-F. 1999. Oxygen isotope fractionation in carbonate and sulfate minerals. Geochemical Journal, 33, 109-126.

Zheng, Y.-F. 2011. On the theoretical calculations of oxygen isotope fractionation factors for carbonate-water systems. Geochemical Journal, 45, 341–354.

Zolensky, M. E., Nakamura, K., Gounelle, M., Mikouchi, T., Kasama, T., Tachikawa, O., & Tonui, E. 2002. Mineralogy of Tagish Lake: An ungrouped type 2 carbonaceous chondrite. Meteoritics and Planetary Science, 37(5), 737–761.

Zolensky, M. E., Bourcier, W. L., & Gooding, J. L. 1989. Aqueous Alteration on the Hydrous Asteroids: Results of EQ3/6 Computer Simulations. Icarus, 78, 411-425.

Zolotov, M. Y. 2012. Aqueous fluid composition in CI chondritic materials: Chemical equilibrium assessments in closed systems. Icarus, 220(2), 713–729.

CHAPTER 4. Nanoscale Chemistry of Magnetite Framboids in the Tarda Meteorite: A Proxy for Fluid Chemistry

Abstract

Tarda is a C2-ungrouped carbonaceous chondrite that preserves a record of low-temperature aqueous alteration on its parent asteroid. While the original fluid has disappeared, constraining its composition is essential for understanding the chemical environment that influenced both secondary mineral formation and prebiotic organic chemistry. Magnetite framboids are an abundant aqueous alteration product in Tarda and likely recorded some of the chemical species from its mother solution during growth, entrained within the framboidal magnetite grain boundaries. To investigate this, we conducted a nanoscale study on five magnetite framboids using transmission electron microscopy (TEM), energy dispersive spectroscopy (EDS), and atom probe tomography (APT). Magnetite framboids in Tarda exhibit a wide range of textures, particle sizes, and packing arrangements, reflecting a progressive sequence of discrete nucleation and growth events likely occurring in isolated water droplets. TEM-EDS analysis reveals trace element enrichments of Ti and Si along ~5 nm thick grain boundaries, with the strongest enrichments observed in the early-formed, fine-grained framboids. Between two APT datasets, we captured a ~ 5 nm thick planar feature enriched in trace abundances of Na, Mg, Ca, Mn, and Si, and numerous ~5 nm wide intracrystalline elemental enrichment clusters of trace Si and Na. These features likely correspond to a magnetite boundary and intracrystalline nanometric pores respectively. The identified chemical species require negative magnetite surface charges during precipitation, constraining fluid pH to values above ~5.4. These findings suggest that magnetite framboids in Tarda formed under generally alkaline and cation-rich conditions that evolved as water–rock interaction progressed. Given the known role of alkaline, metal-rich fluids in promoting prebiotic

organic synthesis, these results provide new compositional constraints on the aqueous environments that influenced both mineral and organic inventories in carbonaceous asteroids.

4.1. Introduction

Radiogenic heating within some primitive carbonaceous asteroids caused accreted ice to melt, forming one of the first aqueous environments present in the Solar System (Brearley, 2006; Cohen & Coker, 2000; Lee et al., 2025). This environment could extensively modify the other accreted asteroid materials, rock and organics, in a process known as aqueous alteration (Brearley, 2006; Glavin et al., 2018; Lee et al., 2025; Suttle et al., 2021). Meteorites from such bodies, termed carbonaceous chondrites, record a diverse suite of secondary minerals and organics that partly reflect the extent of aqueous alteration that each carbonaceous chondrite experienced, with temperatures, pH, and water/rock ratios (etc) ranging from ~0-150˚C, 6-10, and 0.1-1.2, respectively (Brearley, 2006; Glavin et al., 2018; Herd et al., 2011; Krot et al., 2013; Lee et al., 2025, 2014; Schulte & Shock, 2004; Zolensky et al., 1989). These diverse aqueously altered products likely represent bio-relevant material that seeded the young planets prior to biosynthesis, potentially offering insights into the origin of life (Kitadai & Maruyama, 2018; Pizzarello, 2006; Pizzarello & Shock, 2010; Schulte & Shock, 2004).

The composition of the fluid responsible for altering carbonaceous chondrites is an important parameter that drives mineralization and organic synthesis but is incredibly difficult to constrain due to the overall absence of preserved fluid (e.g. Brearley, 2006; Glavin et al., 2018; Kitadai & Maruyama, 2018). Magnetite framboids, however, are an aqueous alteration product in some carbonaceous chondrites and are aggregates of numerous (>1000) and small (≤ 1μm) magnetite particles that likely precipitated from fluid as colloidal crystals (Hua & Buseck, 1998; Kimura et al., 2013; Nozawa et al., 2011; White et al., 2020; Zolensky et al., 2002). Adsorbed ions on

colloidal magnetite surfaces have been previously observed, possibly serving to constrain the composition of the fluid which the magnetite precipitated (Kimura et al., 2013; White et al., 2020).

Here, we investigate the nanoscale chemistry of magnetite framboids in the C2-ungrouped Tarda meteorite; a recently fallen carbonaceous chondrite with evidence of low-temperature aqueous alteration (Bates et al., 2024; Schrader et al., 2024). Using Transmission Electron Microscopy (TEM), Energy Dispersive Spectroscopy (EDS), and Atom Probe Tomography (APT), we characterize the surface and boundary chemistries of individual magnetite particles within multiple framboid clusters. These data are used to infer the chemical conditions of the altering fluid and to assess the formation history of the framboids.

4.2. Materials and Methods

A 2.1 fragment of the Tarda meteorite was loaned from the Royal Ontario Museum (catalog number: ROMESM60117), and was mounted, cut, and polished following Wilson et al., (2024). This procedure used mineral oil and hexane to polish the sample, since they are non-polar and prevent the expansive clay minerals from slaking. Two polished 1-inch-diameter potted butts were produced for analysis.

Magnetite framboids were located for further analysis using the Hitatchi 3500SU Shottky Scanning Electron Microscope (SEM) at the Open Center for the Characterization of Advanced Materials (OCCAM) in Toronto, Canada. Backscatter Electron images were collected with an accelerating voltage of 20 kV with a beam current of 0.7 nA.

A Focused Ion Beam (FIB)-SEM system was employed at the Canadian Centre for Electron Microscopy (CCEM) to lift out targeted sections for TEM and APT analysis. TEM sample preparation utilized a Zeiss Crossbeam 350 FIB-SEM at the Canadian Centre for Electron Microscopy. From a surface polished by a prior FIB cut, the site for the surface-plane oriented

TEM sample was chosen because it contained a variety of magnetite framboid clusters with different particle sizes (Figure 4.1A). The surface plane lift-out orientation ensures that the TEM sample will appear very similar to how this region appears in SEM, compared to a conventional cross-section where most of the sample subsurface is unknown.

The target area was first locally protected by electron beam induced deposition of carbon, followed by a thicker ion beam induced deposition layer of tungsten (Figure 4.1B). The surface plane FIB lift-out (Figure 4.1C) was first attached to a horizontally mounted FIB grid in a custom holder. The grid holder was then repositioned so the FIB grid was held vertically. The FIB processing continued with additional trimming and the deposition of a tungsten protection layer prior to FIB thinning.

Thinning was performed with an ion beam probe starting at 30 kV, 300 pA, and was progressively stepped down to utilize lower currents as the sample became thinner, down to the final current of 20 pA. Following conventional thinning was a ~7° glancing-angle low-voltage cleaning step applied to both sides of the sample with a final 2 kV and 50 pA ion beam (Figure 4.1D).

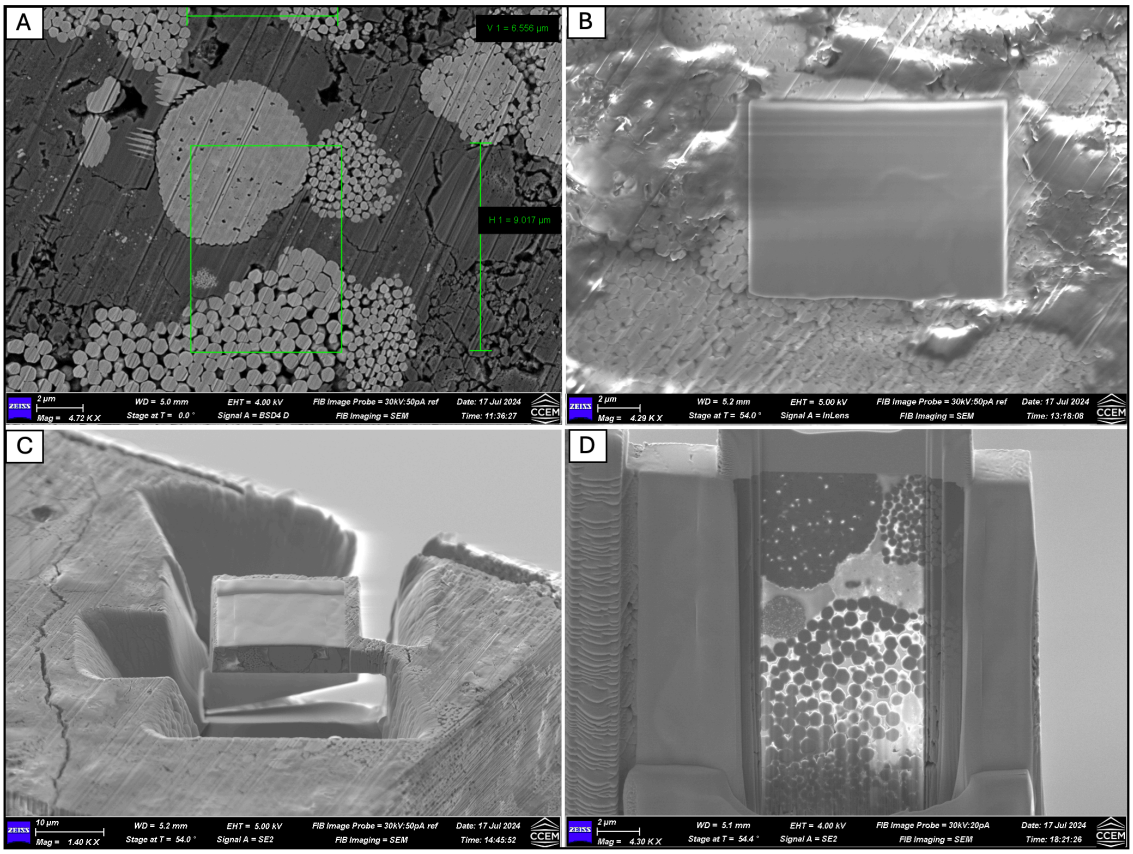

Figure 4.1: SEM images showing different stages of TEM sample preparation. A shows the region selected for TEM (green box), B shows the tungsten deposition, C shows the ion milling required for the liftout, and D shows the final surface produced after section thinning.

Atom probe samples were prepared using a Zeiss Crossbeam 350 FIB-SEM at CCEM. Porous meteorite samples carry the risk of tip fracture during APT acquisition; therefore, using a surface polished by a prior FIB cut, a suitable site for extraction was chosen that was both low in porosity and contained a high density of magnetite framboids (Figure 4.4). Atom probe tips were prepared using traditional FIB-SEM methods, but instead of a conventional silicon coupon, the liftout was segmented and attached to 5 posts of a 200 µm thick Al FIB grid that was custom-made using the Zeiss Crossbeam 350 LaserFIB. The 5 posts were further sharpened and cut using the Ga ion beam to have a flat, ~2µm diameter top. This custom half-grid on CCEM's custom correlative holder to enables correlative TEM analysis on the APT tips before and after the APT acquisition. This method can provide additional correlative sample information and assistance in tip-shape

reconstruction. The blocks were attached to the grid posts using ion beam-induced deposition of tungsten, then shaped by the ion beam using a 30kV accelerating voltage and a series of annular ring patterns with decreasing inner diameters and beam currents (700-50pA). A final sharpening was done with a 5kV 50pA ion beam to help minimize gallium damage in the final tips.

TEM was conducted on the FIB liftout at the Canadian Center for Electron Microscopy (CCEM). The samples were analyzed in the Thermo Fisher Scientific Spectra Ultra, double-corrected HRTEM/STEM operated at 300kV.

The EDS elemental maps were acquired using a Thermo Fisher Ultra X equipped with six Super-X silicon drift detectors (SDD). High Angle Annular Dark Field (HAADF) images were acquired in STEM mode with a probe current of 500pA and 28 mrad convergence angle. The quantitative maps were generated using the Velox program from Thermo Fisher Scientific.

APT analysis was conducted at CCEM on a LEAP 5000 XS. Two specimens yielded good datasets:

i) R5047_35350 was collected using a base temperature of 60K, laser energy of 80pJ, laser pulse rate of 250kHz, and a detection rate of 0.3% (selected since they were successful for Tagish Lake in Lee et al., 2019).
ii) R5047_35357 was collected using a base temperature of 50K, a laser energy of 50pJ, a laser pulse rate of 250kHz, and a detection rate of 0.3%. %. The adjustment of parameters for this second dataset was done in attempt to improve mass spectrum quality (i.e., decreasing heating at the tip apex and reducing thermal tails).

Both datasets were reconstructed using a fixed shank model and the TEM images to measure the initial radius and half-shank angle. The mass spectrum between the samples was very similar.

Additional information on instrument and reconstruction parameters can be found in the supplementary Table B1.

4.3. Results

4.3.1. Magnetite Framboid Variability and Context

Magnetite framboids in Tarda are almost exclusively found in contact with dolomite grains, either entrained within or adjacent. The magnetite framboids exhibit considerable variety, in both cluster size and shape, and the size, shape, and packing of their constituent polyhedral and interlocking magnetite particles (Figure 4.2). The magnetite particles that comprise each framboid cluster are numerous (typically 1000+), ranging from ~90 nm to ~1 μm, with packing tightness/pore space varying predominantly on the particle morphologies (Nozawa et al., 2011). The size of each framboid cluster can range from ~1 to 10+ μm and may be spherical, subspherical, or irregularly shaped.

The region analyzed with TEM contains four distinct magnetite clusters, all of which have unique sizes, shapes, and particle packing arrangements (F1-F4; Figure 4.3). Framboid F1 (Figure 4.3) is a ~7 μm diameter spherical-subspherical framboid cluster, with interlocking particles typically ~230 nm diameter that are tightly packed, often with flush and continuous contact boundaries yielding no pore space. Framboid F2 (Figure 4.3) is a ~4.3 μm diameter subspherical framboid cluster, comprised of interlocking and moderately packed magnetite particles typically ~380 nm in diameter. Framboid F3 (Figure 4.3) is a 1 μm diameter spherical-subspherical cluster, with interlocking magnetite particles typically ~90 nm in diameter that are moderately to well packed, varying with the particle morphology. Framboid F4 (Figure 4.3) is an irregular and elongated magnetite cluster with a short and long axis of approximately 6x11 μm. The constituent magnetite particles have a typical diameter of ~660 nm and are moderately packed. Notably, the

magnetite particles in F1 and F3 were also found to contain numerous nanometric rounded pores, similar to those observed in Ryugu spherulitic magnetite by Dobrică et al. (2023) (Figure 4.5).

APT was performed on an irregular and elongated magnetite framboid, with a long axis of approximately 28 μm (Figure 4.4). The constituent magnetite particles have a typical diameter of ~650 nm and exhibit tight packing with little to no pore space, most suitable for APT ionization.

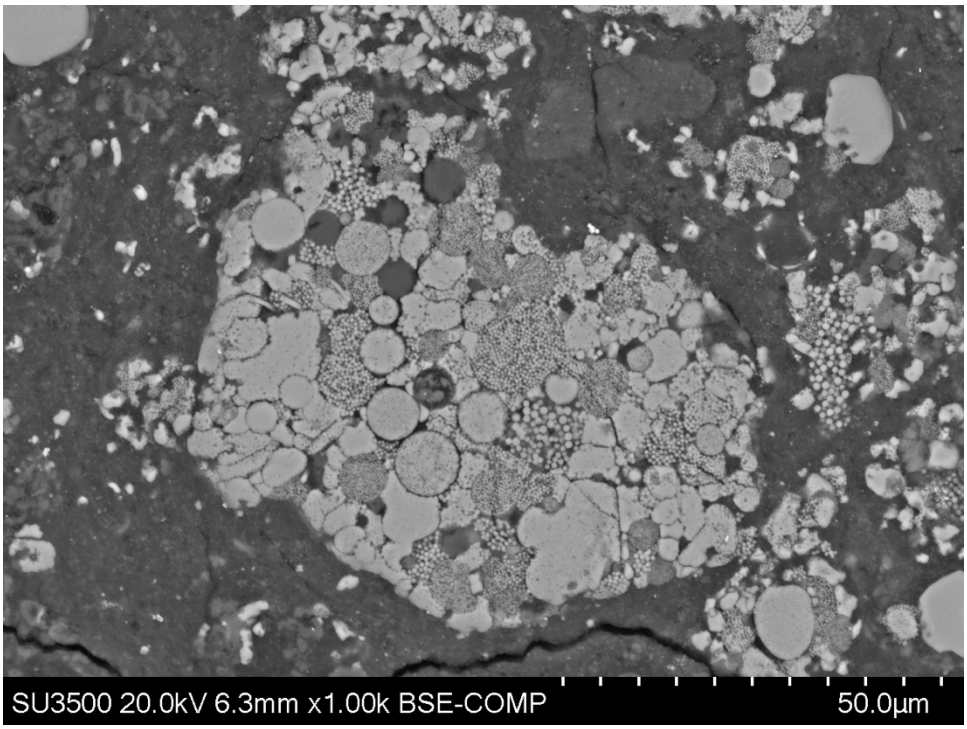

Figure 4.2: Examples of magnetite framboids in the Tarda meteorite that show a range of cluster sizes and shapes, with distinct constituent particle sizes and packing abilities. The large central cluster is likely a magnetite framboid pseudomorph after a euhedral sulfide crystal, similar to that observed in Zolensky et al. (2002) .

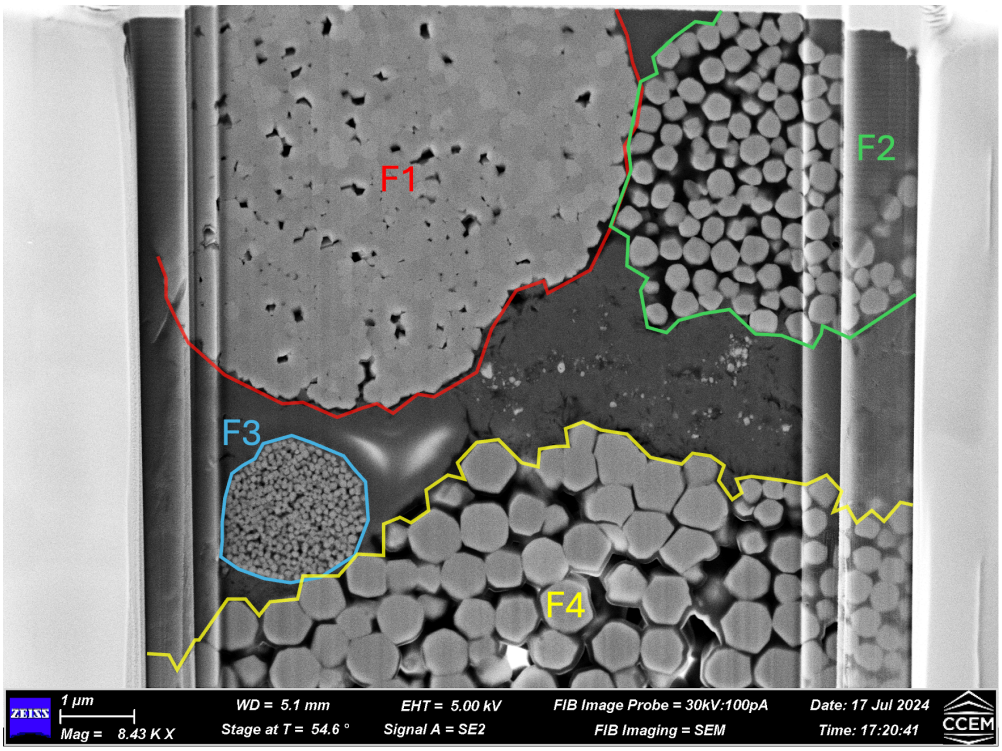

Figure 4.3: SEM image of the location selected for TEM. Four magnetite framboid clusters are observed and outlined, labelled F1-F4.

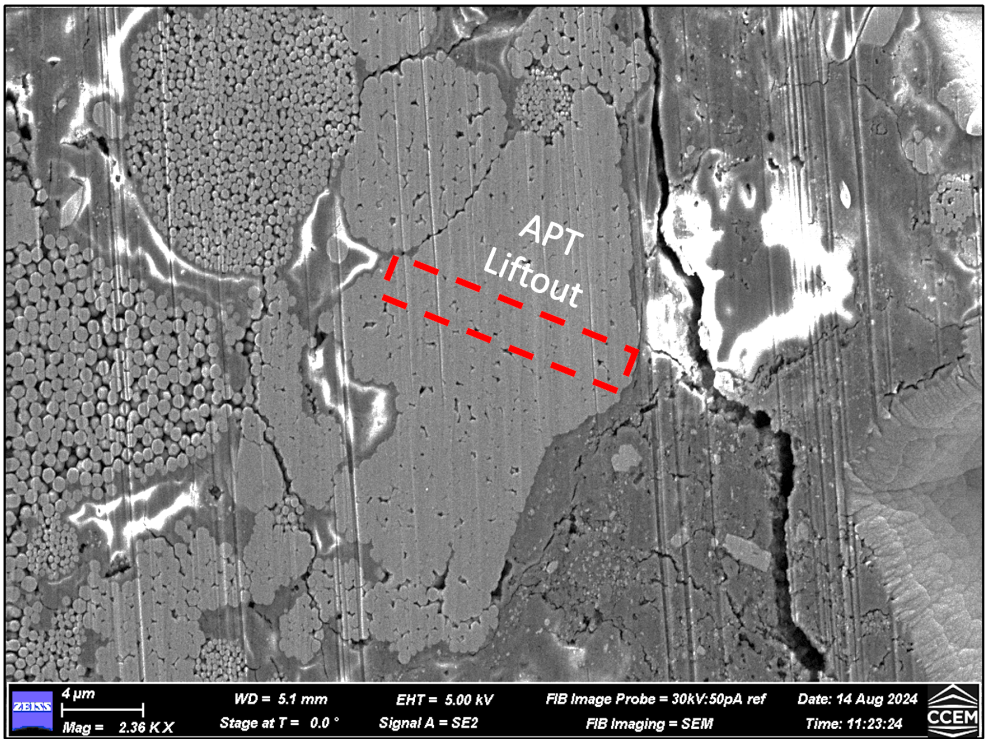

Figure 4.4: SEM image of the magnetite framboid and liftout region selected for APT.

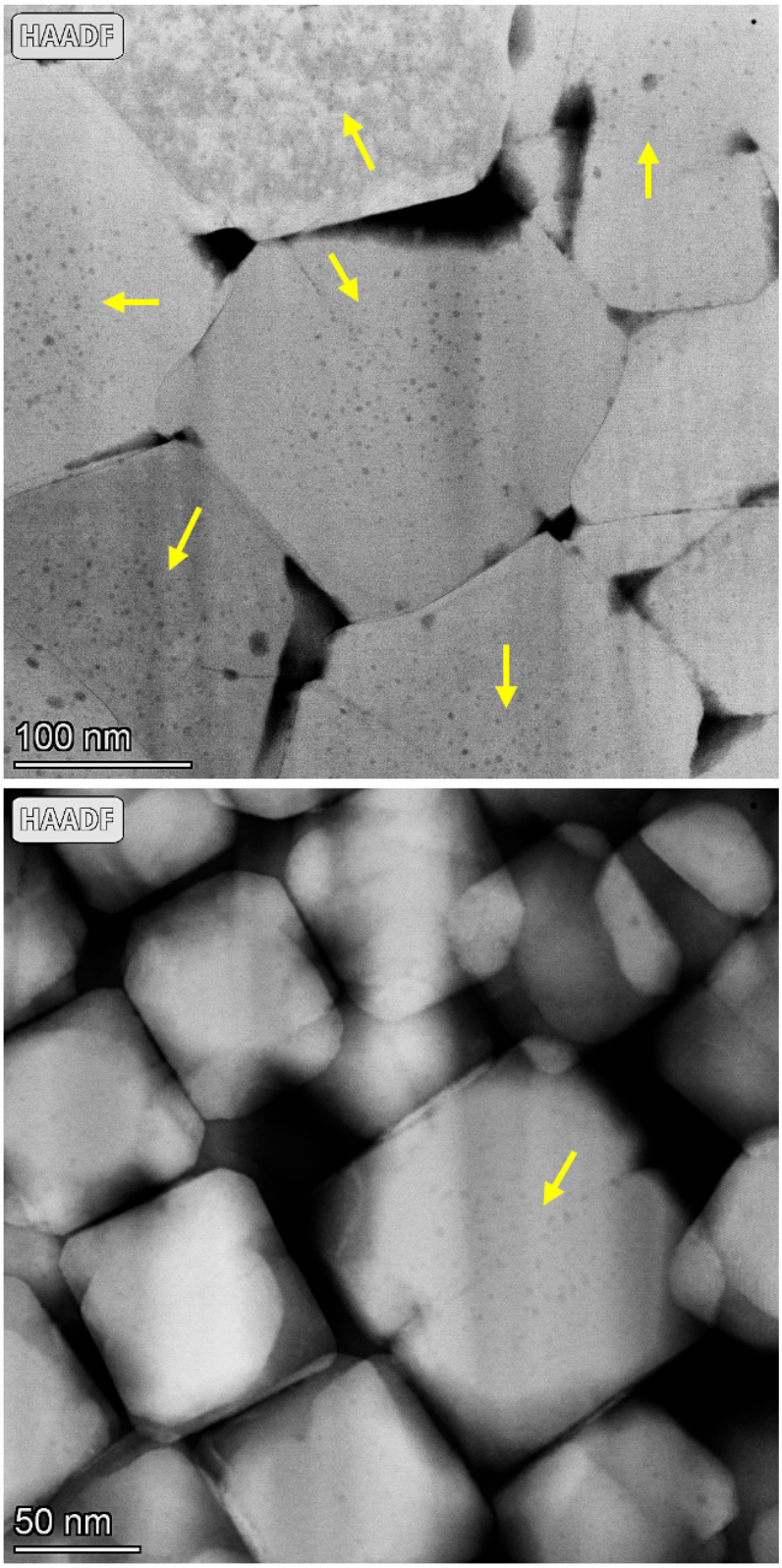

Figure 4.5: HAADF images of framboids F1(top) and F3 (bottom), showing nanometric pores in the magnetite, examples of which are identified by the yellow arrows.

4.3.2. TEM Chemistry

The selected TEM region contains three primary phases (Figure 4.6): (1) magnetite framboids; (2) dolomite; and (3) matrix material, likely consisting of a cryptocrystalline smectite and serpentine (Bates et al., 2024; Gattacceca et al., 2021). Here, we use TEM and EDS to investigate the nanoscale chemistry of the magnetite particles to better reveal the chemistry of the aqueous system from which magnetite precipitated.

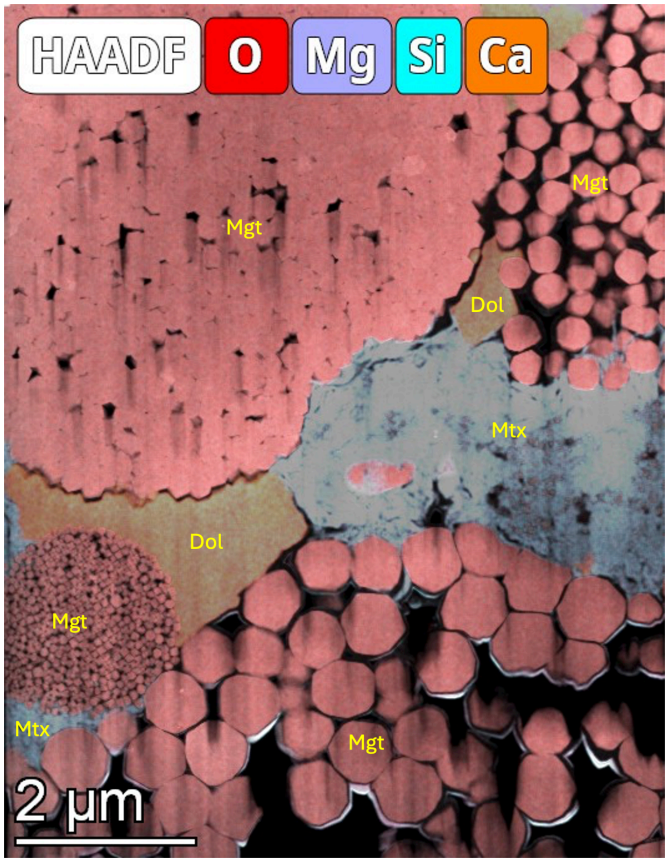

Figure 4.6: TEM section image with O, Mg, Si, and Ca EDS data. Minerals labeled are magnetite (Mgt), dolomite (Dol), and matrix (Mtx) consisting of nanometre-scale crystals of smectite and serpentine.

At the nanometre scale, all observed framboid clusters contain magnetite particles with distinct nano-scale chemistry coating their surfaces. Using TEM and EDS, we see elemental evidence of:

(1) titanium, (2) silicon, (3) magnesium, (4) calcium, (5) sulfur, (6) carbon. The instances of each will be described below.

1. Titanium (Ti) coatings on magnetite particles were observed in each framboid (Figure 4.7A,C,E,G). In all instances, the titanium coatings appear to be ~5 nm thick and may form a continuous or discontinuous border around each affected magnetite particle. Individual magnetite particles in framboids F1 and F3 appear to be most enriched in Ti relative to the background, with boundaries showing over twice the Ti enrichment (Figure B1). F2 displays lesser Ti enrichment, typically as discontinuous boundaries. Ti enrichment in F4 is most sparse, with most occurrences between the magnetite particle border with matrix material.
2. Silicon (Si) coatings on magnetite particles were observed in most framboids, but were more infrequent and weakly detected (Figure 4.7B,D,F,H). Similar to Ti, the Si coatings appear to be ~5 nm thick that form continuous or discontinuous borders around the magnetite particles. In F1 and F3, Si appears be associated with Ti, best viewed in framboid F3 (Figure 4.7E,F). Si occurs most commonly in F1 and F3, with boundaries capturing approximately twice the Si enrichment relative to the background (Figure B1). In F2 and F4, Si is rare and discontinuous.
3. Magnesium (Mg) coatings on magnetite particles were only observed very rarely in framboids F2, F3, and F4. In all observed cases, Si was present as well (Figure 4.8). In F3 and F4, Mg was only observed near the magnetite-matrix boundary. This likely corresponds to a remnant Mg and Si rich phyllosilicate phase.

4. In one rare case, we observed calcium (Ca) and sulfur (S) in F1 (Figure 4.9). Rather than bordering a magnetite particle as seen previously, this Ca and S enrichment occurred as a small ~30 nm cluster, possibly entrained within a magnetite crystal defect.
5. Carbon is ubiquitous within pore space, usually as continuous boundaries around magnetite particles, primarily in framboids F2-F4. The thickness of the carbon-rich domains may vary and extends up to >100 nm. This, however, is likely an artifact of sample preparation, and will be addressed further in the discussion.

Notably, no elemental enrichments beyond Fe and O were correlated with the nanometric pores via EDS, generally similar to the findings of the pores in spherulitic magnetite in Ryugu (Dobrică et al., 2023). This is likely attributed to low x-ray counts that could be additionally masked by the x-rays generated from the electron beam transmitting first through their host magnetite.

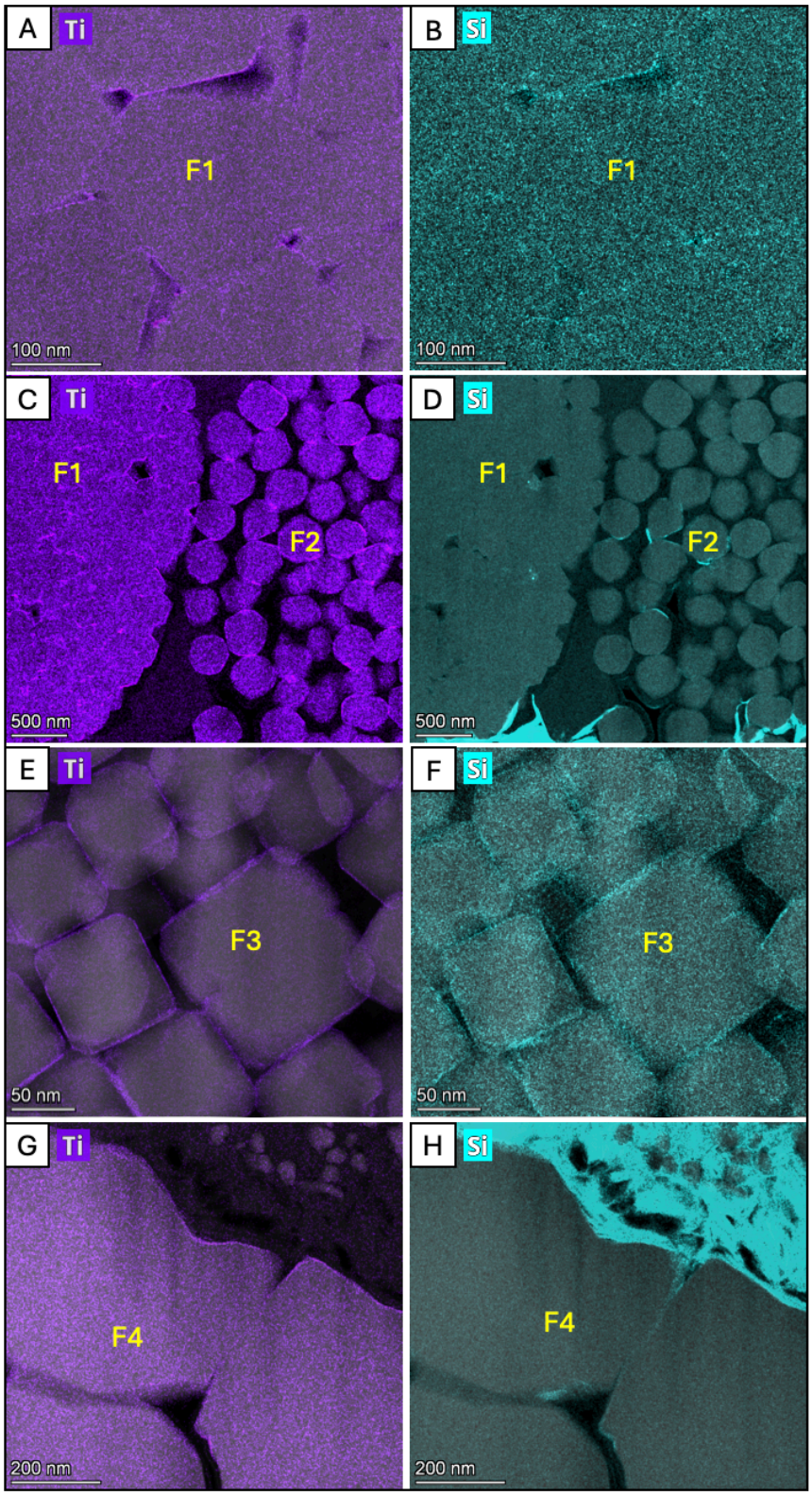

Figure 4.7: Ti and Si EDS maps overlain on some magnetite grains analyzed via TEM. Each image corresponds to magnetite particles from framboids F1-F4 (Figure 4.3).

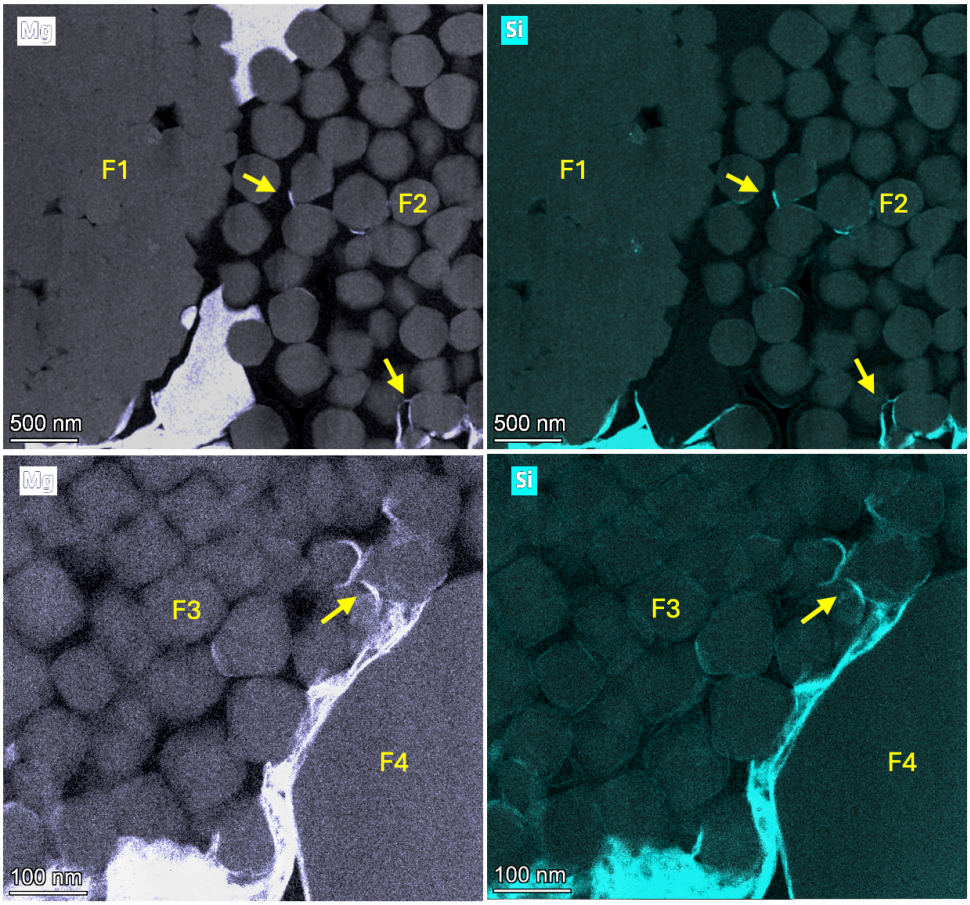

Figure 4.8: Mg and Si content comparison for framboid F2, F3, and F4. Arrows highlight regions that contain both Mg and Si.

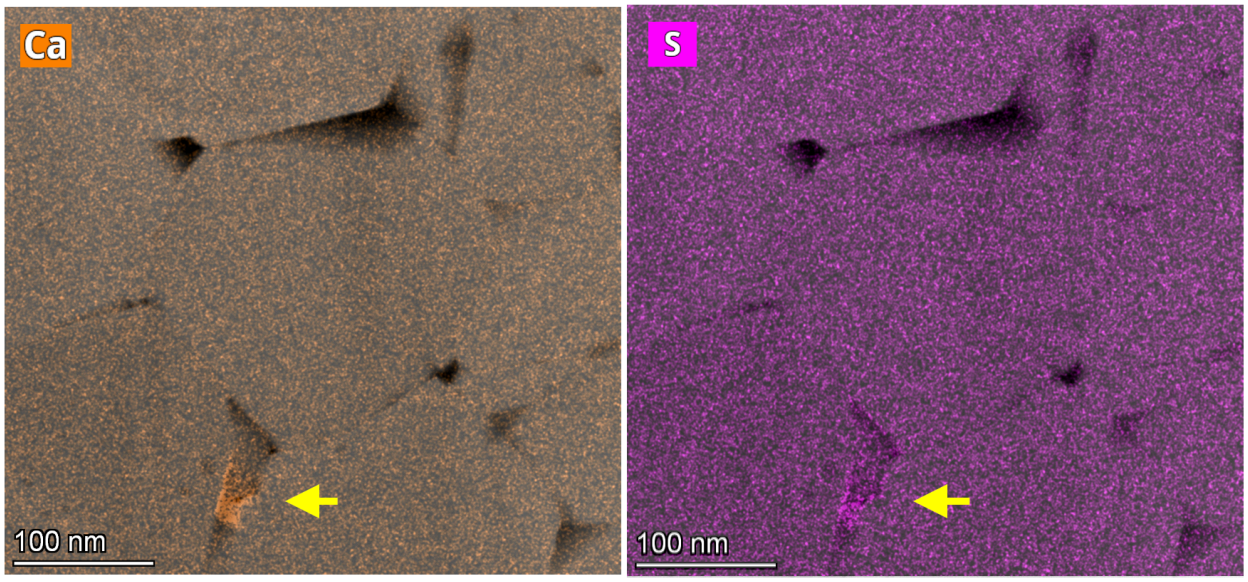

Figure 4.9: Localized enrichment of Ca and S within a darker magnetite feature, denoted by the arrow.

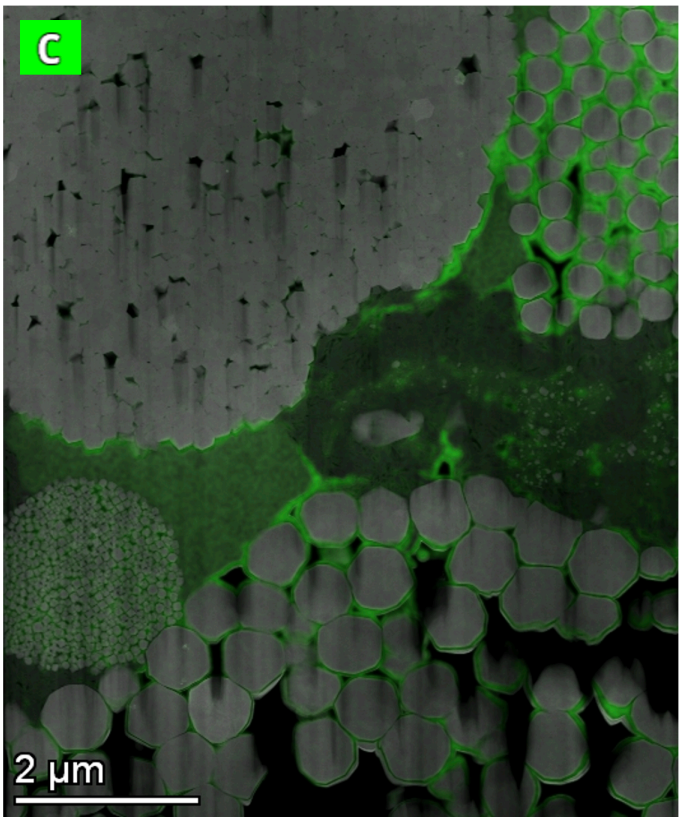

Figure 4.10: EDS map showing the presence of C over the TEM section.

4.3.3. APT Chemistry

Of four prepared tips from the liftout region in Figure 4.4, two failed early during APT analysis, likely due to internal structural heterogeneity resulting in premature fracturing of the material. Datasets R5047_35350 and R5047_35357, however, yielded good data, both capturing unique chemical features. Dataset R5047_35350 captures a ~5 nm thick planar feature enriched in Na, Mg, Ca, Mn, and Si, while dataset R5047_35357 captures small (~5 nm) clusters of Si and Na. The mass-to-charge spectrum is shown below, with the peak families labelled that were used to generate the reconstruction. The solutes of interest, Na, Mg, Ca, and Mn, appear doubly charged. Si appears as both doubly charged single ions and as singly charged molecular ions of SiO. The natural isotopic abundances of SiO were used to increase confidence in this species along the interface, due to a possible overlap with FeO_2^{2+} ions.

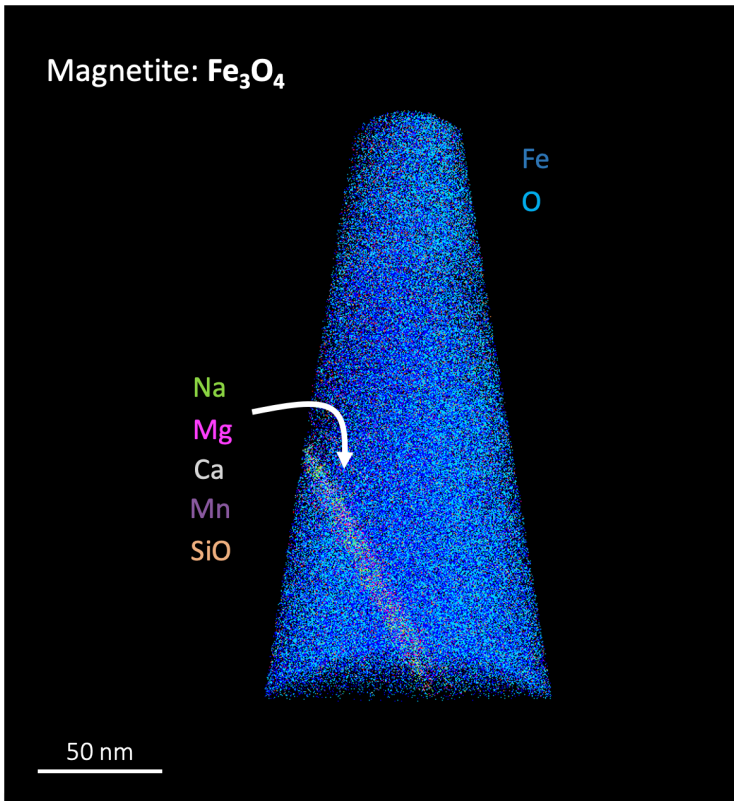

Figure 4.11: APT tip reconstruction for dataset R5047_35350 showing a planar feature in magnetite that is enriched in Na, Mg, Ca, Mn, and SiO

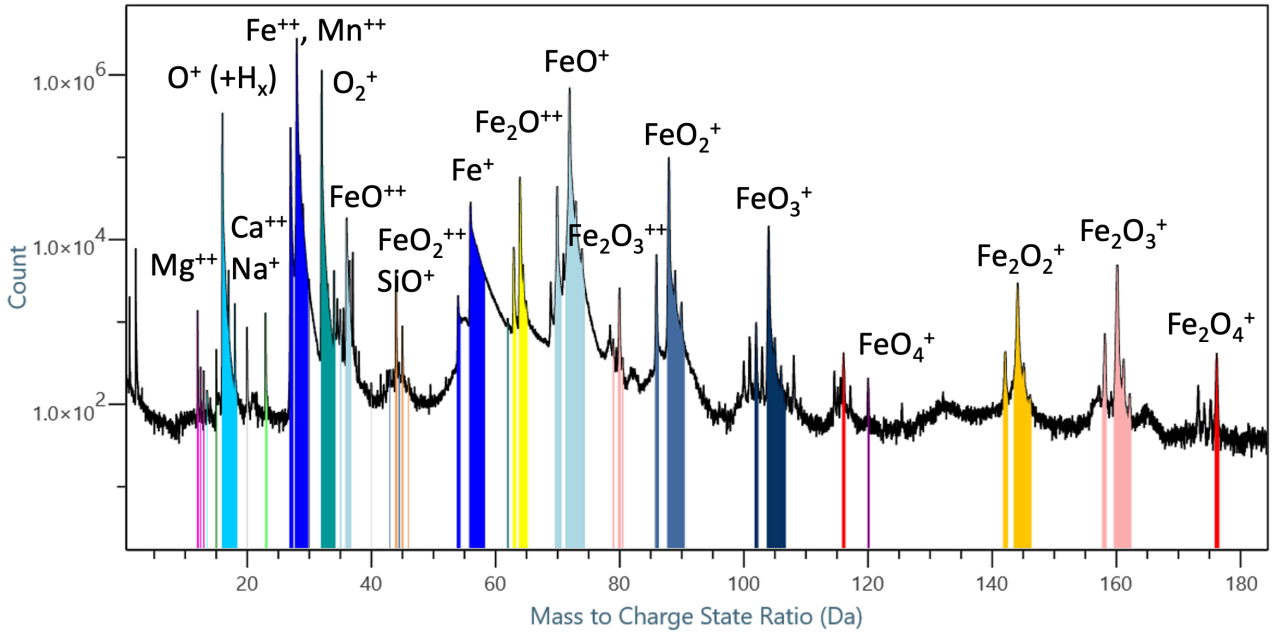

Figure 4.12: Mass to charge state ratio plot for dataset R5047_35350, showing the labeled peaks.

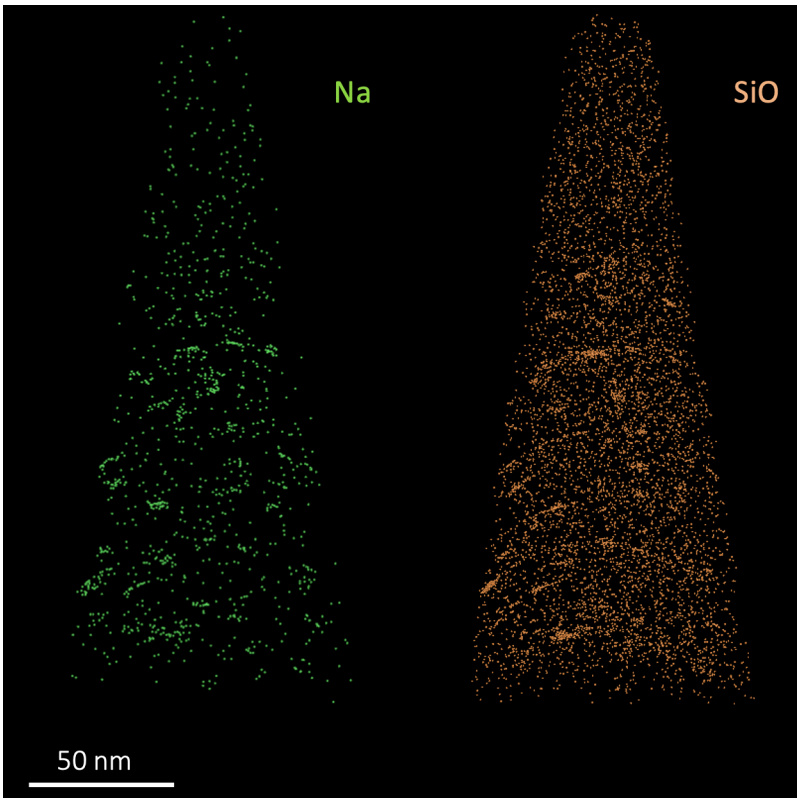

Figure 4.13: APT tip reconstruction for dataset R5047_35357 showing clusters of Na and Si dispersed throughout the magnetite.

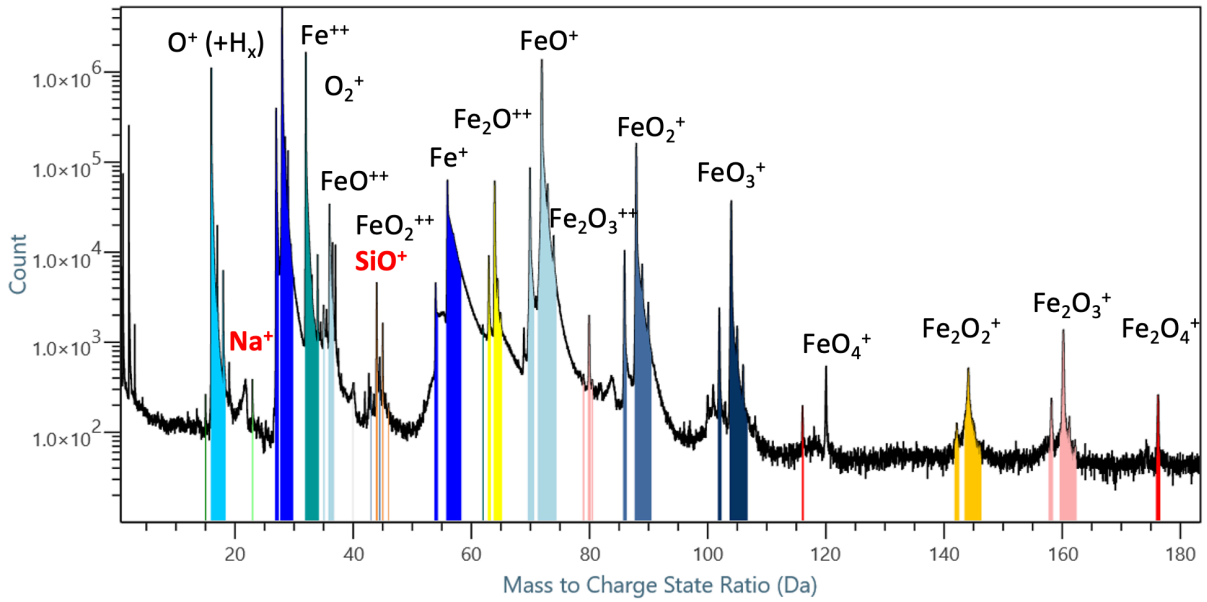

Figure 4.14: Mass to charge state ratio for data R5047_35357. Na and SiO are shown in red, and correlate to the clusters observed in Figure 4.13.

4.4. Discussion

4.4.1. Reliability of TEM EDS Chemistry Data

Transmission Electron Microscopy (TEM) requires intensive sample preparation, which introduces multiple opportunities for sample contamination and/or chemical modification. To ensure that the reported elemental distributions are meaningful, it is critical to first establish that the observed chemistries are (1) indigenous to the sample and (2) have remained in place.

Several materials used during sample preparation could contribute exogenous elements:

- Carbon (C) and Tungsten (W) were used as protective coating. Prior to ion milling, a thin C coat was followed by a thicker W layer to protect the region of interest.
- The ion beam used gallium (Ga) for milling.
- Copper (Cu) and Yttrium (Y) originate from the TEM grid.

In our sample, C is observed extensively in open pores. While C may indeed be expected to adsorb to magnetite, boundary thicknesses for adsorbed atoms are expected to be < 10 nm (Kimura et al., 2013; Lee et al., 2020) which is in stark contrast to the observed C surface features that are often >80 nm in thickness (Figure 4.10). Additionally, C is also found lining pores within matrix material, and SEM imaging shows that these C-rich magnetite boundaries only appear after milling. Thus, C is interpreted to be a contaminant and is excluded from further interpretation in the TEM dataset.

The other potential contaminants (W, Ga, Cu, and Y) were typically detected as background throughout the sample in trace quantities. Since they were not expected in Tarda, they were removed.

During ion milling, sputtered material may resettle nearby on the sample, possibly modifying the local chemistry. However, since the ion milling uses a Ga beam, Ga would be expected to

locally redeposit with any other excavated particles, acting as a chemical tracer. Thus, all TEM regions were screened for anomalously high Ga concentrations and any region containing significant Ga enrichment was excluded from interpretations.

While TEM offers high spatial resolution, its invasive sample preparation poses a risk of altering chemical signatures. In contrast, Atom Probe Tomography (APT) samples are prepared differently, with the final milling step using a 5 kV beam to minimize gallium damage. In addition, ions from the direct surface of the specimen are not collected, as those ion trajectories are beyond the angular FOV of the instrument and are therefore not included in the final reconstructed datasets In our APT dataset, a ~5 nm interior planar feature is resolved, consistent in scale with the chemical boundary thicknesses identified via TEM and EDS. This cross-validation provides confidence that the chemical enrichment features detected via TEM are real, rather than artifacts introduced during sample preparation.

4.4.2. Magnetite Framboid Crystallization Conditions

Magnetite framboids are common in aqueously altered carbonaceous material, and are usually associated with other aqueous mineral phases, including smectite and serpentine matrix material, carbonates, and/or sulfides (Brearley, 2006; Chan et al., 2016; Harju et al., 2014; Kerridge et al., 1979; Kimura et al., 2013; Lee et al., 2025; Rubin & Ma, 2017). From petrographic relationships and in situ oxygen isotopes from individual phases (section 3.3) magnetite is generally known to precipitate from the altering fluid early in the aqueous alteration crystallization sequence, prior to carbonates and after sulfides (occasionally as their pseudomorphs), consistent with their occurrences in other carbonaceous material (Kimura et al., 2013; McCain et al., 2023; Tonui et al., 2014; White et al., 2020; Zolensky et al., 2002). The pH for magnetite crystallization is generally alkaline, constrained by the presence of saponite and surface charges of magnetite (Kimura et al.,

2013; White et al., 2020), which agrees with observed trend in computer models and analogous aqueous alteration laboratory experiments (Kikuchi et al., 2022; Zolensky et al., 1989). In an Fe, S, and O system, magnetite tends to be more stable at lower temperatures, however higher temperatures seem to benefit analogous terrestrial framboid pyrite crystallization (Crerar et al., 1978; Ohfuji & Rickard, 2005). Additionally, these laboratory experiments find that supersaturation is required for framboid synthesis, such that the crystal nucleation rate is significantly greater than the rate of crystal growth. This is then followed by rapid crystal growth, which consumes the crystal nutrients at greater rates than they are supplied, exhausting the system to prevent the growth of a more massive crystalline structure (Kimura et al., 2013; Nozawa et al., 2011; Ohfuji & Rickard, 2005). In meteorites, this likely occurs either from direct precipitation in fluid, or through pseudomorph of Fe-sulfide framboids in oxidizing conditions (Kimura et al., 2013; White et al., 2020; Zolensky et al., 2002). While terrestrial magnetite framboids can pseudomorph after Fe-sulfide framboids, this mechanism, however, appears unlikely in meteorites since Fe-sulfide framboids have never been found, and central voids observed in magnetite particles after pseudomorphing terrestrial pyrite are absent (Suk et al., 1990). Thus, magnetite framboids in meteorites likely precipitate directly from solution.

Magnetite framboids, therefore, formed as colloidal crystals; a type of material that has been extensively studied due to their ability to model atomic systems at observable scales, and their applications to optics and photonic crystals, etc (e.g. Gasser, 2009; Hou et al., 2018; Lee & Lee, 2023; Nozawa et al., 2011; Schroden et al., 2002). Colloidal crystals balance attractive and repulsive forces to organize into well-ordered structures. For magnetite, van der waals and magnetic forces attract each particle, requiring suitable repulsive forces to prevent agglomeration (Derjaguin & Landau, 1941; Kimura et al., 2013; Nozawa et al., 2011; Verwey & Overbeek, 1948;

White et al., 2020). This repulsive force originates from the surface charge of the magnetite, which depends on temperature and pH of the solution. At temperatures between 30-100˚C, the point of zero charge generally occurs between a pH range of 5.4-6.8, with more acidic and alkaline solutions forming positive and negative surface charges respectively (Kimura et al., 2013; Regazzoni et al., 1983; Tewari & Mclean, 1972).

The relatively uniform sizes of magnetite particles within each framboid suggest each framboid experienced homogeneous nucleation within a closed system. In a low gravity planetesimal, this is likely achieved in water droplets, with the surface tension of the water forming the closed system boundary (Kimura et al., 2013). Once the framboid nucleation conditions in each droplet were met, magnetite crystal growth must have occurred more rapidly than water evaporation. If external factors such as impact shock was responsible for driving the nucleation of the water droplet, homogenous nucleation and growth of framboids would not be expected (Kimura et al., 2013).

The sizes, shapes, and packing structures of the colloidal particles can be used to help determine a framboid crystallization sequence, probably on the local scale, since the supersaturation of magnetite crystal nutrients would gradually decrease as magnetite continues to form (Bates et al., 2024; Ono et al., 2024; Tsuchiyama et al., 2022). This would lower the nucleation rate, permitting larger crystals to grow, leading to a fine to coarse grained framboid crystallization sequence (Kimura et al., 2013; Ohfuji & Rickard, 2005; Tsuchiyama et al., 2022).

4.4.3. Crystallization Conditions of Framboids in Tarda

4.4.3.1. Temperature

In Tarda, magnetite generally forms between dolomite and sulfides in the aqueous alteration crystallization sequence, evidenced by dolomite grains engulfing magnetite crystals, oxygen isotopes analyzed in section 3.3, and magnetite framboid replacement of original sulfide crystals

(Bates et al., 2024; Figure 4.2). Thus, the temperature of magnetite precipitation can be constrained by the temperature of pre-forming sulfides, likely precipitating in equilibrium at 100-135˚C (Schrader et al., 2024), and the temperature of the first carbonates that likely precipitated at $90.4^{+29.9}_{-25.0}$˚C, identified from a co-precipitating magnetite-dolomite pair (section 3.4.3). Thus, we will assume magnetite precipitated at ~100˚C.

4.4.3.2. Crystallization Sequence

In the TEM region, the framboid magnetite particles in F1-F4 vary in size, where F1 (~90 nm) < F3 (~230 nm) < F2 (~380 nm) <F4 (~660 nm), possibly suggesting a crystallization sequence in that order. This agrees well with petrographic relationships between magnetite framboids found elsewhere in Tarda, which show that magnetite framboids with larger crystals tend to have more irregular framboid shapes and form rims around framboids with smaller crystals, implying later formation (Figure 4.15).

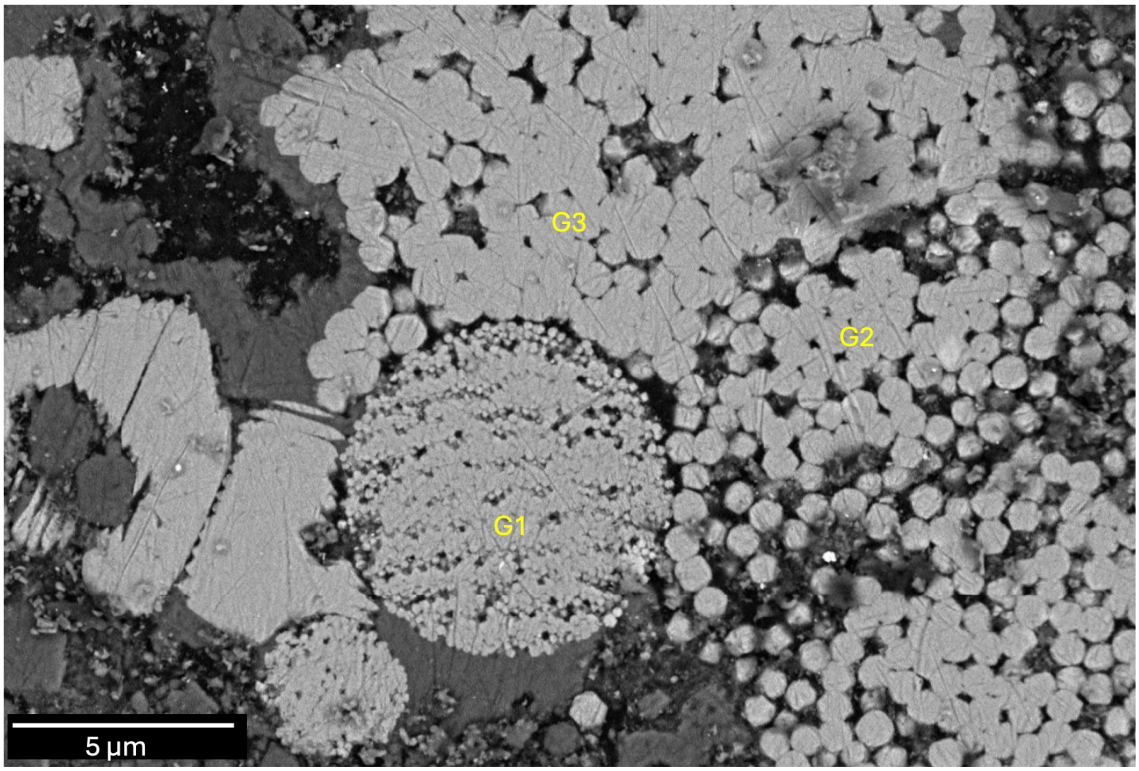

Figure 4.15: Magnetite textures in Tarda showing crystallization sequences based on petrographic relationships. The first, second, and third generations are labeled G1, G2, and G3, respectively.

4.4.3.3. Fluid Chemistry

Here, we report cations (such as titanium) adsorbed to magnetite particles in each magnetite framboid suggesting that the surface charge of magnetite was negative during growth. This requires that the pH of the aqueous solution from which magnetite precipitated was greater than 5.4, which is the point of zero charge for magnetite at ~100˚C (Regazzoni et al., 1983; Tewari & Mclean, 1972). This agrees well with the expected pH (>7) of altering fluid in carbonaceous chondrites (Kikuchi et al., 2022; White et al., 2020; Zolensky et al., 1989). Furthermore, the elements detected via EDS and APT constrain the cations that was present in the fluid while magnetite was forming.

Using EDS, we detected boundary enrichment of Ti and Si predominantly in F3 and F1, followed by F2 and then F4. This agrees well with the inferred crystallization order of the analyzed

framboids, possibly suggesting that the ionic strength of these elements decreased as subsequent framboids precipitated. Notably, the enrichment of Ca and S also occurs in framboid F1 but precipitated as a small (~10 nm) cluster, rather than coating the magnetite particle surface as observed with Ti and Si. Thus, this is probably not attributed to the same adsorption processes responsible for Ti and Si, however, could still be remnants of the fluid from which the magnetite precipitated, possibly precipitating in a crystal defect as the droplet evaporated. More evidence, however, is required for improved interpretations.

Atom Probe Tomography was performed on an irregular magnetite framboid with particle diameters of approximately 650 nm (Figure 4.4). This framboid rims nearby framboids, implying it formed later in the crystallization sequence. Thus, the APT target framboid is most similar to irregular framboid F4 in the TEM region (Figure 4.3). The APT dataset R5047_35350 mostly captured homogenously distributed Fe and O ions consistent with magnetite, but with a distinct ~5 nm thick planar feature that displays significant enrichments of Na, Si, Mg, Ca, and Mn relative to the surrounding crystal, all of which are present in trace amounts (< 0.5 at%). This planar feature additionally corresponds to a decrease in Fe and O. This relates well to the 5 nm thick features identified via TEM and EDS, and likely represents a boundary between two colloidal magnetite crystals, with the element enrichment representing adsorbed ions onto the magnetite particle surfaces. These ions were, therefore, likely present in the mother solution from which the magnetite precipitated, and preferentially accumulated in the grain boundaries as colloidal magnetite growth progressed.

The APT has notably captured a distinct set of boundary-enriched elements not detected by TEM-EDS. This discrepancy may be attributed to the following:

1. Different localized fluid chemistry: It is possible that the altering fluid had different chemical compositions governed by local mineral dissolution. Thus, the APT and TEM/EDS may reflect real chemical differences that reflect heterogeneous aqueous alteration conditions.
2. Analytical limitations: Elemental detection via EDS performs best when analyzing higher atomic numbers and abundances (e.g. Ritchie et al., 2018; Williams & Carter, 2009). Thus, aside from Si (which was infrequently and weakly observed via EDS), the other elements that were detected in the APT mass spectrum were likely too light and/or scarce to be detected by the EDS above the background. Notably, however, the TEM and EDS captured the largest abundance/background ratio for Ti, which was not detected via APT. The mass to charge state ratio of Ti^{+} and Ti^{2+} would be ~48 Da and ~24 Da respectively, of which no peaks were present (Figure 4.12). It is possible, however, that Ti could ionize with oxygen, as Ti_xO_x, but many of these peaks would overlap with Fe_xO_x, or O_x which is expected to dominate the spectrum and could mask any contribution from Ti.

The feature described here has also been reported by White et al. (2020), who conducted APT on a magnetite framboid in the C2-ung meteorite Tagish Lake. Tagish Lake is thought to have shared a parent asteroid with Tarda, possibly enabling fluid chemistry to be assessed spatially, while conditions were similar (Bates et al., 2024; Marrocchi et al., 2021; Schrader et al., 2024). White et al., (2020) report a captured boundary between two magnetite framboids, enriched in primarily Na, Ca, Mg, and Mn. They do not report Si, however, which was found in our dataset. This discrepancy may be due to the mass-to-charge spectrum overlap between SiO^{+} and FeO_2^{2+}, resolved in this study using typical isotopic abundances. Additionally, Riciputi et al. (1994) conducted SIMS analysis of carbonates in four CM (Mighei-like) chondrites and one CI (Ivuna-

like) chondrite, finding considerable trace abundances of Na, Fe, Mg, and Mn, relative to Ca, which the authors attributed to fluid chemical enrichments. Notably, Si was used to screen for contamination in their experiment. Thus, the results by Riciputi et al. (1994) are in excellent agreement with the results presented here, and for Tagish Lake by White et al. (2020), possibly suggesting similar fluid chemistries during both magnetite and carbonate formation, despite spatial, compositional, and temporal variations.

The second successful APT dataset (R5047_35357) was similarly dominated by uniform Fe and O, expected for magnetite. This dataset did not capture a planar feature associated with element enrichment, and peaks of Ca, Mg, and Mn were unable to be resolved from the background (Figure 4.13). Na and Si peaks, however, have remained but are constrained to nanometric (~5 nm) clusters, that are similar in size and shape to the nanometric pores observed in Figure 4.5. Using TEM, previous studies have identified similar nanometric pores in Ryugu, entrained within magnetite spherulites – a magnetite morphology that likely predates framboidal magnetite (Dobrică et al., 2023; Tsuchiyama et al., 2022). One magnetite spherulite analyzed by Dobrică et al. (2023) contained nanometer-scale acicular fibers that displayed enrichment of amorphous Si and Mg, which the authors suggest may be remnants of early fluid chemistry, similar to fluid inclusions found in chondritic halite (e.g. Zolensky et al., 1999). Dobrică et al. (2023) further attributes these pores to non-equilibrium magnetite growth, possibly governed by supersaturated conditions during the earliest stages of magnetite precipitation.

Thus, the agreement between size, and chemistry of the chemical clusters present in APT dataset R5047_35357, and the nanometric pores observed in TEM here and by Dobrică et al. (2023), suggests the nanometric pores in framboidal magnetite have been captured via APT. The nanometric clusters in APT are enriched in Si and Na, but Mg remained absent, differing from the

TEM-EDS signature identified by Dobrică et al., (2023). Since the magnetite framboids analyzed here likely precipitate later in the aqueous alteration sequence than the spherulitic magnetite analyzed by Dobrică et al., (2023) the distinct pore fluid chemistries between the two systems may highlight a decrease in Mg as magnetite precipitation progresses, and/or also reflect compositional differences between the Tarda and Ryugu parent bodies.

The pores entrained within the magnetite framboids must have predated the adsorbed ions on the magnetite surfaces. Since this was likely a closed chemical system confined to a water droplet (Kimura et al., 2013), this may suggest the droplet originally had higher concentrations of Si and Na, relative to Ca, Mg, and Mn, and were capable of segregating into the magnetite pores at concentrations suitable for detection via APT. Continuous magnetite growth and water evaporation then later enabled the remaining dissolved ions to precipitate at sufficient concentrations on the magnetite surfaces. Furthermore, the presence of the pores in late-stage magnetite framboid formation suggests that non-equilibrium magnetite precipitation could extend well beyond what was previously recognized (Dobrică et al., 2023). I therefore caution against assuming equilibrium magnetite growth in models such as oxygen isotope thermometry.

4.5. Implications for Organics

Aqueous alteration is known to modify organics, likely influencing the final organic content of the chondrite (e.g. Glavin et al., 2018; Herd et al., 2011; Pizzarello et al., 2006; Pizzarello et al., 2013). Thus, varying fluid conditions are expected to be captured by the organic content, with some environments being particularly conducive to life-relevant organics (e.g. Cooper et al., 2001, 2011; Schulte & Shock, 2004)

In the previous section, we have placed constraints on the fluid from which, at least, framboidal magnetite precipitated from. The temperature (~100˚C), pH (>5.4) and fluid chemistry (Na, Ti, Si,

Mg, Ca, Mn, and S) describe this fluid and, to an extent, its supply of reactants. Determining the influence these reactants would have on organics, however, is a challenging endeavor since diversity and abundance of the organic content in meteorites exhibits a considerable range, and seemingly displays a degree of randomness that is at odds with the relatively systematic organic inventory of the Earth (Glavin et al., 2018; Pizzarello et al., 2006; Pizzarello & Shock, 2010). Additionally, the influence that these parameters have on organics within the context of early planetesimals, is relatively unexplored. Glavin et al. (2018) pointedly notes that "… to date, there is no quantitative or even qualitative work of the influences of fluid composition, secondary mineralogy, and temperature on the organic contents of chondrites.".

Thus, while the influence of these parameters have not been directly investigated in carbonaceous chondrites, Glavin et al. (2010) has determined that meteorites with high degrees of aqueous alteration (such as petrologic type 1 samples) contain lower abundances of amino acids than their less altered counterparts (such as petrologic type 2 samples), suggesting that amino acid formation and/or preservation is better achieved under milder aqueous alteration conditions (Glavin et al., 2010, 2012). Physicochemical modeling of a rock with average CM (Mighei-type carbonaceous chondrite) suggests greater temperatures increase many organic compound abundances, including amino acids, amines, and ketones (Schulte & Shock, 2004). Additionally, analogous terrestrial thermodynamic models and laboratory experiments suggest that alkaline fluids, warmer temperatures, and catalytic metals (such as Mg^{2+}) are conducive for production of life-relevant organic molecules (Barge et al., 2019; Kitadai, 2015; Kitadai & Maruyama, 2018; Martin & Russell, 2007), suggesting that the aqueous conditions during magnetite precipitation supported organic synthesis. This is confirmed by Tunney et al. (2022), who directly analyzed organic compounds in Tarda and found complex organic molecules including amino acids,

although their abundances were not reported. In comparison, Tagish Lake was also altered by a chemically similar fluid (White et al., 2020), yet displays highly variable amino acid abundances (<0.1-5.4 ppm) between different samples, with some samples yielding abundances below detection limits (Glavin et al., 2012; Pizzarello et al., 2001). This highlights that the environment constrained in Tarda, while potentially favorable for organic synthesis, may differ in key reactants such as aldehydes or ammonia (White et al., 2020) or may spatially vary. Alternatively, intensive aqueous alteration may have degraded the organic content in specific regions (Glavin et al., 2012). Targeted laboratory experiments simulating a range of plausible fluid chemistries and alteration conditions could help clarify how these factors influence organic production on early planetesimals.

4.6. Conclusion

This nanoscale investigation of magnetite framboids in the Tarda meteorite provides insight into the fluid chemistry responsible for altering the Tarda meteorite while, at least, magnetite was precipitating. Using TEM, EDS, and APT, we detected chemical enrichment of Ti, Na, Si, Mg, Ca, S, and Mn on scales of 5–10 nm, which we interpret as chemical remnants of the mother solution from which the magnetite precipitated. The implied surface charge of the magnetite is negative which generally requires alkaline conditions. This is consistent with prior models for carbonaceous chondrite alteration and suggests that the aqueous system was enriched in a diverse suite of cations.

Framboidal magnetite textures and particle sizes suggest that magnetite formation occurred in a series of discrete nucleation and growth events, beginning with spherical framboids composed of smaller particles (such as ~90 nm), eventually progressing to irregular framboids composed of large particles (~1 μm). This progressive crystallization sequence, and the changing fluid

chemistry inferred from boundary compositions in EDS, imply that the availability of ionic species evolved as water–rock interactions proceeded.

The detection of trace Ti, Na, Mg, Ca, Mn, Si, and S in framboidal magnetite boundaries, coupled with alkaline and moderately warm (~100°C) conditions, highlights the potential for this fluid to promote organic synthesis. While the relationship between these specific fluid conditions and organic molecule production in Tarda remains uncertain, the chemistry inferred here aligns with experimental and theoretical work that suggests alkaline fluids and cation-rich environments may support prebiotic synthesis pathways. This work provides compositional constraints for future experiments studying the influence of aqueous environments on organic and mineral production.

4.7. References

Barge, L. M., Flores, E., Baum, M. M., Velde, D. G. V., & Russell, M. J. 2019. Redox and pH gradients drive amino acid synthesis in iron oxyhydroxide mineral systems. *Proceedings of the National Academy of Sciences of the United States of America*, *116*(11), 4828–4833. https://doi.org/10.1073/pnas.1812098116

Bates, H. C., Aspin, R., Fu, C. Y., Harrison, C. S., Feaver, E., Branagan-Harris, E., King, A. J., Bryson, J. F. J., Sridhar, S., & Nichols, C. I. O. 2024. Extent of alteration, paleomagnetic history, and infrared spectral properties of the Tarda ungrouped carbonaceous chondrite. *Meteoritics and Planetary Science*. https://doi.org/10.1111/maps.14224

Brearley, A. J. (2006). The Action of Water. *Meteorites and the Early Solar System II*, 587–624.

Chan, Q. H. S., Zolensky, M. E., Martinez, J. E., Tsuchiyama, A., & Miyake, A. 2016. Magnetite plaquettes are naturally asymmetric materials in meteorites. *American Mineralogist*, *101*(9), 2041–2050. https://doi.org/10.2138/am-2016-5604

Cohen, B. A., & Coker, R. F. 2000. Modeling of Liquid Water on CM Meteorite Parent Bodies and Implications for Amino Acid Racemization. *Icarus*, *145*(2), 369–381. https://doi.org/10.1006/icar.1999.6329

Cooper, G., Kimmich, N., Belisle, W., Sarinana, J., Brabham, K., & Garrel, L. 2001. *Carbonaceous meteorites as a source of sugar-related organic compounds for the early Earth*. *414*(6866), 879–883. https://doi.org/10.1038/414879a

Cooper, G., Reed, C., Nguyen, D., Carter, M., & Wang, Y. 2011. Detection and formation scenario of citric acid, pyruvic acid, and other possible metabolism precursors in carbonaceous meteorites. *PNAS*, *108*(34), 14015–14020. https://doi.org/10.1073/pnas.1105715108/-/DCSupplemental

Crerar, D. A., Susak, N. J., Borcsik, M., & Schwartz, S. 1978. Solubility of the buffer assemblage pyrite + pyrrhotite + magnetite in NaCl solutions from 200 to 350°C. *Geochimica et Cosmochimica Acta*, *42*, 1427–1437.

Derjaguin, B., & Landau, L. 1941. Theory of the Stability of Strongly Charged Lyophobic Sols and of the Adhesion of Strongly Charged Particles in Solutions of Electrolytes. *Acta Physiochim*, *14*, 633–662.

Dobrică, E., Ishii, H. A., Bradley, J. P., Ohtaki, K., Brearley, A. J., Noguchi, T., … Tsuda, Y. 2023. Nonequilibrium spherulitic magnetite in the Ryugu samples. *Geochimica et Cosmochimica Acta*, *346*, 65–75. https://doi.org/10.1016/j.gca.2023.02.003

Gasser, U. 2009. Crystallization in three-and two-dimensional colloidal suspensions. *Journal of Physics Condensed Matter*, *21*(20). https://doi.org/10.1088/0953-8984/21/20/203101

Gattacceca, J., McCubbin, F. M., Grossman, J., Bouvier, A., Bullock, E., Chennaoui Aoudjehane, H., Debaille, V., D'Orazio, M., Komatsu, M., Miao, B., & Schrader, D. L. 2021. The Meteoritical Bulletin, No. 109. *Meteoritics and Planetary Science*, *56*(8), 1626–1630. https://doi.org/10.1111/maps.13714

Glavin, D P, Alexander, D., Aponte, J. C., Dworkin, J. P., Elsila, J. E., & Yabuta, H. 2018. The Origin and Evolution of Organic Matter in Carbonaceous Chondrites and Links to Their Parent Bodies. In *Primitive Meteorites and Asteroids: Physical, Chemical, and Spectroscopic Observations Paving the Way to Exploration* (pp. 205–271).

Glavin, Daniel P., Callahan, M. P., Dworkin, J. P., & Elsila, J. E. 2010. The effects of parent body processes on amino acids in carbonaceous chondrites. *Meteoritics and Planetary Science*, *45*(12), 1948–1972. https://doi.org/10.1111/j.1945-5100.2010.01132.x

Glavin, Daniel P., Elsila, J. E., Burton, A. S., Callahan, M. P., Dworkin, J. P., Hilts, R. W., & Herd, C. D. K. 2012. Unusual nonterrestrial l-proteinogenic amino acid excesses in the Tagish Lake meteorite. *Meteoritics and Planetary Science*, *47*(8), 1347–1364. https://doi.org/10.1111/j.1945-5100.2012.01400.x

Harju, E. R., Rubin, A. E., Ahn, I., Choi, B. G., Ziegler, K., & Wasson, J. T. 2014. Progressive aqueous alteration of CR carbonaceous chondrites. *Geochimica et Cosmochimica Acta*, *139*, 267–292. https://doi.org/10.1016/j.gca.2014.04.048

Herd, C. D. K., Blinova, A., Simkus, D. N., Huang, Y., Tarozo, R., Alexander, C. M. O'D., … Stroud, R. M. 2011. Origin and evolution of prebiotic organic matter as inferred from the Tagish Lake meteorite. *Science*, *332*(6035), 1304–1307. https://doi.org/10.1126/science.1203290

Hou, J., Li, M., & Song, Y. 2018. Patterned Colloidal Photonic Crystals. *Angewandte Chemie*, *57*, 2544–2553. https://doi.org/10.1002/ange.201704752

Hua, X., & Buseck, P. R. 1998. Unusual forms of magnetite in the Orgueil carbonaceous chondrite. *Meteoritics and Planetary Science*, *33*, 215–220. https://doi.org/10.1111/j.1945-5100.1998.tb01335.x

Kerridge, J. F., Mackay, A. L., & Boynton, W. V. 1979. Magnetite in CI Carbonaceous Meteorites: Origin by Aqueous Activity on a Planetesimal Surface. *Science*, *205*, 395–397.

Kikuchi, S., Shibuya, T., Abe, M., & Uematsu, K. 2022. Experimental chondrite–water reactions under reducing and low-temperature hydrothermal conditions: Implications for incipient aqueous alteration in planetesimals. *Geochimica et Cosmochimica Acta*, *319*, 151–167. https://doi.org/10.1016/j.gca.2021.11.006

Kimura, Y., Sato, T., Nakamura, N., Nozawa, J., Nakamura, T., Tsukamoto, K., & Yamamoto, K. 2013. Vortex Magnetic Structure in Framboidal Magnetite Reveals Existence of Water Droplets in an Ancient Asteroid. *Nature Communications*, *4*, 1–8. https://doi.org/10.1038/ncomms3649

Kitadai, N. 2015. Energetics of Amino Acid Synthesis in Alkaline Hydrothermal Environments. *Origins of Life and Evolution of Biospheres*, *45*(4), 377–409. https://doi.org/10.1007/s11084-015-9428-3

Kitadai, N., & Maruyama, S. 2018. Origins of building blocks of life: A review. *Geoscience Frontiers*, *9*(4), 1117–1153. https://doi.org/10.1016/j.gsf.2017.07.007

Krot, A. N., Keil, K., Scott, E. R. D., Goodrich, C. A., & Weisberg, M. K. 2013. Classification of Meteorites and Their Genetic Relationships. In *Treatise on Geochemistry: Second Edition* (2nd ed., Vol. 1). https://doi.org/10.1016/B978-0-08-095975-7.00102-9

Lee, J., & Lee, S. 2023. Colloidal Optics and Photonics: Photonic Crystals, Plasmonics, and Metamaterials. *Current Optics and Photonics*, *7*(6), 608–637. Retrieved from http://creativecommons.

Lee, M. R., Alexander, C. M. O'D., Bischoff, A., Brearley, A. J., Fujiya, W., Le, C., Ashley, G., Dobric, E., Kooten, E. Van, Krot, A. N., Leitner, J., Marrocchi, Y., Remusat, L., Telus, M., Tsuchiyama, A., & Vacher, L. G. 2025. Low-Temperature Aqueous Alteration of Chondrites. *Space Science Reviews*, *221*(11). https://doi.org/10.1007/s11214-024-01132-8

Lee, M. R., Lindgren, P., & Sofe, M. R. 2014. Aragonite, breunnerite, calcite and dolomite in the CM carbonaceous chondrites: High fidelity recorders of progressive parent body aqueous alteration. *Geochimica et Cosmochimica Acta*, *144*, 126–156. https://doi.org/10.1016/j.gca.2014.08.019

Marrocchi, Y., Avice, G., & Barrat, J.-A. 2021. The Tarda Meteorite: A Window into the Formation of D-type Asteroids. *The Astrophysical Journal Letters*, *913*(1), 1–8. https://doi.org/10.3847/2041-8213/abfaa3

Martin, W., & Russell, M. J. (2007). On the origin of biochemistry at an alkaline hydrothermal vent. *Philosophical Transactions of the Royal Society B: Biological Sciences*, Vol. 362, pp. 1887–1926. https://doi.org/10.1098/rstb.2006.1881

McCain, K. A., Matsuda, N., Liu, M. C., McKeegan, K. D., Yamaguchi, A., Kimura, M., … Tsuda, Y. 2023. Early fluid activity on Ryugu inferred by isotopic analyses of carbonates and magnetite. *Nature Astronomy*, *7*(3), 309–317. https://doi.org/10.1038/s41550-022-01863-0

Nozawa, J., Tsukamoto, K., Van Enckevort, W., Nakamura, T., Kimura, Y., Miura, H., Satoh, H., Nagashima, K., & Konoto, M. 2011. Magnetite 3D colloidal crystals formed in the early solar system 4.6 billion years ago. *Journal of the American Chemical Society*, *133*(23), 8782–8785. https://doi.org/10.1021/ja2005708

Ohfuji, H., & Rickard, D. 2005. Experimental syntheses of framboids - A review. *Earth-Science Reviews*, *71*(3–4), 147–170. https://doi.org/10.1016/j.earscirev.2005.02.001

Ono, H., Tsuchiyama, A., Matsumoto, M., Miyake, A., Matsuno, J., Nakamura, T., Yasutake, M., Takeuchi, A., & Tachibana, S. 2024. Development of 3D Crystal Shape Description Including Orientation Using XNCT and TEM and Its Application to Ryugu Sample. *55th Lunar and Planetary Science Conference*, (1488). https://doi.org/10.1126/science

Pizzarello, S. 2006. The chemistry of life's origin: A carbonaceous meteorite perspective. *Accounts of Chemical Research*, *39*(4), 231–237. https://doi.org/10.1021/ar050049f

Pizzarello, S, Cooper, G. W., & Flynn, G. J. 2006. The Nature and Distribution of the Organic Material in Carbonaceous Chondrites and Interplanetary Dust Particles. In *Meteorites and the Earth Solar System II*. Retrieved from www.nrao.edu,

Pizzarello, S., Huang, Y., Becker, L., Poreda, R. J., Nieman, R. A., Cooper, G., & Williams, M. 2001. The organic content of the Tagish Lake meteorite. *Science*, *293*(5538), 2236–2239. https://doi.org/10.1126/science.1062614

Pizzarello, S, & Shock, E. 2010. The organic composition of carbonaceous meteorites: the evolutionary story ahead of biochemistry. *Cold Spring Harbor Perspectives in Biology*, *2*(3), 1–20. https://doi.org/10.1101/cshperspect.a002105

Pizzarello, Sandra, Davidowski, S. K., Holland, G. P., & Williams, L. B. 2013. Processing of meteoritic organic materials as a possible analog of early molecular evolution in planetary environments. *Proceedings of the National Academy of Sciences of the United States of America*, *110*(39), 15614–15619. https://doi.org/10.1073/pnas.1309113110

Regazzoni, A. E., Blesa, M. A., & Maroto, A. J. G. 1983. Interfacial Properties of Zirconium Dioxide and Magnetite in Water. *Journal of Colloid And Interface Science*, *91*(2), 560–570.

Riciputi, L. R., Mcsween, H. Y., Johnson, C. A., & Prinz, M. 1994. Minor and trace element concentrations in carbonates of carbonaceous chondrites, and implications for the compositions of coexisting fluids. *Geochimica et Cosmochimica Acta*, *58*(4), 1343–1378.

Ritchie, N. W. M., Newbury, D. E., Lowers, H., & Mengason, M. 2018. Exploring the limits of EDS microanalysis: Rare earth element analyses. *IOP Conference Series: Materials Science and Engineering*, *304*(1). https://doi.org/10.1088/1757-899X/304/1/012013

Rubin, A. E., & Ma, C. 2017. Meteoritic minerals and their origins. *Chemie Der Erde*, Vol. 77, pp. 325–385. https://doi.org/10.1016/j.chemer.2017.01.005

Schrader, D. L., Cloutis, E. A., Applin, D. M., Davidson, J., Torrano, Z. A., Foustoukos, D., Alexander, C. M. O. D., Domanik, K. J., Matsuoka, M., Nakamura, T., Zega, T. J., Brennecka, G. A., & Render, J. 2024. Tarda and Tagish Lake: Samples from the same outer Solar System asteroid and implications for D- and P-type asteroids. *Geochimica et Cosmochimica Acta*, *380*(September 2023), 48–70. https://doi.org/10.1016/j.gca.2024.07.007

Schroden, R. C., Al-Daous, M., Blanford, C. F., & Stein, A. 2002. Optical properties of inverse opal photonic crystals. *Chemistry of Materials*, *14*(8), 3305–3315. https://doi.org/10.1021/cm020100z

Schulte, M., & Shock, E. 2004. Coupled organic synthesis and mineral alteration on meteorite parent bodies. *Meteoritics and Planetary Science*, *39*(9), 1577–1590. https://doi.org/10.1111/j.1945-5100.2004.tb00128.x

Suk, D., Peacor, D. R., & Van der Voo, R. 1990. Replacement of pyrite framboids by magnetite in limestone and implications for palaeomagnetism. *Nature*, *345*, 611–613.

Suttle, M. D., King, A. J., Schofield, P. F., Bates, H., & Russell, S. S. 2021. The aqueous alteration of CM chondrites, a review. *Geochimica et Cosmochimica Acta*, Vol. 299, pp. 219–256. https://doi.org/10.1016/j.gca.2021.01.014

Tewari, P. H., & Mclean, A. W. 1972. *Temperature Dependence of Point of Zero Charge of Alumina and Magnetite*. *40*(2), 267–272.

Tonui, E., Zolensky, M., Hiroi, T., Nakamura, T., Lipschutz, M. E., Wang, M. S., & Okudaira, K. 2014. Petrographic, chemical and spectroscopic evidence for thermal metamorphism in carbonaceous chondrites I: CI and CM chondrites. *Geochimica et Cosmochimica Acta*, *126*, 284–306. https://doi.org/10.1016/j.gca.2013.10.053

Tsuchiyama, A., Matsumoto, M., Matsuno, J., Nakamura, T., Noguchi, T., Yasutake, M., … Watanabe, S. 2022. 3D Morphologies of Magnetite, Sulfides, Carbonates and Phosphates in Ryugu Samples and Their Crystallization Sequence During Aqueous Alteration. *85th Annual Meeting of The Meteoritical Society 2022*, *15*, 7944–7951.

Tunney, L. D., Hill, P. J. A., Herd, C. D. K., & Hilts, R. W. 2022. Organic compounds in the Tarda C2 ungrouped carbonaceous chondrite: Evaluating the sources of contamination in a desert fall. *Meteoritics and Planetary Science*, *57*(4), 850–865. https://doi.org/10.1111/maps.13800

Verwey, E. J. W., & Overbeek, J. T. G. 1948. *Theory of the stability of lyophobic colloids*. Elsevier Publishing Company.

White, L. F., Tait, K. T., Langelier, B., Lymer, E. A., Černok, A., Kizovski, T. V., Ma, C., Tschauner, O., & Nicklin, R. I. 2020. Evidence for sodium-rich alkaline water in the Tagish Lake parent body and implications for amino acid synthesis and racemization. *Proceedings of the National Academy of Sciences of the United States of America*, *117*(21), 11217–11219. https://doi.org/10.1073/pnas.2003276117

Williams, D. B., & Carter, C. B. 2009. *Transmission Electron Microscopy: A Textbook for Material Science*. Springer.

Wilson, B. J. K., Cecco, V. E. D. I., Garvie, L. A. J., Tait, K. T., & Daly, M. G. 2024. A sample preparation guide for clay-rich carbonaceous chondrites. *Meteoritics and Planetary Science*, *59*(3), 560–567. https://doi.org/10.1111/maps.14140

Zolensky, M. E., Nakamura, K., Gounelle, M., Mikouchi, T., Kasama, T., Tachikawa, O., & Tonui, E. 2002. Mineralogy of Tagish Lake: An ungrouped type 2 carbonaceous chondrite. *Meteoritics and Planetary Science*, *37*(5), 737–761. https://doi.org/10.1111/j.1945-5100.2002.tb00852.x

Zolensky, Michael E, Bodnar, R. J., Gibson Jr, E. K., Nyquist, L. E., Reese, Y., Shih, C.-Y., & Wiesmann, H. 1999. Asteroidal Water Within Fluid Inclusion-Bearing Halite in an H5 Chondrite. *Science*, *285*(10), 1377–1379. Retrieved from www.sciencemag.org

Zolensky, Michael E, Bourcier, W. L., & Gooding, J. L. 1989. Aqueous Alteration on the Hydrous Asteroids: Results of EQ3/6 Computer Simulations. *Icarus*, *78*, 411–425.

CHAPTER 5. Conclusion

In this dissertation, constraints were placed on the temperature, timing, chemical evolution, and composition of the fluid responsible for altering the Tarda meteorite. Additionally, a new sample preparation method was developed, enabling the high-resolution study of Tarda and other fragile clay-rich meteorites.

Chapter 2 addressed the unique sample preparation challenges associated with the swelling clays that dominate the matrix of Tarda. Conventional polishing methods typically use polar liquids which causes the sample to rapidly crumble, preventing high-quality surface preparation. To overcome this, a non-polar, clay-sensitive polishing procedure was developed that preserves the textural integrity of the sample while producing surfaces suitable for sensitive microanalytical techniques. This method enabled the analyses presented in subsequent chapters, while also providing a practical methodology for the preparation of other polar-sensitive extraterrestrial materials, such as samples from Ryugu, Bennu, or similarly altered meteorites.

In Chapter 3, in situ SIMS was employed to investigate the isotopic composition of dolomite and magnetite in Tarda and make comparisons to, primarily, Tagish Lake. Oxygen, carbon, and manganese-chromium isotopic analyses were used to constrain the temperature, timing, and fluid evolution during aqueous alteration. Oxygen-isotope thermometry indicates that dolomite precipitated at approximately 100°C, while Mn-Cr dating suggests that dolomite precipitation occurred ~4.563 billion years ago. Oxygen and carbon isotopes suggest significant water-rock interaction, revealing that Tarda was probably more aqueously altered than Tagish Lake.

In Chapter 4, the nanoscale geochemistry of five magnetite framboids in Tarda was studied to constrain the composition of the altering fluid. Using TEM and EDS, fluid trace element enrichments were identified. Further APT analysis captured a ~5 nm thick planar feature enriched

in Na, Si, Mg, Ca, and Mn, and numerous ~5 nm clusters enriched in Si and Na, likely revealing the chemistry within a captured magnetite grain boundary and nanometric pores, respectively. This cation enriched chemistry implies negative magnetite surface charge conditions, generally requiring precipitation from an alkaline fluid. Textural and chemical variability between framboid generations further suggest progressive changes in fluid composition during local alteration.

Overall, this work provides an extensive characterization of the fluid that altered the unique Tarda meteorite. In the broader context, these results help constrain the fluid conditions experienced by some primitive asteroids prior to delivering their contents to the early planets. Additionally, the fluid parameters identified in this work provide a foundation for future experimental studies and modeling efforts aimed at understanding the chemical pathways that may have contributed to prebiotic organic synthesis in the early Solar System.

FUTURE WORK

The results presented in this dissertation highlight four themes that could warrant future study. Each theme will be explained below.

Theme 1 – Further exploring the relationship between Tarda and Tagish Lake: Tarda and Tagish Lake are two of only few meteorites that have a P- and D-type spectral reflectance signature (Hiroi et al., 2001; Schrader et al., 2024). Furthermore, they are thought to record heterogeneous aqueous alteration from the same parent body (Bates et al., 2024; Marrocchi et al., 2021; Schrader et al., 2024). Isotopic analyses, however, on secondary minerals in Tagish Lake are sparse, limiting our understanding of its aqueous alteration history. Future work should collect C and triple O isotopes in Tagish Lake, while taking care to log the lithologies from which the analyses came. Additionally, the effect aqueous alteration has on their spectral signatures should be explored.

Theme 2 – Aqueous alteration laboratory experiments: This dissertation provides new constraints on the temperature, timing, and chemistry of the fluid that altered Tarda. However, the effect that temperature, fluid composition, and mineralogy have on organic production in chondrites has never been explored in detail (Glavin et al., 2018). Thus, a series of controlled laboratory experiments should be conducted, each injecting realistic and varying fluid into chondrite simulants with the goal of determining productive fluid environments for biorelevant organic molecules on chondrites.

Theme 3 – Quantifying abundances of organics in Tarda: The new fluid parameters identified in this dissertation would have affected the production of organics in Tarda. The organic inventory of Tarda, however, remains largely uncharacterized. Future work should investigate both soluble and insoluble organic matter within Tarda to assess how its unique alteration history influenced organic synthesis and preservation. Additionally, this should be compared with the

organic content of Tagish Lake to determine how their unique aqueous alteration histories on similar accretionary components may affect organic production.

Theme 4 – Assessing spatial and temporal effects on aqueous alteration: All fluid parameters constrained in this dissertation come from the analysis of dolomite and magnetite, and thus, represent the fluid conditions while dolomite and magnetite were precipitating. All analyses were also performed from a 2.1-gram Tarda sample. As such, these results likely capture a snapshot of the aqueous environment in both time and space. To develop a more spatially representative understanding of parent body fluid composition, future work should analyze additional Tarda (and probably Tagish Lake) samples. Furthermore, expanding isotopic and geochemical studies to include other secondary phases, such as phyllosilicates or sulfides, would help track the temporal evolution of the fluid.

Bates, H. C., Aspin, R., Fu, C. Y., Harrison, C. S., Feaver, E., Branagan-Harris, E., King, A. J., Bryson, J. F. J., Sridhar, S., & Nichols, C. I. O. 2024. Extent of alteration, paleomagnetic history, and infrared spectral properties of the Tarda ungrouped carbonaceous chondrite. *Meteoritics and Planetary Science*. https://doi.org/10.1111/maps.14224

Glavin, D. P., Alexander, D., Aponte, J. C., Dworkin, J. P., Elsila, J. E., & Yabuta, H. 2018. The Origin and Evolution of Organic Matter in Carbonaceous Chondrites and Links to Their Parent Bodies. In *Primitive Meteorites and Asteroids: Physical, Chemical, and Spectroscopic Observations Paving the Way to Exploration* (pp. 205–271).

Hiroi, T., Zolensky, M. E., & Pieters, C. M. 2001. The Tagish Lake meteorite: A possible sample from a D-type asteroid. *Science*, *293*(5538), 2234–2236. https://doi.org/10.1126/science.1063734

Marrocchi, Y., Avice, G., & Barrat, J.-A. 2021. The Tarda Meteorite: A Window into the Formation of D-type Asteroids. *The Astrophysical Journal Letters*, *913*(1), 1–8. https://doi.org/10.3847/2041-8213/abfaa3

Schrader, D. L., Cloutis, E. A., Applin, D. M., Davidson, J., Torrano, Z. A., Foustoukos, D., Alexander, C. M. O'D., Domanik, K. J., Matsuoka, M., Nakamura, T., Zega, T. J., Brennecka, G. A., & Render, J. 2024. Tarda and Tagish Lake: Samples from the same outer Solar System asteroid and implications for D- and P-type asteroids. *Geochimica et Cosmochimica Acta*, *380*(September 2023), 48–70. https://doi.org/10.1016/j.gca.2024.07.007

APPENDICES

A: Chapter 2 Supplementary

SIMS Bias Corrections

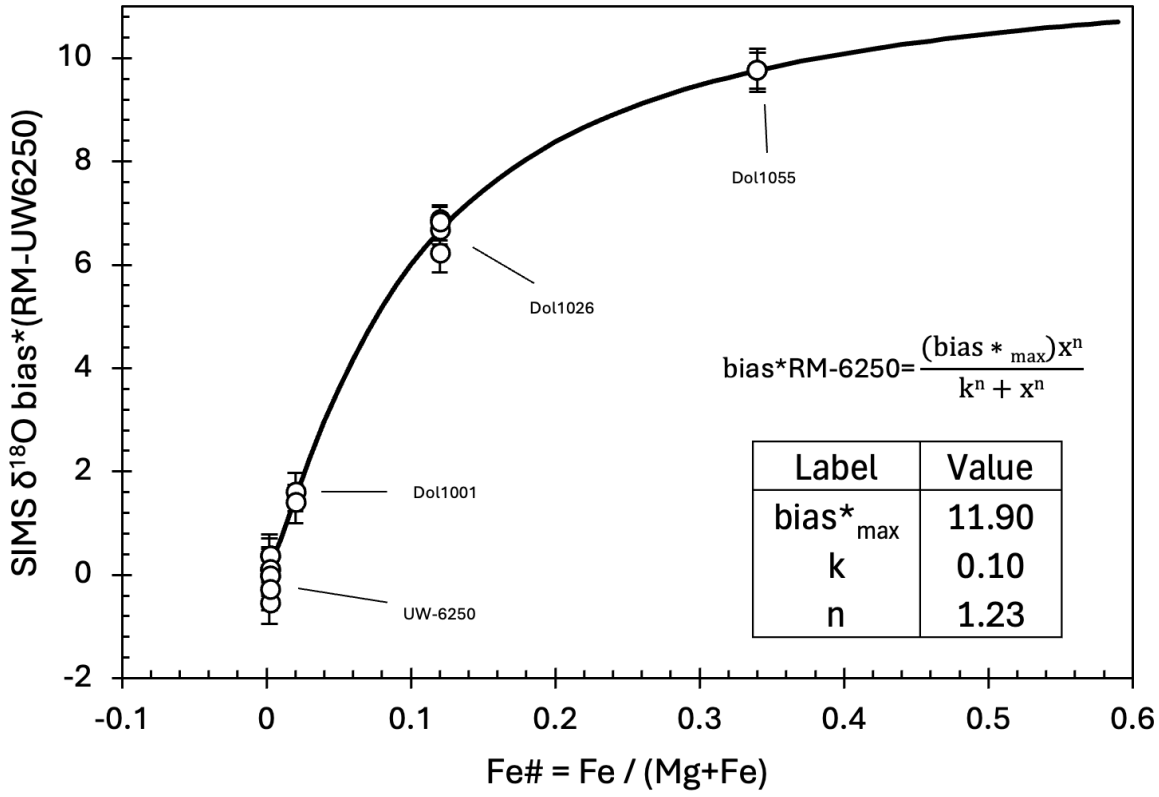

Figure A1: Instrumental $\delta^{18}O$ bias correction for a series of dolomite reference material (RM) ranging in Fe# fitted with a hill function (Śliwiński et al., 2016a). This curve was used to correct the instrument bias for the dolomite grains measured in Tarda.

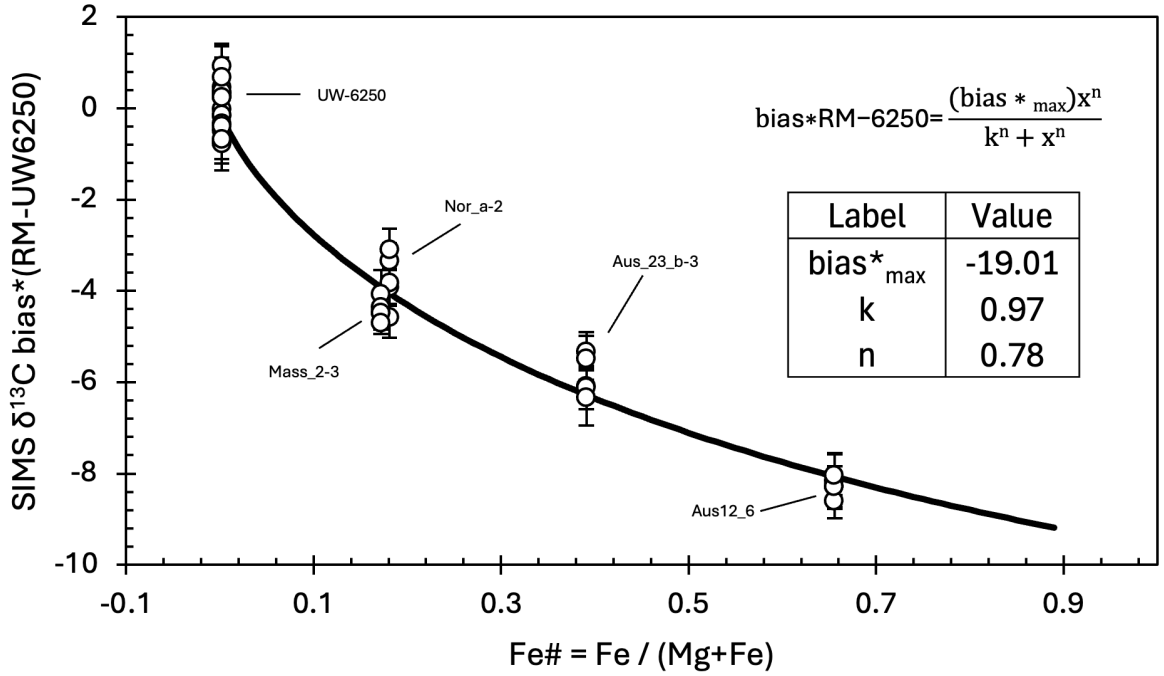

Figure A2: Instrumental $\delta^{13}C$ bias correction for instrument session one using a series of dolomite reference materials (RM) ranging in Fe# fitted with a hill function (Śliwiński et al., 2016b). This curve was used to correct the instrument bias for the dolomite grains measured in Tarda.

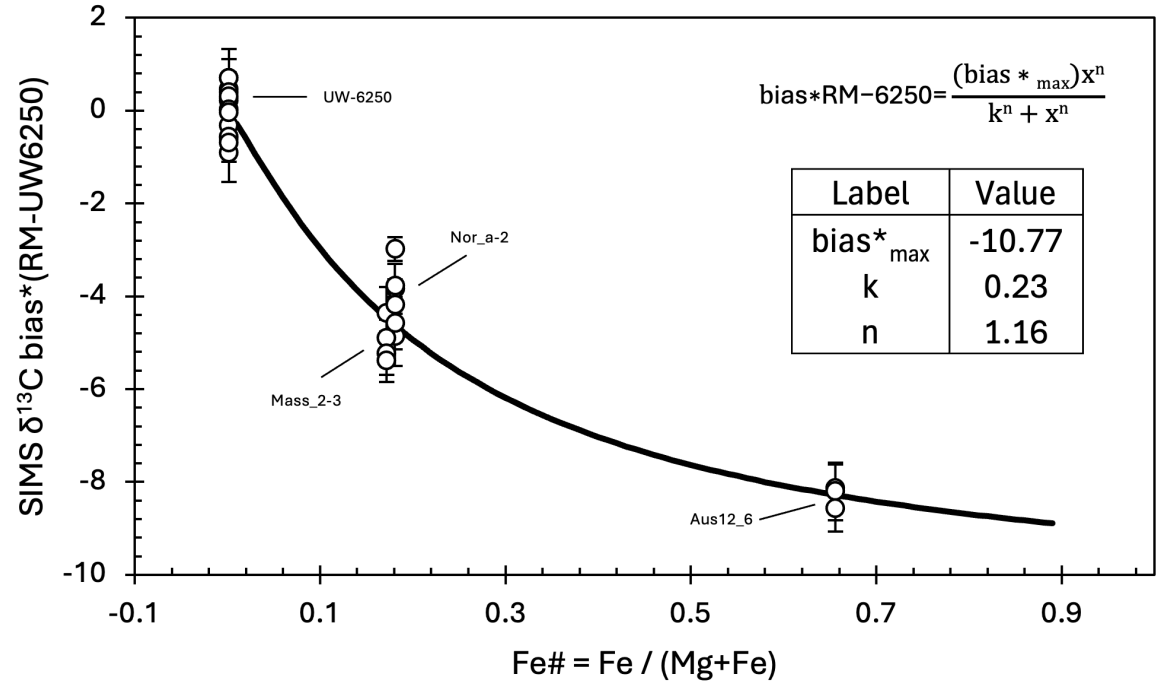

Figure A3: Instrumental $\delta^{13}C$ bias correction for instrument session two using a series of dolomite reference materials (RM) ranging in Fe# fitted with a hill function (Śliwiński et al., 2016b). This curve was used to correct the instrument bias for the dolomite grains measured in Tarda.

Contextual imaging of representative SIMS sites

While dolomite and magnetite crystals are ubiquitous throughout the matrix, only the rarer coarse-grained crystals were suitable for SIMS analysis with the CAMECA ims-1280, due to beam size constraints and the need for homogeneous, inclusion-free domains (Figure A4). Grains larger than ~10μm that were generally free of fractures, pores, or mineral inclusions were selected to minimize isotopic contamination during analysis (Figure A4; Figure A5). Backscattered electron (BSE) images of representative SIMS target grains (Figure A4) and resultant SIMS pits (Figure A5) are shown below.

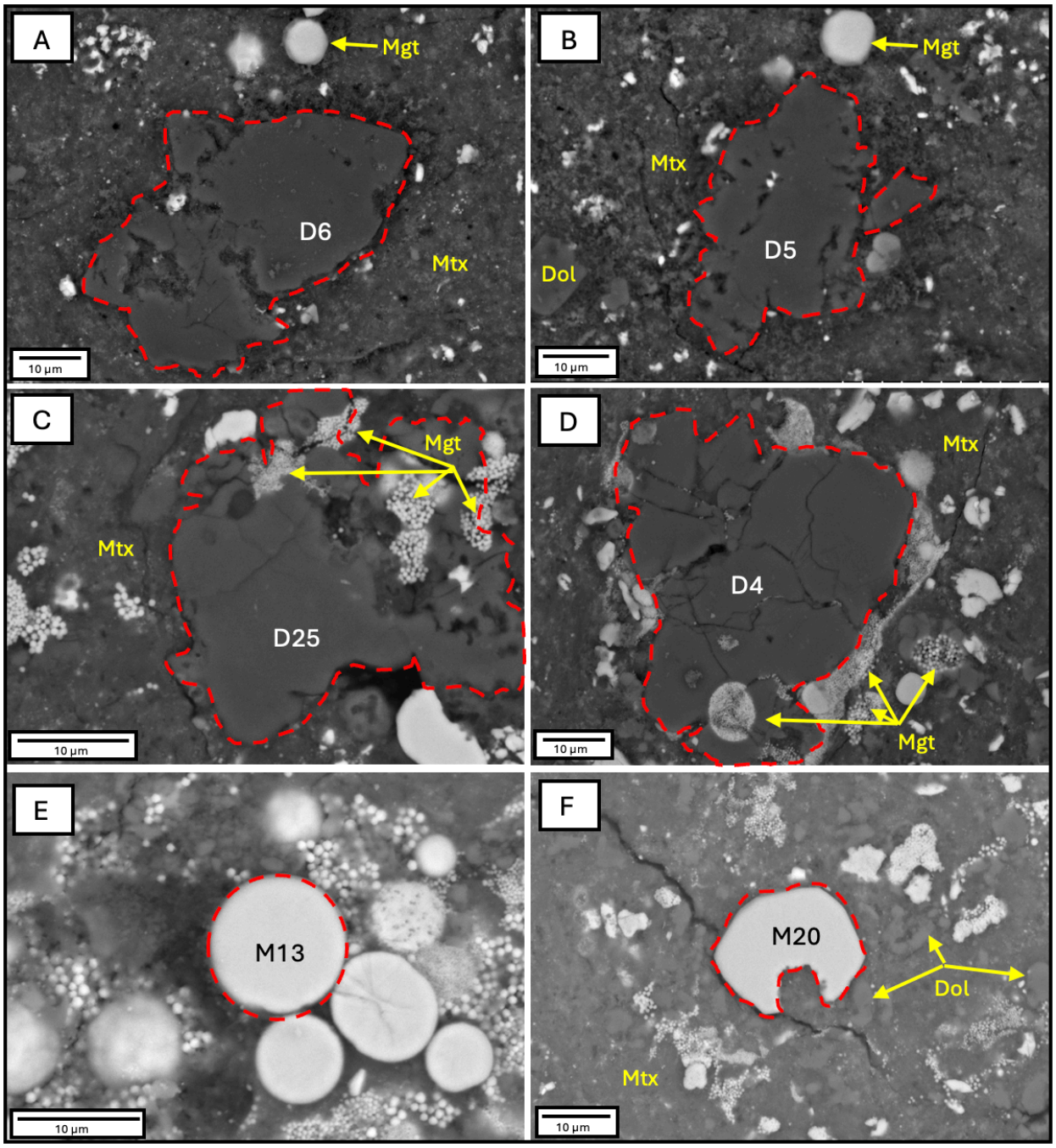

Figure A4: Backscatter electron images of some dolomite (A-D) and magnetite (E,F) grains that were analyzed via SIMS in this study. Analyzed dolomite and magnetite grains are outlined in red with the corresponding analysis ID in the centre of the outlined grain (Table 1; Table 2). Some examples of magnetite (Mgt), dolomite (Dol), and matrix (Mtx) are labelled in the images.

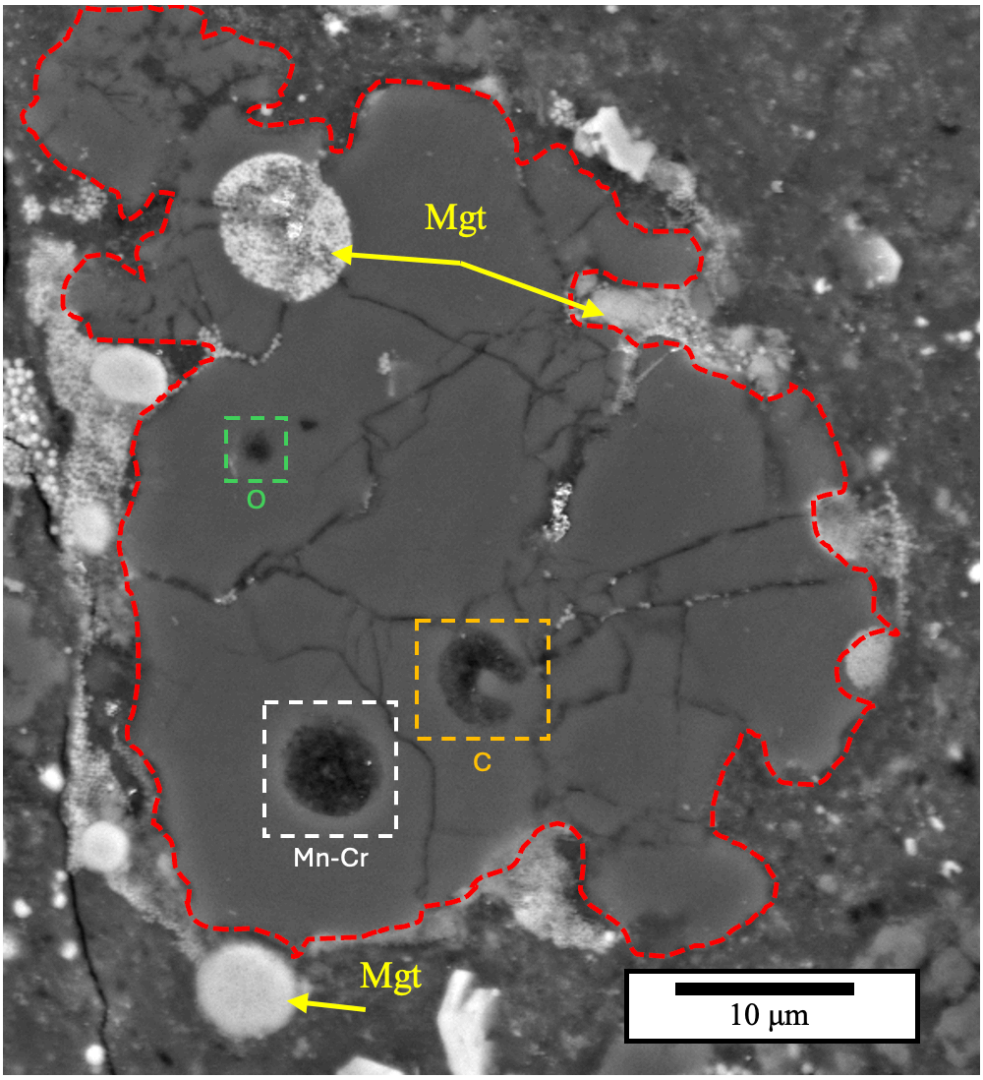

Figure A5: BSE image of a dolomite crystal (analysis ID D4; Table 1) with pits produced by the SIMS ion beam after Mn-Cr (white box), C (orange box), and O (green box) isotope measurements. The dolomite crystal is outlined in red, and some examples of associated magnetite are labelled (Mgt).

Isotope thermometry data

Table A1: Oxygen isotope data for all SIMS points collected from the dolomite and magnetite assemblage in Figure 7. Bolded values identify the two measurements selected for oxygen isotope thermometry based on proximity, magnetite morphology, and overlapping $\Delta^{17}O$ values (section 4.3).

Analysis ID	Phase	$\delta^{18}O$ (‰)	2σ	$\delta^{17}O$ (‰)	2σ	$\Delta^{17}O$ (‰)	2σ
DM1D1	Dol	24.77	0.97	13.01	1.58	0.13	1.73
DM1D2	**Dol**	**25.66**	**1.05**	**14.51**	**1.37**	**1.17**	**1.63**
DM1D3	Dol	25.12	0.95	13.19	1.43	0.13	1.59
DM1D4	Dol	24.26	0.83	13.34	1.73	0.73	1.99
DM1M1	Mgt (pla.)	0.71	2.29	3.27	1.25	2.91	1.70
DM1M2	**Mgt (eq.)**	**-0.83**	**2.48**	**-0.13**	**1.07**	**0.31**	**1.70**

Context for analysis D6

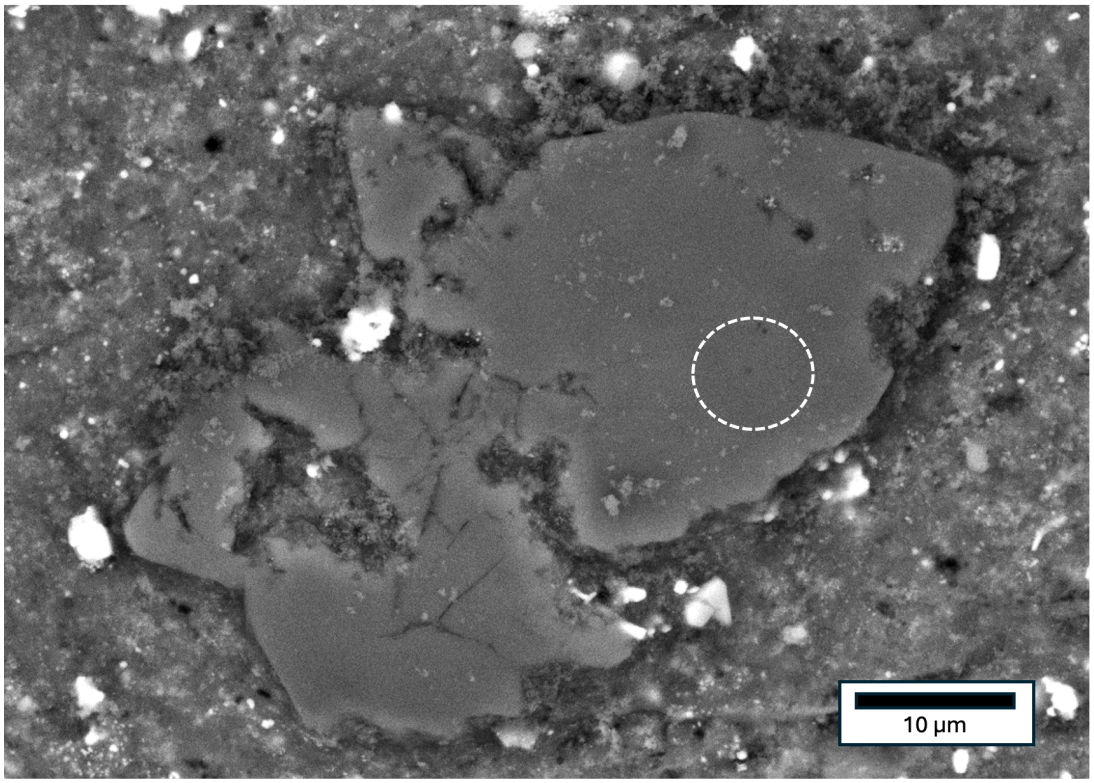

Figure A6: Backscattered electron image of the dolomite (analysis ID: D6) that did not plot on the Mn-Cr isochron in Figure 5. White dashed circle is the approximate location of the Mn-Cr SIMS measurement.

Literature isotope data of carbonates and magnetite in Tagish Lake

While triple O-isotope values can help unravel the conditions under which these carbonates formed, literature values of secondary minerals in Tagish Lake are sparse. To date, there is no published work investigating the triple O-isotope signature of magnetite, and triple-O signatures of carbonates can only be found in three conference abstracts, two of which were published >20 years ago at the time of this writing (Engrand et al., 2001; Leshin et al., 2001; Ushikubo et al., 2023). Of these three studies, Engrand et al. (2001), performed SIMS measurements of two calcite crystals that were standardized to a non-matrix-matched San Carlos Olivine, yielding results that are likely biased and will not be used for comparison. Ushikubo et al. (2023) recently used SIMS to measure triple-O isotopes in Tagish Lake calcite (n=13), but did not report the values. Leshin et al. (2001) used a phosphoric acid technique to dissolve the carbonates from a crushed and "degraded" aliquot of Tagish Lake and measured the whole-rock calcite and dolomite triple-O isotope compositions of the CO_2 released by the acid. Grady et al. (2002), however, employed the same method on a "pristine" sample of Tagish Lake but measured $\delta^{18}O$ and $\delta^{13}C$ only. The $\delta^{18}O$ values for both calcite and dolomite are consistent between the three studies, thus we compare our results to Ushikubo et al. (2023) and Leshin et al. (2001).

References

Engrand, C., Gounelle, M., Duprat, J., & Zolensky, M. E. 2001. In-situ oxygen isotopic composition of individual minerals in Tagish Lake, a unique type 2 carbonaceous chondrite. *32nd Lunar and Planetary Science Conference.*

Grady, M. M., Verchovsky, A. B., Franchi, I. A., Wright, I. P., & Pillinger, C. T. 2002. Light element geochemistry of the Tagish Lake C12 chondrite: Comparison with CI1 and CM2 meteorites. *Meteoritics and Planetary Science*, *37*(5), 713–735. https://doi.org/10.1111/j.1945-5100.2002.tb00851.x

Leshin, A., Farquhar, J., Guan, Y., Pizzarello, S., Jackson, T. L., & Thiemens, M. H. 2001. Oxygen Isotopic Anatomy of Tagish Lake: Relationship to Primary and Secondary Minerals in CI and CM Chondrites. *32nd Lunar and Planetary Science Conference*.

Śliwiński, M. G., Kitajima, K., Kozdon, R., Spicuzza, M. J., Fournelle, J. H., Denny, A., & Valley, J. W. 2016a. Secondary Ion Mass Spectrometry Bias on Isotope Ratios in Dolomite–Ankerite, Part I: δ18O Matrix Effects. *Geostandards and Geoanalytical Research*, *40*(2), 157–172. https://doi.org/10.1111/j.1751-908X.2015.00364.x

Śliwiński, M. G., Kitajima, K., Kozdon, R., Spicuzza, M. J., Fournelle, J. H., Denny, A., & Valley, J. W. 2016b. Secondary Ion Mass Spectrometry Bias on Isotope Ratios in Dolomite–Ankerite, Part II: δ13C Matrix Effects. *Geostandards and Geoanalytical Research*, *40*(2), 173–184. https://doi.org/10.1111/j.1751-908X.2015.00380.x

Ushikubo, T., Yamaguchi, A., Weisberg, M. K., Kimura, M., & Ebel, D. S. 2023. Evidence for High δ13C and Δ17O Fluid in Small Bodies Accreted in a Cold and Distant Region from the Sun. *54th Lunar and Planetary Science Conference*.

B: Chapter 3 Supplementary

Table B1: Atom Probe Tomography collection specifications for datasets R5047_35350 and R5047_35357.

Dataset	**R5047_35350**	**R5047_35357**
Instrument Model	LEAP 5000XS	LEAP 5000XS
Instrument Settings		
Laser wavelength (nm)	355	355
Laser pulse energy (pJ)	80	50
Pulse frequency (kHz)	250	250
Target detection rate (ions/pulse)	0.003	0.003
Nominal flight path (mm)	100	100
Base temperature (K)	60	50
Chamber pressure (Torr)	4.4E-11	3.8E-11
Data Summary		
Analysis software	IVAS 6.3	IVAS 6.3
Total ions:	27,479,861	64,721,090
Single (%)	52	56
Multiple (%)	47	43
Partial (%)	1	1
Reconstructed ions:	25,195,526	41,142,880
Ranged (%)	91	91
Volt./bowl corr. peaks (Da)	28, 32, 72	28, 32, 72
M/ΔM (FWHM)	384	515
Time-indep. Background (ppm/nsec)	5	8
Reconstruction		
Final specimen state	Fractured	Fractured
Radius evolution model	Shank	Shank
Initial Radius (nm)	30	35
Half Shank Angle (°)	18	12
Field factor (k)	3.3	3.3
Image compression factor	1.65	1.65
Assumed E-field (V/nm)	33	18
Detector efficiency (%)	0.8	0.8
V_{intial};V_{final} (V)	3.9;4.7	3.8;5.8

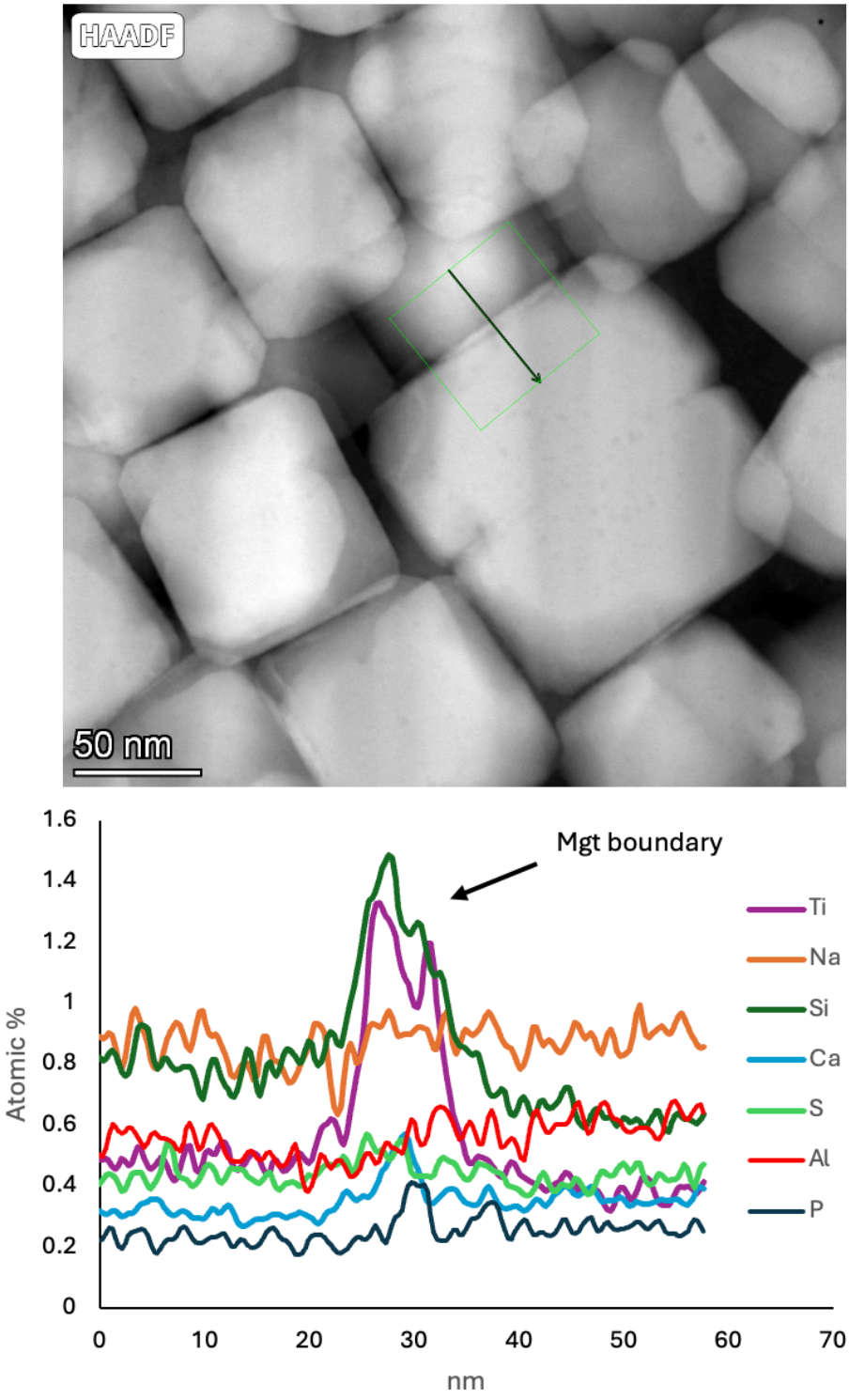

Figure B1: Top image shows a HAADF TEM image of magnetite framboid F4. A line scan was measured from this region, denoted by the black arrow. The bottom plot shows the elemental composition along the line scan, in atomic %. The peaks of Ti and Si correspond to the magnetite boundary in the top image.